MODELING AND ANALYSIS OF APERTURE COUPLED CYLINDRICAL DIELECTRIC RESONATOR ANTENNAS

by

Mhamed Chabi

A thesis submitted

to the Department of Electrical and Computer Engineering

University of Manitoba

Winnipeg, Manitoba, Canada

In partial fulfillment of the requirements for

the degree

Master of Science

ISBN 0-612-13018-5

Canada

Name Mhamed CHABI

Dissertation Abstracts International is arranged by broad, general subject categories. Please select the one subject which most nearly describes the content of your dissertation. Enter the corresponding four-digit code in the spaces provided.

Electrical
SUBJECT TERM

0544
SUBJECT CODE

U·M·I

Subject Categories

THE HUMANITIES AND SOCIAL SCIENCES

COMMUNICATIONS AND THE ARTS
Architecture 0729
Art History 0377
Cinema 0900
Dance 0378
Fine Arts 0357
Information Science 0723
Journalism 0391
Library Science 0399
Mass Communications 0708
Music 0413
Speech Communication 0459
Theater 0465

EDUCATION
General 0515
Administration 0514
Adult and Continuing 0516
Agricultural 0517
Art 0273
Bilingual and Multicultural 0282
Business 0688
Community College 0275
Curriculum and Instruction 0727
Early Childhood 0518
Elementary 0524
Finance 0277
Guidance and Counseling 0519
Health 0680
Higher 0745
History of 0520
Home Economics 0278
Industrial 0521
Language and Literature 0279
Mathematics 0280
Music 0522
Philosophy of 0998
Physical 0523
Psychology 0525
Reading 0535
Religious 0527
Sciences 0714
Secondary 0533
Social Sciences 0534
Sociology of 0340
Special 0529
Teacher Training 0530
Technology 0710
Tests and Measurements 0288
Vocational 0747

LANGUAGE, LITERATURE AND LINGUISTICS
Language
- General 0679
- Ancient 0289
- Linguistics 0290
- Modern 0291

Literature
- General 0401
- Classical 0294
- Comparative 0295
- Medieval 0297
- Modern 0298
- African 0316
- American 0591
- Asian 0305
- Canadian (English) 0352
- Canadian (French) 0355
- English 0593
- Germanic 0311
- Latin American 0312
- Middle Eastern 0315
- Romance 0313
- Slavic and East European 0314

PHILOSOPHY, RELIGION AND THEOLOGY
Philosophy 0422
Religion
- General 0318
- Biblical Studies 0321
- Clergy 0319
- History of 0320
- Philosophy of 0322

Theology 0469

SOCIAL SCIENCES
American Studies 0323
Anthropology
- Archaeology 0324
- Cultural 0326
- Physical 0327

Business Administration
- General 0310
- Accounting 0272
- Banking 0770
- Management 0454
- Marketing 0338

Canadian Studies 0385
Economics
- General 0501
- Agricultural 0503
- Commerce-Business 0505
- Finance 0508
- History 0509
- Labor 0510
- Theory 0511

Folklore 0358
Geography 0366
Gerontology 0351
History
- General 0578
- Ancient 0579
- Medieval 0581
- Modern 0582
- Black 0328
- African 0331
- Asia, Australia and Oceania 0332
- Canadian 0334
- European 0335
- Latin American 0336
- Middle Eastern 0333
- United States 0337

History of Science 0585
Law 0398
Political Science
- General 0615
- International Law and Relations 0616
- Public Administration 0617

Recreation 0814
Social Work 0452
Sociology
- General 0626
- Criminology and Penology 0627
- Demography 0938
- Ethnic and Racial Studies 0631
- Individual and Family Studies 0628
- Industrial and Labor Relations 0629
- Public and Social Welfare 0630
- Social Structure and Development 0700
- Theory and Methods 0344

Transportation 0709
Urban and Regional Planning 0999
Women's Studies 0453

THE SCIENCES AND ENGINEERING

BIOLOGICAL SCIENCES
Agriculture
- General 0473
- Agronomy 0285
- Animal Culture and Nutrition 0475
- Animal Pathology 0476
- Food Science and Technology 0359
- Forestry and Wildlife 0478
- Plant Culture 0479
- Plant Pathology 0480
- Plant Physiology 0817
- Range Management 0777
- Wood Technology 0746

Biology
- General 0306
- Anatomy 0287
- Biostatistics 0308
- Botany 0309
- Cell 0379
- Ecology 0329
- Entomology 0353
- Genetics 0369
- Limnology 0793
- Microbiology 0410
- Molecular 0307
- Neuroscience 0317
- Oceanography 0416
- Physiology 0433
- Radiation 0821
- Veterinary Science 0778
- Zoology 0472

Biophysics
- General 0786
- Medical 0760

EARTH SCIENCES
Biogeochemistry 0425
Geochemistry 0996
Geodesy 0370
Geology 0372
Geophysics 0373
Hydrology 0388
Mineralogy 0411
Paleobotany 0345
Paleoecology 0426
Paleontology 0418
Paleozoology 0985
Palynology 0427
Physical Geography 0368
Physical Oceanography 0415

HEALTH AND ENVIRONMENTAL SCIENCES
Environmental Sciences 0768
Health Sciences
- General 0566
- Audiology 0300
- Chemotherapy 0992
- Dentistry 0567
- Education 0350
- Hospital Management 0769
- Human Development 0758
- Immunology 0982
- Medicine and Surgery 0564
- Mental Health 0347
- Nursing 0569
- Nutrition 0570
- Obstetrics and Gynecology 0380
- Occupational Health and Therapy 0354
- Ophthalmology 0381
- Pathology 0571
- Pharmacology 0419
- Pharmacy 0572
- Physical Therapy 0382
- Public Health 0573
- Radiology 0574
- Recreation 0575
- Speech Pathology 0460
- Toxicology 0383

Home Economics 0386

PHYSICAL SCIENCES
Pure Sciences
Chemistry
- General 0485
- Agricultural 0749
- Analytical 0486
- Biochemistry 0487
- Inorganic 0488
- Nuclear 0738
- Organic 0490
- Pharmaceutical 0491
- Physical 0494
- Polymer 0495
- Radiation 0754

Mathematics 0405
Physics
- General 0605
- Acoustics 0986
- Astronomy and Astrophysics 0606
- Atmospheric Science 0608
- Atomic 0748
- Electronics and Electricity 0607
- Elementary Particles and High Energy 0798
- Fluid and Plasma 0759
- Molecular 0609
- Nuclear 0610
- Optics 0752
- Radiation 0756
- Solid State 0611

Statistics 0463

Applied Sciences
Applied Mechanics 0346
Computer Science 0984
Engineering
- General 0537
- Aerospace 0538
- Agricultural 0539
- Automotive 0540
- Biomedical 0541
- Chemical 0542
- Civil 0543
- Electronics and Electrical 0544
- Heat and Thermodynamics 0348
- Hydraulic 0545
- Industrial 0546
- Marine 0547
- Materials Science 0794
- Mechanical 0548
- Metallurgy 0743
- Mining 0551
- Nuclear 0552
- Packaging 0549
- Petroleum 0765
- Sanitary and Municipal 0554
- System Science 0790

Geotechnology 0428
Operations Research 0796
Plastics Technology 0795
Textile Technology 0994

PSYCHOLOGY
General 0621
Behavioral 0384
Clinical 0622
Developmental 0620
Experimental 0623
Industrial 0624
Personality 0625
Physiological 0989
Psychobiology 0349
Psychometrics 0632
Social 0451

MODELLING AND ANALYSIS OF APERTURE COUPLED CYLINDRICAL DIELECTRIC RESONATOR ANTENNAS

BY

MHAMED CHABI

A Thesis submitted to the Faculty of Graduate Studies of the University of Manitoba in partial fulfillment of the requirements of the degree of

MASTER OF SCIENCE

ABSTRACT

Dielectric resonator antennas offer many attractive features such as low cost, small size, easy fabrication, freedom from metallic loss, wider bandwidth, high radiation efficiency, and easy coupling to all transmission line. These important characteristics enable dielectric resonator antennas (DRAs) to have a potential application in the *mm* wave band, in which the conductor loss of the metallic antennas becomes too large to ignore. With a proper feeding structure for the DRA, this type of antenna can also be easily integrated into microwave integrated circuits (MIC).

In this thesis, an aperture coupled cylindrical dielectric resonator antenna, excited by the $HEM_{11\delta}$ dominant mode is studied both theoretically and experimentally. In the theoretical analysis, two methods are used to model the DR, namely the magnetic wall model (MWM) and the dual dielectric waveguide model (DWM). The latter method is developed for accurately determining the wavenumbers inside the DR. The knowledge of the wavenumbers leads directly to the evaluation of the resonant frequency, Q–factor and the near– and far– fields of a dielectric resonator antenna. The accuracy of the computed results using the DWM model for DR is demonstrated by comparison with exact numerical and empirical formulation available in the literature.

An experimental investigation of the resonant frequency, input impedance, and radiation pattern of a dielectric resonator antenna have been carried out in this thesis. The resonant frequency and input impedance have been measured for dielectric resonators of various geometrical aspect ratios and dielectric constants 10.2 and 10.5. The radiation pattern of the antenna was measured at various frequencies and for two resonators that provide good matching conditions. Experimental results show that the antenna displays the expected radiation pattern and has a wide operating frequency bandwidth.

Very good agreement was obtained between the developed dual dielectric waveguide model for the DR and the experimental results for both the resonant frequency and radiation pattern.

This thesis is dedicated to my Father.

May Allah grant him paradise.

Amen.

ACKNOWLEDGEMENTS

I would like to express my sincere gratitude to my advisor Professor G. Bridges for his valuable advice, patience, guidance, and assistance during the course of this research.

I would like to thank my committees members, Professor A. Sebak and Professor N. Sepehri for their willingness to examine this work.

Also special Thanks goes to B. Tabachnick for his assistance in doing the experimental part of the thesis

I wish to extend my appreciation to my Mother, my Hanna, and all my Brothers and Sisters for their continued support and encouragement.

Finally, I would like to acknowledge the financial assistance of the Natural Science and Engineering Research Council of Canada, Federal Networks of Centres of Excellent / Micro-net.

TABLES OF CONTENTS

LIST OF FIGURES

LIST OF TABLES

CHAPTER 1

1.1 Introduction to Dielectric Resonator (DR)

Dielectric resonators are simply pieces of high dielectric constant ceramic's, their shapes being usually a short and solid cylinder, but one can also find spherical and parallelpiped designs. They were first studied by R.D. Richtmyer of Stanford University when he showed that unmetalized dielectric objects can function as Microwave Resonators [1]. However, their first practical application did not appear until the mid 60's when they were used as resonating elements in waveguide filters [2]. Nevertheless, dielectric resonators were still far from any true practical usage in the microwave industry, since the dielectric materials that were available at that time, such as rutile, lacked temperature stability causing large resonant frequency changes. A breakthrough in ceramics technology in the 1970's was with the development of the first temperature stable, low loss barium tetratitanate resonator by Raytheon [3]. Later, a modified barium tetratitanate with improved performance was reported by Bell labs [4], and a stable dielectric material Zr–Sn Tio ceramics developed by Japan [5]. These temperature stable materials have led to the actual implementation of dielectric resonators as microwave components.

In todays technology of MIC (Microwave Integrated Circuits) and MMIC (Monolithic Microwave Integrated Circuits), low cost and the small size are the two most important criteria in designing microwave circuit components. In this respect, dielectric resonators (DRs) that are fabricated out of low loss material $\tan(\delta) \approx 10^{-4}$ and high dielectric constant $\varepsilon_{r_{DR}} \approx (20\text{–}100)$ are widely used in shielded microwave circuits. They replace the bulky and expansive metallic cavities in constructing high performance narrow band filters, and highly stable fundamental frequency oscillators. In these applications, the DR's unloaded quality factor Q_u can vary from 5000 to 50000 [6]. When the DR is placed in an open environment, the power lost is mainly due to radiation, the unloaded quality factor Q_u of the lowest order modes of the DR are in the order of (10–100). This makes them a good candidate in designing wide band antennas.

Recently attention has also been focussed on the design of microwave antennas that take advantage of the technology developed for MICs. These antennas are required to be cost–effective, smaller in size, easy to fabricate and have a high performance. Also, these antennas are required to operate not only in the microwave band but also in the millimeter and near millimeter region (100–300 Ghz). In this trends, microstrip antennas [7] have taken the attention of most of microwave antenna researchers since they offer many advantages in the microwave frequency range. However, they suffer from narrow–band performance (1–5%) of the operating frequency, pattern distortion due to surface wave modes excited around the microstrip patch edge, and relatively large conductor losses in the metal portion of the antenna which increases with frequency. Nevertheless, microstrip patch antenna researchers [7] have developed ways of solving some of these disadvantages, except the conductor losses, which become too great for a systems requiring efficient operation at high frequencies.

Dielectric resonator antennas offer many attractive features and have some advantages over microstrip patch antennas. These are illustrated by the following:

- The dimensions of a DR antenna are of the order of $\lambda_0 / \sqrt{\varepsilon_r}$, where λ_0 is the free space wavelength and ε_r is the dielectric constant of the resonator material. For the microstrip patch antenna, dimensions are of the order of $\lambda_0 / \sqrt{\varepsilon_r}$. However, a high value of ε_r (10–100) can be used to manufacture the DR, thus the size of the DR antenna can be made much smaller than the microstrip antenna.

- The dielectric resonator has no conductor loss. This leads to high radiation efficiency of the antenna, especially in *mm*–wave antennas where the loss in metal fabricated antennas such as the microstrip antenna can be high.

- DRs can be easily coupled to nearly all transmission lines geometries used at microwave and *mm*–wave frequencies. This makes them suitable for integration into

different planar technologies.

- Each radiating mode of the DR has a unique internal and external field distribution. Thus one can obtained different radiating patterns by exciting different radiating modes of the DR.

- A wider bandwith of the operating frequency (4–10%) can be easily obtained using a lower order mode of the DR.

1.2 Modes of a Cylindrical Dielectric Resonator

There are many resonant modes which can be excited in dielectric resonators. These modes can be divided into three main families; transverse electric (TE), transverse magnetic (TM), and hybrid modes. Each of the three families has an infinite variety of individual modes. The fields of the TE and TM modes are axisymmetric, therefore, they are independent on the variation of ϕ , while the fields of the Hybrid modes are dependant on the variation of ϕ . The hybrid modes can also be subdivided into two groups; HEM and EHM [8]. For the HEM modes, the H_z component is much smaller than the E_z component and therefore the other remaining field components for the HEM modes can be obtained from knowledge of E_z component only. The reverse is also true for the EHM modes.

To classify the different modes of each family of the DR, mode indices are indicated using subscripts. The *TE*, *TM*, *HEM* and *EHM* modes are then classified as $TE_{0mp+\delta}$, $TM_{0mp+\delta}$, $HEM_{nmp+\delta}$ and $EHM_{nmp+\delta}$ respectively. The first index ($n = 0,\ 1,\ 2,\ \ldots$) denotes the variation of the field in the ϕ direction. Note that n is equal to zero for TE and TM modes. The index ($m = 1,\ 2,\ \ldots\ldots$) denotes the order of variation of the fields along the radial direction and the index $p+\delta$, ($p = 0,\ 1,\ 2,\ \ldots\ldots$) denotes the order of variation of fields along the z–direction. The nomenclature δ signifies a non–integer number, smaller than unity. As explained in [8] and [9], this notation is adopted to take into consideration that some of the fields leaks out of the resonator and eventually decays expo-

nentially in its vicinity.

The $TE_{01\delta}$ and $HEM_{11\delta}$ are the two lowest radiating modes of an isolated DR. These modes have many good features that make them a good candidate in antenna applications. They have a very low quality factor (high radiation loss). Also, they have a plane of symmetry that behaves as an electric wall, and therefore, one can use half of this structure with a metallic wall placed at the plane of symmetry. The metallic wall is required when building an antenna to provide a mechanical support for the antenna and its feed structure.

To excite a specific mode in the DR while suppressing an unwanted one, one must know the field configuration inside the DR. Kajfez et. al. [9] and [10] provide a catalog for the electric and magnetic patterns inside a DR for several low–order resonant modes. With reference to Fig. 1.1, Figs. (1.2)–(1.3) shows the field distribution inside the DR for the $TE_{01\delta}$ mode, while Figs. (1.3)–(1.7) shows the fields distribution for $HEM_{11\delta}$ mode. These figures were taken from [7].

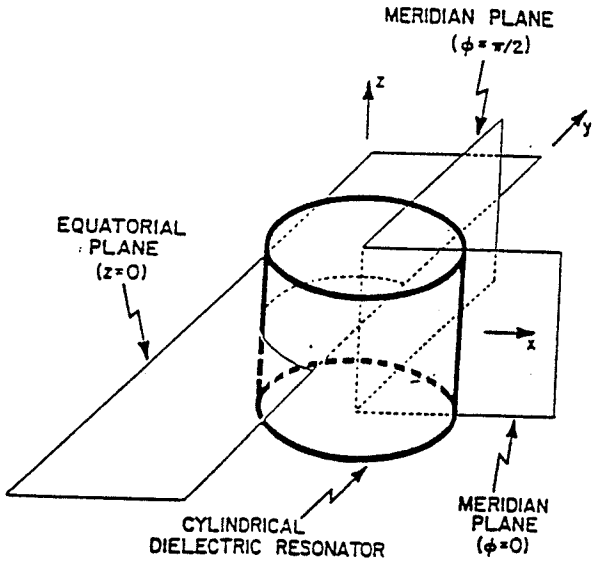

Figure 1.1 The definition of the planes used for analyzing the field inside the dielectric resonator [9]

In all Figs. (1.2)–(1.7), the double arrows indicates the region where the field is less than 3 dB below the maximum, while the longer lines indicate a level between 3 and 10 dB below the maximum. The shorter lines indicate a level between 10 and 20 dB below the maximum. When the level of the field is more than 20 dB below the maximum value of the field, the

points are left blank.

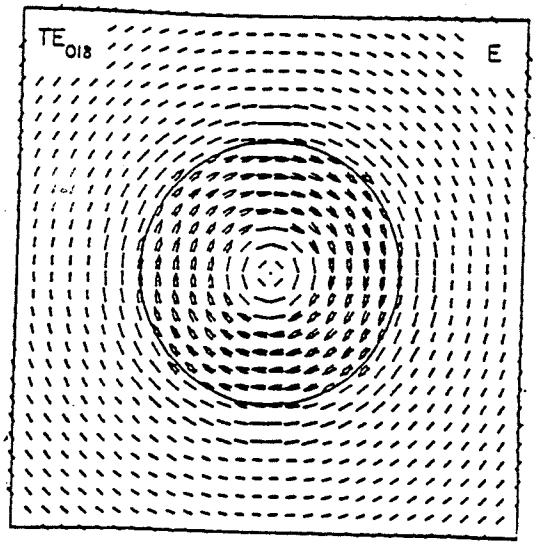

Figure 1.2 The E filed of $TE_{01\delta}$ mode in equatorial plane [9]

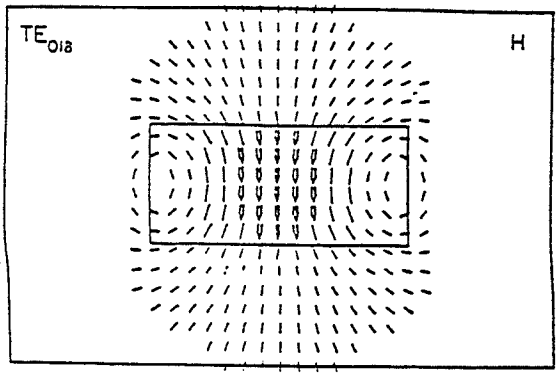

Figure 1.3 The H filed of $TE_{01\delta}$ mode in meridian plane [9]

The electric field for the $TE_{01\delta}$ is shown to be very strong everywhere within the equatorial plane of the dielectric resonator except near its center as in Fig. 1.2. The magnetic field for the $TE_{01\delta}$ mode in the equatorial plane is perpendicular to the electric field shown in Fig. 1.2 and its maximum occurs one–quarter period later in time [9]. Also, as indicated in Fig. 1.3 the magnetic field is strong down at the center of the resonator. The magnetic field for the $HEM_{11\delta}$ mode in the equatorial plane of the dielectric resonator is shown in Fig. 1.4. The electric field is shown in Fig. 1.5 in a plane that is parallel to the equatorial plane but

displaced by an offset of $2.15\,mm$ in the $z = 0$ from it. In both of Figs. 1.4 and 1.5, the fields are shown to be strong inside DR while weak outside it.

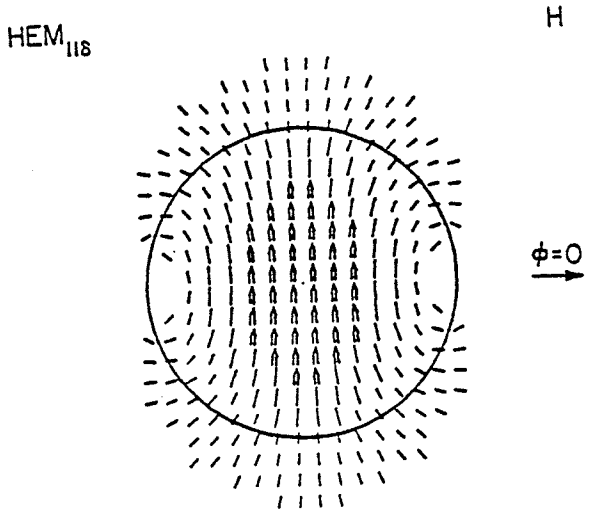

Figure 1.4 The H filed of $HEM_{11\delta}$ mode in equatorial plane [9]

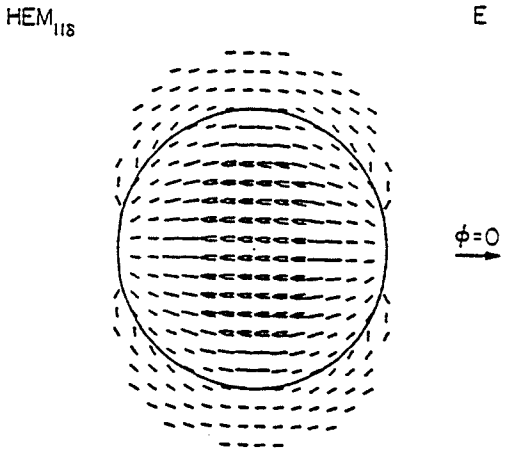

Figure 1.5 The E filed of $HEM_{11\delta}$ mode in plane parallel to equatorial plane [9]

The meridian plane fields are shown in Figs. 1.6 and 1.7. In this plane, the electric field intensity reaches its maximum at ($\phi = 0$) as in Fig. 1.6, while the maximum magnetic field intensity occurs in the meridian plane at ($\phi = \pi/0$) as in Fig. 1.7. Also in the meridian plane, the

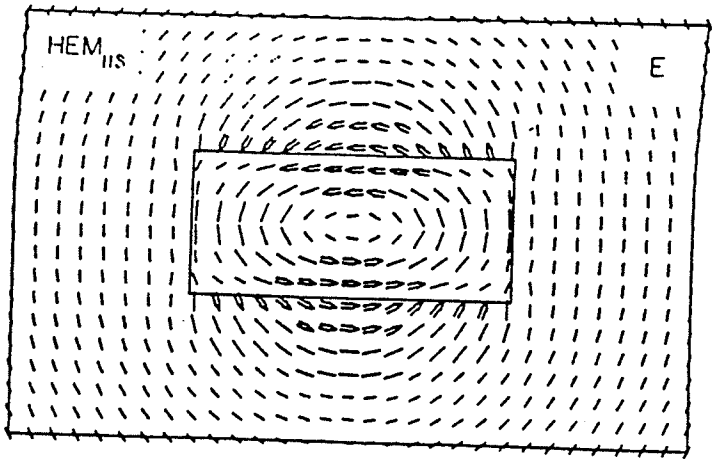

Figure 1.6 The E filed of $HEM_{11\delta}$ mode in meridian plane at $\phi = 0$ [9]

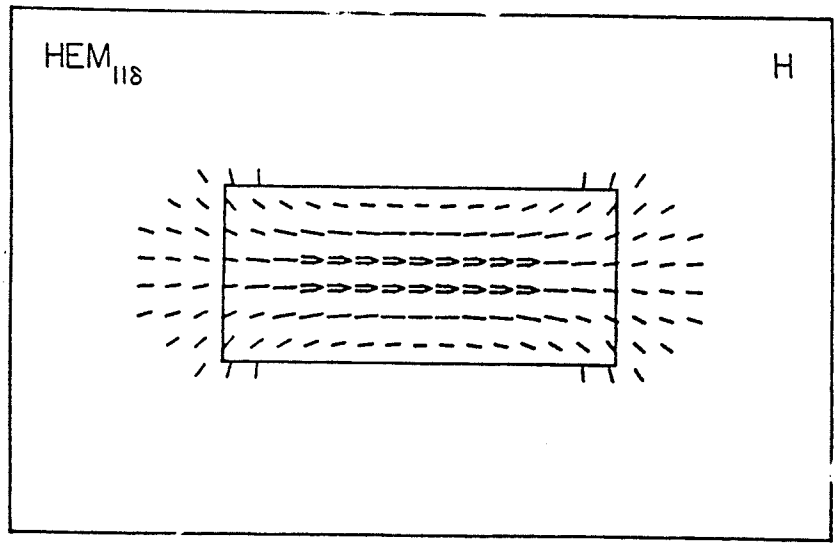

Figure 1.7 The H filed of $HEM_{11\delta}$ mode in meridian plane at $\phi = \frac{\pi}{2}$ [9]

electric field is shown to be very weak outside the resonator, while the magnetic field is shown to be strong.

1.3 Literature Review on Dielectric Resonator Antenna (DRA)

Long et. al. [11] were among the first research groups to investigate the use of a dielectric resonator as an antenna element. They used a magnetic wall boundary condition to formulate the resonant frequency and the radiation pattern for the DRA. They excited the resonator on a ground plane in the $HEM_{11\delta}$ mode by drilling a hole in the resonator near the edge and inserting a short monopole probe as shown in Fig. 1.8. The resonance frequency and the radiation pattern was measured for a DR of various aspect ratios (a/h), dielectric constants $\varepsilon_{r_{DR}}$, and size of feeding probe. They found that for all the tested samples that the DR antenna excited in the $HEM_{11\delta}$ mode radiated efficiently in a direction normal to the ground plane

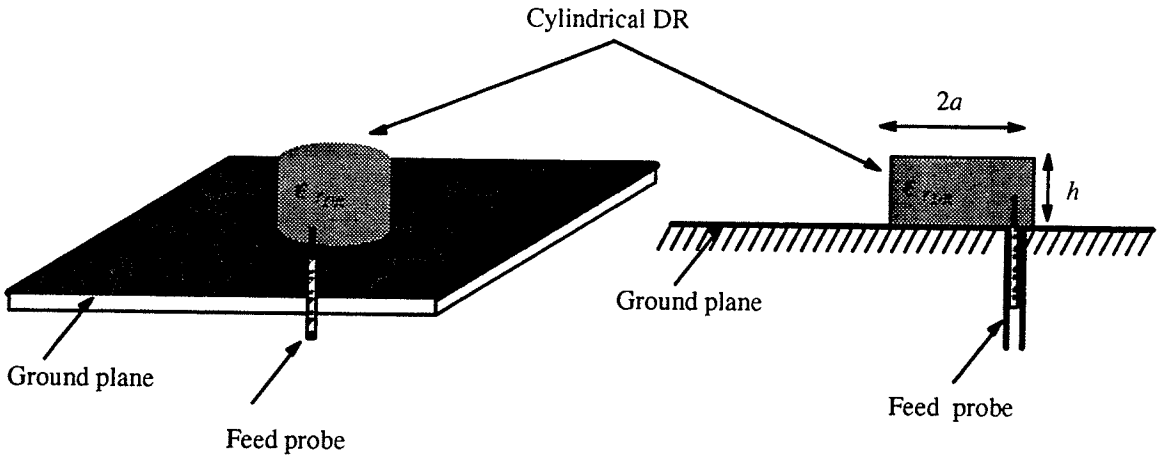

Figure 1.8 Cylindrical dielectric resonator excited by a monopole

In [12], Mongia proposed a cylindrical DR antenna which utilized the $TE_{01\delta}$ mode of the resonator. In his report, he placed a lateral split cylindrical DR on its side on a ground plane and then fed it with a coaxial cable as shown in Fig. 1.9. As was expected, it was shown that this antenna radiated like a magnetic dipole orientated along the longitudinal center of the DR. It was also reported that this antenna has a bandwith of 8% of the operating frequen-

cy.

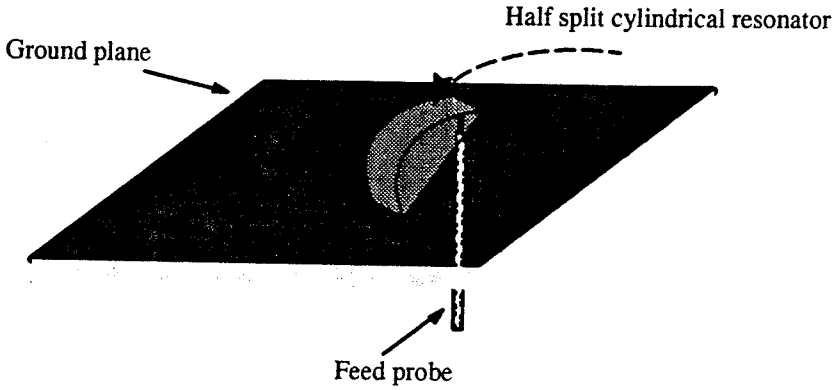

Figure 1.9 Cylindrical dielectric resonator excited by a monopole

McAllister et. al. [13] examined the radiation pattern and the input impedance of a rectangular parallelpiped resonator. They found that this type of antenna is an efficient radiator in the direction normal to the ground plane when it is excited by short monopole probe placed near its edge as shown in Fig. 1.10. It was also found that a maximum antenna gain can be obtained when the height of this resonator is smaller than its width.

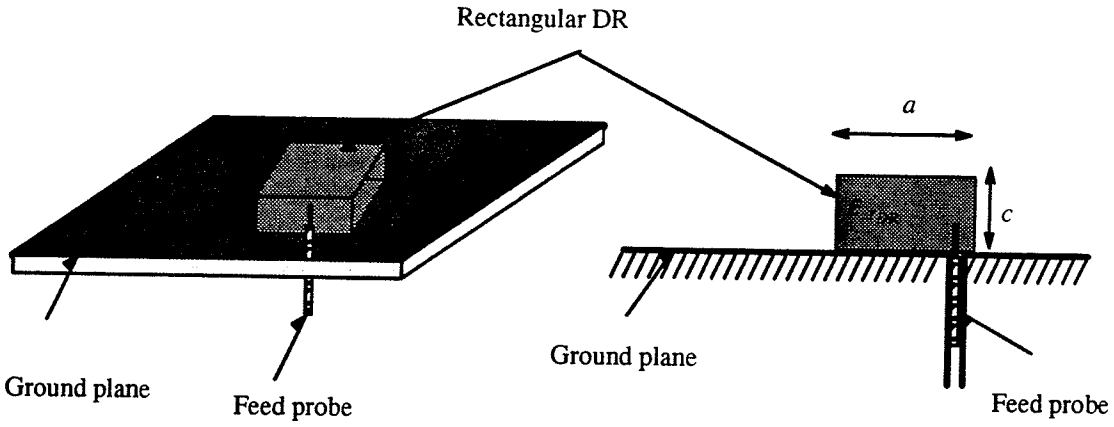

Figure 1.10 Rectangular dielectric resonator excited by a monopole

McAllister et. al. [14] used similar technique as the cylindrical and rectangular parallelpiped resonators to investigate the radiation pattern and the input impedance of hemispherical dielectric resonator antennas on a ground plane excited by a probe as shown in Fig. 1.11. Because of the spherical shape of this resonator, they were able to obtain an exact solution for the field and the resonant frequency. It was found that the hemispherical DR radiated

in its dominant mode similar to that reported for cylindrical and rectangular DR antennas.

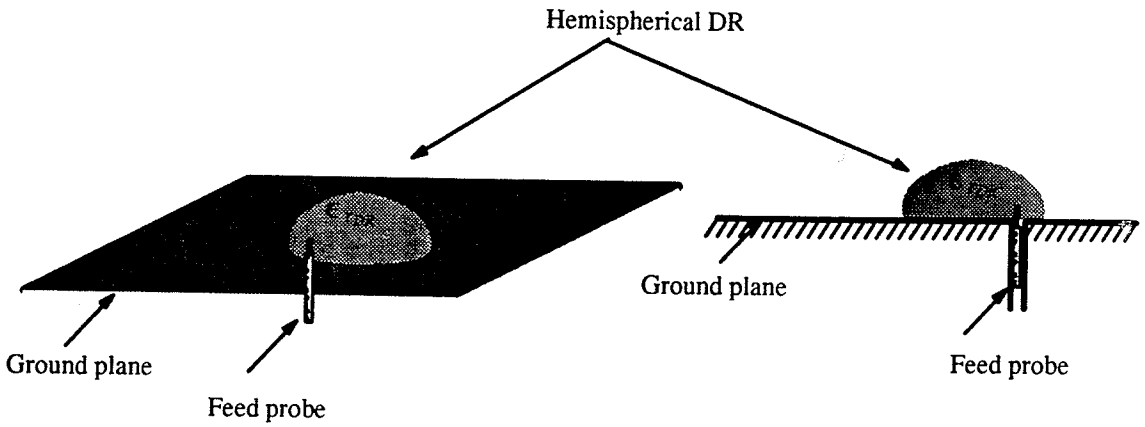

Figure 1.11 Hemispherical dielectric resonator excited by a monopole

Kranenburg and Long [15] examined the use of microstrip feed structures for the DR. They placed a cylindrical DR directly on top of a common microstrip feed line as shown in Fig. 1.12. By varying the position of the DR with respect to the end of the microstrip line, they measured the insertion loss of the antenna and they found that a strong coupling between the two occurs when the termination of the line is located slightly less than one quarter of the dielectric wavelength past the nearest edge of the DR. A deterioration of the radiated pattern was observed when the end of the line is terminated near the center of the cylinder, this latter occurring because of the placement of the DR and the feed structure on the same side of the substrate.

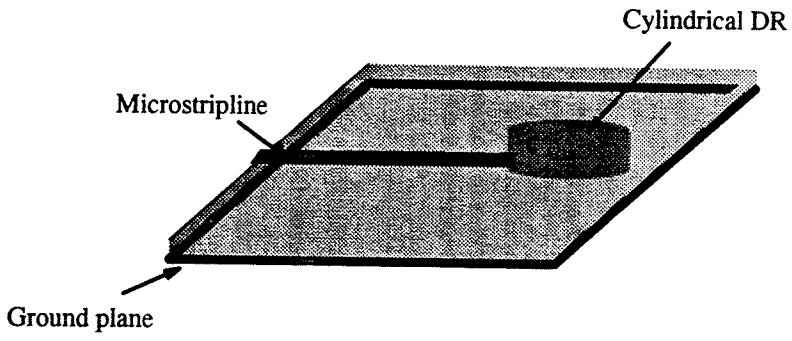

Figure 1.12 Dielectric resonator antenna fed by microstrip transmission line

Kranenburg et al [16] showed that a coplanar waveguide can be an effective feeding structure for the cylindrical DR antenna. The configuration of this antenna is shown in Fig. 1.13. In their report, they examined experimentally the coupling behavior and the radiation pattern for DR cylinders with various aspect ratios, dielectric constants, and feed positions. The measured results for the radiation pattern and the resonant frequency agreed well with ones obtained theocratically using a magnetic wall boundary condition model.

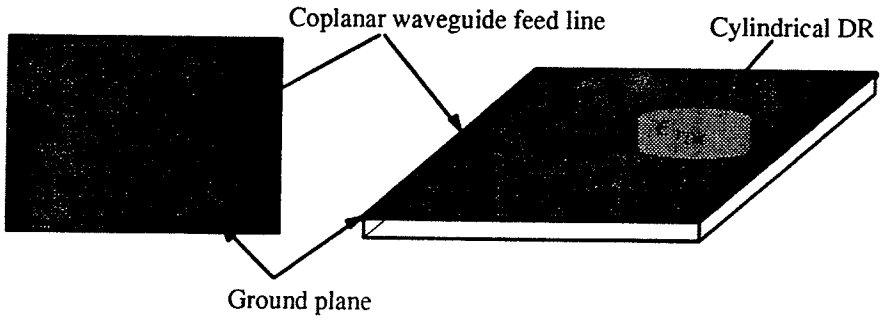

Figure 1.13 Dielectric resonator antenna fed by a coplanar waveguide

A planar array composed of a pair unit of dielectric resonator antennas was reported by M.Haneishi and H.Takazawa [17]. The configuration of this antenna is shown in Fig. 1.14. Each element of the pair unit was fed uniformly in power from orthogonal points F_1 and F_2. It was shown that a subarray made of two pair–units (Fig. 1.14b) yielded a 2 dB ellipticity with a bandwidth of 15%. The same result was also obtained when using an array of 8 pair–unit (Fig. 1.14c)

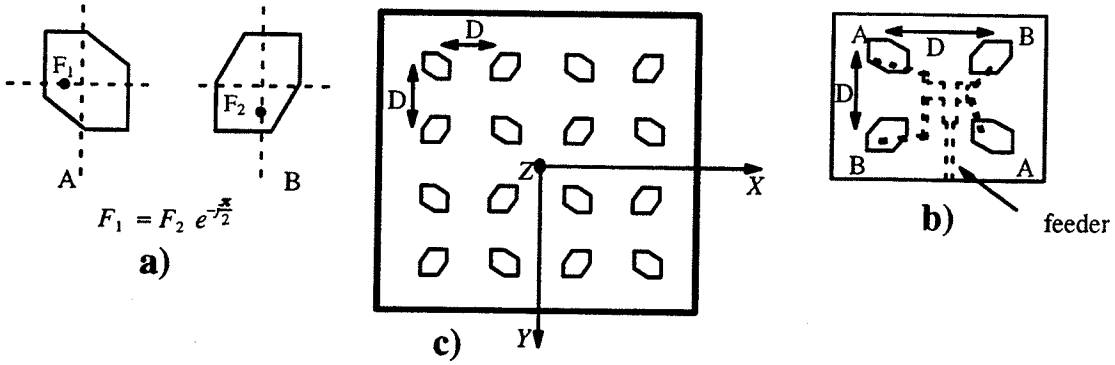

Figure 1.14 Configuration for DRA planar array

a) Pair–unit
b) Subarray
c) Array

Finally, the microstrip aperture coupling technique has been also used and proved to be an efficient mechanism for feeding dielectric resonators [18]– [22]. This technique was first introduced by Pozar [24] & [25] as an alternative to the traditional feeding structures, such as probe feeding, for antennas that have a potential used at millimeter–wave frequency and are compatible with MIC's. The slot–coupling has numerous advantages, as listed below:

- With the slot coupling, the radiating element is separated from the feeding structure by a ground plane. Therefore no direct contact between the two is needed. Furthermore, the feeding circuit will not degrade the radiation pattern and at the same time the radiation from the antenna will not interfere with the feed circuit performance.
- This technique saves space on the radiating surfaces. Thus the active circuitry such as phase shifters and amplifiers can be placed along the feed network on the lower substrate. Shielding of the circuitry is provided by the ground plane separating the lower substrate and the radiating element.
- The slot of the feeding network can be designed so that it excite only the dominant mode of the antenna, couples efficiently the energy from the microstrip line to the antenna, and to have no effect on the characteristic of the radiating element.

More discussion and analysis regarding the use of this coupling technique will be presented in Chapter 2 of this thesis.

1.4 Thesis Objectives

The objective of this thesis is to proceed in investigating theoretically and experimentally the cylindrical dielectric resonator antenna fed by an aperture on the ground plane of a microstrip line as shown in Fig. 1.15.

Theoretically, the aim is to use the dielectric waveguide model [29] as a starting point and

to modify it for a slot coupling DR antenna. This would enable us determining without extensive computation the parameters of the resonator, such as, the resonant frequency and wavenumbers, and therefore be able to find all the characteristics of the antenna.

Previous investigations have been either to analyze the DR as a cavity model [11] and [18], or to analyze it using the moment method [20] and [21]. The cavity model assumes that the surface of the DR is a perfect magnetic conductor. This yields an error of approximately 10% for the resonant frequency of the DR, and more than 20% for the radiated quality factor. The moment method predicts accurately all the parameters of the resonator, however, it requires extensive computation as compared with simple approximation methods.

Experimentally, the objective is to verify the analysis technique developed in this thesis and to confirm the use of the DR as a radiating element.

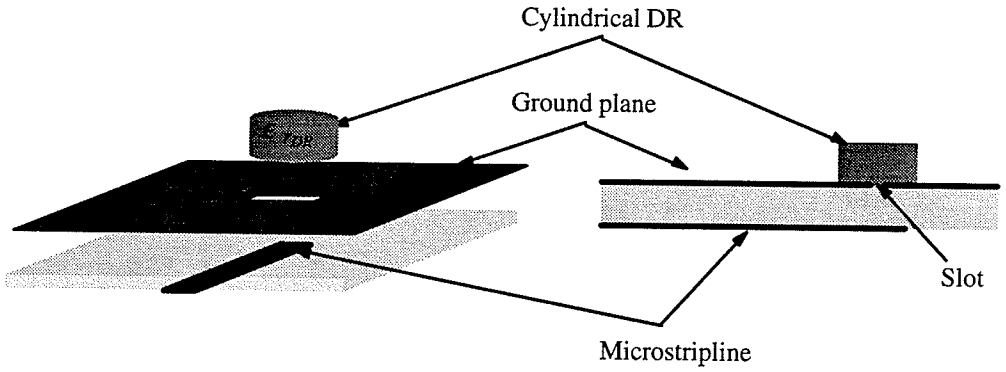

Figure 1.15 Aperture coupled cylindrical dielectric resonator antenna

1.5 Thesis Outline

This chapter presents an introduction to the dielectric resonator and a historical background of its usage as a radiating element. The objectives of this thesis was also discussed in this chapter.

Chapter 2 discusses the theoretical analysis of the aperture coupled antenna of Fig. 1.15. This chapter starts with a presentation of the antenna configuration and then discusses the methods of analysis for an isolated dielectric resonator; namely the cavity model and the dual dielectric waveguide model. Using these two models for the DR, equations for the reso-

nant frequency and wavenumbers of the DR are developed. Hence, all the field components inside and outside the DR are obtained. The results of the resonant frequency and the radiated quality factor of this antenna are computed and compared to the ones obtained numerically using a moment method [20] and [21], and to those reported in the literature[26]. The results of the radiated field were presented and compared with the one computed rigorously in [23]. The near field results of an isolated DR were also determined in this chapter. Finally, following the steps that were outlined in [23] and [27], an equivalent circuit of the antenna is presented.

Chapter 3 outlines the design and fabrication of the feedline and DR of our antenna structure. Also, a comparison of theoretical and experimental results for the resonant frequency and the radiation pattern of this antenna are discussed in this chapter.

Chapter 4 includes the conclusion and the recommendations from this thesis work.

CHAPTER 2

THEORY

2.1 Antenna Configuration

The dielectric resonator antenna (DRA), we consider in detail in this thesis is shown in Fig.2.1. The dielectric resonator antenna consists of a cylindrical dielectric resonator (DR) of height h, radius a and dielectric constant $\epsilon_{r_{DR}}$. This DR is placed on the top of a guided

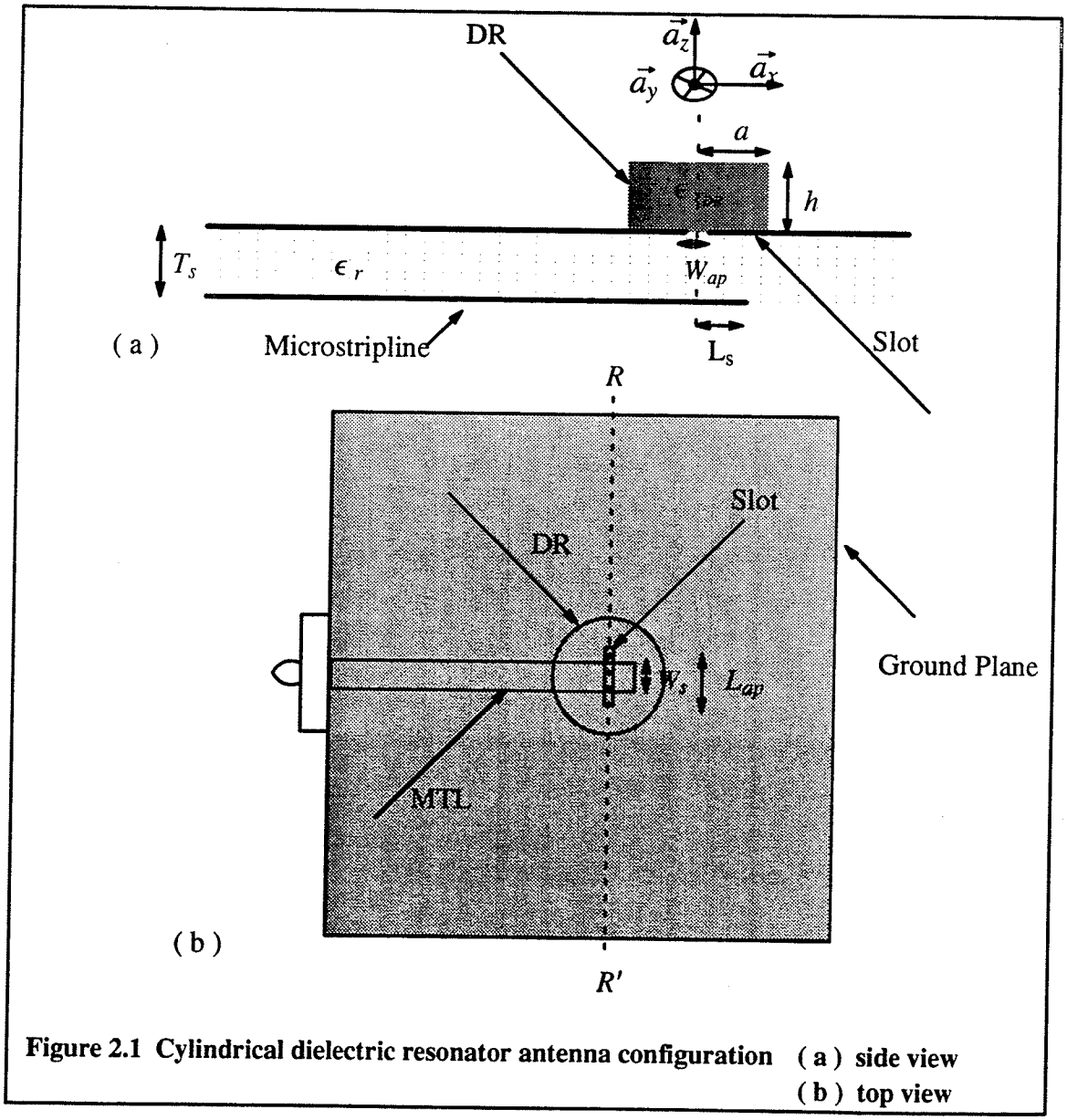

Figure 2.1 Cylindrical dielectric resonator antenna configuration (a) side view (b) top view

dielectric slab with a rectangular thin slot as feed for the DR. The slot is of width W_{ap} and of length L_{ap}. The slot is etched on the ground plane of a microstripline (MTL) and thus couples energy from the feed line to the dielectric resonator (DR). The grounded dielectric slab has a dielectric constant ϵ_r and a thickness T_s, whereas the MTL feed line has a width W_s and an open circuit stub length L_s from the slot reference plane $R-R'$. For the mode of interest, the maximum coupling from the MTL to DR occurs when the DR is centered along the axis of symmetry of the slot [25]. The slot width is usually chosen to be significantly smaller than the microstrip feed line guided wavelength, so it can be modelled by a magnetic current oriented in the $\vec{y}$ direction as in Fig. 2.2. At microwave frequencies ($1-60$ GHz), the finite ground plane will be assumed to be electrically very large, so it can be considered as an infinite ground plane. Using the image theory, this antenna can then be modelled by an isolated DR of radius $r=a$ and of height double the one used above the ground plane. Thus, as shown in Fig. 2.2, the antenna can be assumed to be an isolated DR, excited by a magnetic current $\vec{M}$ placed at the center axis of the DR $z=0$.

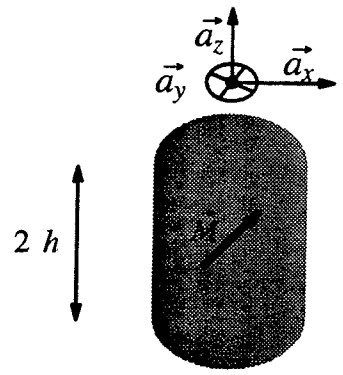

Figure 2.2 The equivalent model for the DRA

To study the important characteristics of this antenna such as; resonant frequency, radiation pattern, bandwidth, input impedance and quality factor, the electric and magnetic fields inside the isolated DR are first found by the use of a simple cavity model. Due to the inadequacies of this model, a more accurate dual dielectric waveguide model is introduced.

This model is then latter compared to the exact numerical and empirical solution formulation found in the literature.

2.2 Methods of Analysis for an Isolated Dielectric Resonator

To solve for the electric and magnetic fields inside and outside the isolated dielectric resonator antenna of Fig. 2.2, a simple cavity and a more complex waveguide models are used. In the cavity model the top, bottom and side walls of the DR are assumed to be perfect magnetic conductors. Therefore, the electromagnetics fields are confined inside the DR. On the other hand, the waveguide model considers the fields outside the DR walls, assuming to decay in both ϱ and z directions. Since the DR is assumed to be cylindrical, the scalar Helmholtz equation in cylindrical coordinate is used to solve for the fields inside and outside the DR. The boundary condition set by both DR models are then applied to obtain the final solutions.

2.2.1 Wave Equation Solution in Cylindrical Coordinates

In a homogeneous, linear and isotropic medium the electric and the magnetic potential vector equations are given, respectively, as follows[28]

$$\nabla^2\vec{A} + k^2\vec{A} = 0 \tag{2.1}$$

$$\nabla^2\vec{F} + k^2\vec{F} = 0 \tag{2.2}$$

where k is the wave number and is defined by

$$k = \sqrt{(\omega^2\mu\,\epsilon)} \tag{2.3}$$

where

$$\epsilon = \varepsilon_o\,\varepsilon_{r_{DR}}$$

Here $\epsilon_o = 8.854\ 10^{-12}$ (Farad/m) is the permittivity of free space, and $\varepsilon_{r_{DR}}$ is the relative dielectric constant of the medium. The scalar longitudinal components of the electric vector potential A_z and magnetic vector potential F_z both satisfy the scalar Helmholtz equa-

tion,

$$\nabla^2\psi + k^2\psi = 0 \tag{2.4}$$

In cylindrical coordinate system Fig. 2.3, $\frac{\partial^2\psi}{\partial\varrho^2}+\frac{1}{\varrho}\frac{\partial\psi}{\partial\varrho}+\frac{1}{\varrho^2}\frac{\partial^2\psi}{\partial\phi^2}+\frac{\partial 2\psi}{\partial z^2}+k^2\psi=0$ (2.5)

where $\psi = \begin{cases} \psi^m = A_z & \text{for TM modes} \\ \psi^e = F_z & \text{for TE modes} \end{cases}$

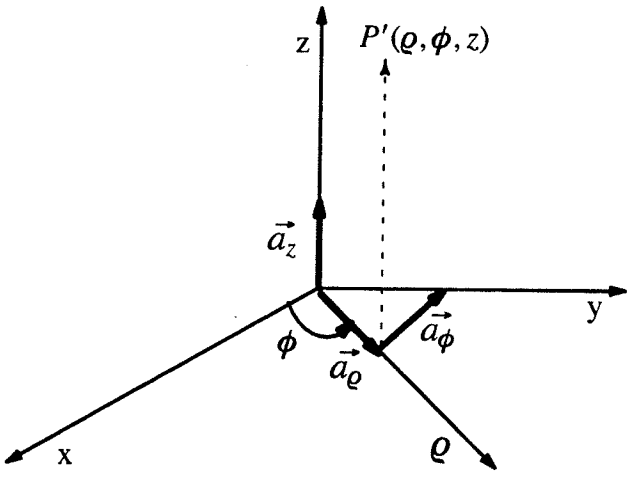

Figure 2.3 The cylindrical coordinates system

Using the method of separation of variable, the wave function ψ is first set into a product of three independent functions

$$\psi = Z(z)\ F(\phi)\ P(\varrho). \tag{2.6}$$

By substituting (2.6) into (2.5), the following system of three ordinary differential equations is obtained

$$\begin{cases} \dfrac{1}{Z}\dfrac{d^2Z}{dz^2} + k_z^2 = 0 \\ \dfrac{1}{F}\dfrac{d^2F}{dz^2} + k_\phi^2 = 0 \\ \varrho\dfrac{d}{d\varrho}\left(\varrho\dfrac{dP}{d\varrho}\right) + \left((\ k_p\ \varrho)^{\,2} - m^2\right)\ P = 0 \end{cases} \tag{2.7}$$

where, $$k^2 = k_z^2 + k_p^2 \tag{2.8}$$

Each of these ordinary differential equations determines only one of the functions P,F or Z. The first two equations are harmonic equations, whose solutions are harmonic functions. The last equation is the Bessel equation of the m^{th} order, whose solution is a Bessel function. For a cylindrical cavity structure, such as the dielectric resonator of Fig. 2.2, a solution for the system of equations (2.7) inside dielectric region would be of the form,

$$\begin{cases} Z(z) = A_z \cos(\ k_z\ z) + B_z \sin(\ k_z\ z) \\ F(\phi) = A_\phi \cos(\ k_\phi\ \phi\ ) + B_\phi \sin(\ k_\phi\ \phi) \\ P(\varrho) = A_p\ J_m(\ k_p\ \varrho\ ) + B_p\ Y_m(\ k_p\ \varrho) \end{cases} \tag{2.9}$$

Substituting the system (2.9) into (2.6), the scalar wave function ψ then can be expressed as

$$\begin{aligned} \psi = A_p\ J_m(\ k_p\ \varrho\ ) \cdot &\left(A_z\ cos(\ k_z\ z) + B_z\ sin(\ k_z\ z)\right) \\ \cdot &\left(A_\phi \cos(\ k_\phi\phi) + B_\phi\ \sin(\ k_\phi\ \phi)\right) \end{aligned} \tag{2.10}$$

The scalar wave function ψ must be finite for all values of ϱ, z and ϕ inside the DR. Since the function Y_m becomes infinite for $\varrho = 0, B_p = 0$. The choices of k_z, k_ϕ and the other constants A_z and B_z depend on the dimensions of the dielectric resonator, the boundary conditions applied, and the conditions of the fields to be supported by the DR.

The electric field E and magnetic field H can be expressed in terms of the scalar wave equation ψ^e and ψ^m [28], respectively, as follow

for TM^z case ,

$$H_\varrho = \frac{1}{\varrho}\frac{\partial \psi^m}{\partial \phi} \tag{2.11}$$

$$H_\phi = -\frac{\partial \psi^m}{\partial \varrho} \tag{2.12}$$

$$H_z = 0 \tag{2.13}$$

$$E_\varrho = \frac{1}{j\omega\epsilon}\frac{\partial^2 \psi^m}{\partial \varrho\ \partial z} \tag{2.14}$$

$$E_\phi = \frac{1}{j\omega\epsilon\varrho}\frac{\partial^2 \psi^m}{\partial \phi\ \partial z} \tag{2.15}$$

$$E_z = \frac{1}{j\omega\epsilon}(\frac{\partial^2}{\partial^2 z} + k^2)\ \psi^m \tag{2.16}$$

for TE^z case ,

$$H_\varrho = \frac{1}{j\omega\mu}\frac{\partial^2 \psi^e}{\partial \varrho\ \partial z} \tag{2.17}$$

$$H_\phi = \frac{1}{j\omega\mu\varrho}\frac{\partial^2 \psi^e}{\partial \phi\ \partial z} \tag{2.18}$$

$$H_z = \frac{1}{j\omega\mu}(\frac{\partial^2}{\partial^2 z} + k^2)\ \psi^e \tag{2.19}$$

$$E_\varrho = -\frac{1}{\varrho}\frac{\partial \psi^e}{\partial \phi} \tag{2.20}$$

$$E_z = 0 \tag{2.21}$$

$$E_\phi = \frac{\partial \psi^e}{\partial \varrho} \tag{2.22}$$

In the scope of this thesis, we are only interested in the dominant mode that is excited by the slot on the ground plane. This mode is denoted by $HEM_{11\delta}$ and it is predominantly transverse magnetic, therefore, only the field expansion of TM to z direction (TM^z) are to be considered.

2.2.2 The Concept of Perfect Magnetic Conductor (PMC)

The electromagnetic waves inside the dielectric resonator can be viewed as a summation of plane waves, incident at all angles, upon the surface of the DR. Therefore, an understanding of the propagation properties of a plane wave in a dielectric medium with a high permittivity incident at an interface to a dielectric medium with a low dielectric constant will give a clear idea about the fields inside the DR as well as the concept of perfect magnetic wall PMC.

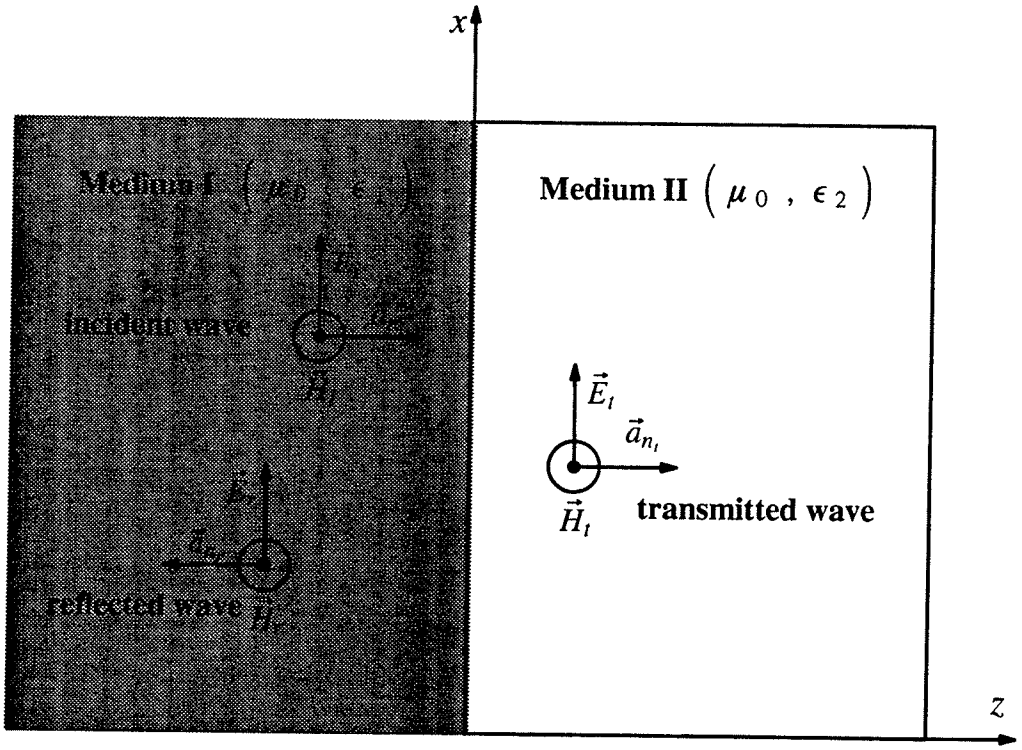

Figure 2.4 Plane wave incident to the interface of two dielectric Media

Consider a uniform plane wave normally incident upon a boundary surface that separates two different dielectric mediums as in Fig. 2.4. These mediums are denoted by medium I and medium II. The two mediums are characterized by (μ_o , ϵ_1) and (μ_o , ϵ_2), respectively, and they are assumed to be isotropic.

The incident wave (E_i, H_i) traveling in the positive z direction is given by,

$$\vec{E}_i = \vec{a}_x \, E_{io} \, e^{-j k_1 z} \tag{2.23}$$

$$\vec{H}_i = \vec{a}_y \, \frac{E_{io}}{n_1} \, e^{-j k_1 z} \tag{2.24}$$

where η_1 is the intrinsic impedance of medium I, $\eta_1 = \sqrt{\frac{\mu_0}{\epsilon_1}}$ (2.25)

and k_1 is the propagation constant of the medium I, $k_1 = \omega \sqrt{(\mu_o \, \epsilon_1)}$. (2.26)

E_{io} is the magnitude of E_i at $z = 0$. Due to the discontinuity at the interference between the two mediums, the incident wave is partly reflected back into medium I and partly transmitted into medium II. The reflected wave is defined by

$$\vec{E}_r = \vec{a}_x \, E_{ro} \, e^{j k_1 z} \tag{2.27}$$

$$\vec{H}_r = -\vec{a}_y \, \frac{E_{ro}}{n_1} \, e^{j k_1 z} \tag{2.28}$$

where E_{ro} is the magnitude of E_r at $z = 0$. The transmitted wave is defined by,

$$\vec{E}_t = \vec{a}_x \, E_{t0} \, e^{-j k_2 z} \tag{2.29}$$

$$\vec{H}_t = \vec{a}_y \, \frac{E_{t0}}{n_2} \, e^{-j k_2 z} \tag{2.30}$$

where E_{to} is the magnitude of E_t at $z = 0$. η_2 is the intrinsic impedance of the medium II, which is defined by $\eta_2 = \sqrt{\frac{\mu_0}{\epsilon_2}}$ (2.31)

and k_2 is the propagation constant of the medium II $k_2 = \omega \sqrt{(\mu_o \, \varepsilon_2)}$. (2.32)

At the dielectric interference, the tangential components of the electric field and the magnetic field intensities must be continuous as

$$E_{io} + E_{ro} = E_{to} \tag{2.33}$$

$$\frac{1}{\eta_1} \, (E_{io} - E_{ro}) = \frac{E_{to}}{\eta_2} \tag{2.34}$$

By arranging the two above equations, and using (2.25) and (2.31)

$$\Gamma = \frac{E_{ro}}{E_{io}} = \frac{\eta_2 - \eta_1}{\eta_2 + \eta_1} = \frac{1 - \sqrt{\frac{1}{\epsilon_r}}}{1 + \sqrt{\frac{1}{\epsilon_r}}} \tag{2.35}$$

$$\tau = \frac{E_{to}}{E_{io}} = \frac{2\,\eta_2}{\eta_2 + \eta_1} = \frac{\sqrt{\frac{1}{\epsilon_r}}}{1 + \sqrt{\frac{1}{\epsilon_r}}} \tag{2.36}$$

where Γ is the reflection coefficient and τ is the transmission coefficient. As ϵ_r increases, the value of the reflection coefficient Γ approaches unity while the transmission coefficient τ approaches zero.This can be demonstrated by

$$\lim_{\epsilon_r \to \infty} \Gamma = \lim_{\epsilon_r \to \infty} \frac{1 - \sqrt{\frac{1}{\epsilon_r}}}{1 + \sqrt{\frac{1}{\epsilon_r}}} = 1 \tag{2.37}$$

$$\lim_{\epsilon_r \to \infty} \tau = \lim_{\epsilon_r \to \infty} \frac{2\sqrt{\frac{1}{\epsilon_r}}}{1 + \sqrt{\frac{1}{\epsilon_r}}} = 0 \tag{2.38}$$

Consequentially, if medium I is of a high dielectric constant ϵ_r most of the incident wave propagating from medium I in the direction of medium II will be reflected back to medium I and only a small portion of it will be transmitted to medium II. Furthermore, as ϵ_r approaches infinity a total reflection of the incident energy is achieved at the boundary between medium I and medium II ($z = 0$). In circuit terminology, this boundary can be considered as an open circuit boundary condition. Thus, the surface of a medium with a very high permittivity can be assumed to be covered by a perfect magnetic conductor (PMC) which corresponds to an open circuit boundary condition.

2.2.3 The Magnetic Wall Model (Cavity Model)

In this model, the electromagnetic fields inside the DR are calculated by assuming that the surfaces of the DR are covered with a perfect magnetic conductor PMC as shown in Fig. 2.5. For this situation, the normal component of the electric field E_n and the tangential component of the magnetic field H_t are set to zero at all the surfaces of the DR.

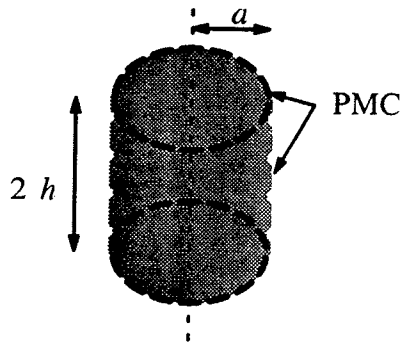

Figure 2.5 The cavity model for DR

Considering the TM^z mode, at the side surface of the DR :

$$E_p/_{\rho=a} = 0$$

and from (2.10) and either (2.12) or (2.14), the following is obtained

$$J'_m(k_p\ a) = 0 \qquad => \qquad k_p = \frac{x'_{mn}}{a} \qquad n = 1\ ,2\ ,\ 3\ \ldots . \qquad (2.39)$$

where $J'_m\ (x)$ is the derivative of the Bessel function of order m and x'_{mn} represents the n^{th} zeros of $J'_m\ (x)$. The index m defines the allowed azimuthal modes which are

$$\begin{cases} \cos(\ k_\phi\ \phi\ ) \\ \\ \sin(\ k_\phi\ \phi\ ) \end{cases} , \ k_\phi = m.$$

Similarly, at top and bottom surface of the DR

$$E_z/_{(z=\pm h)} = 0 \qquad \text{and} \qquad H_p/_{(z=\pm h)} = 0.$$

By using (2.10) and either (2.12) or (2.16), the following is obtained

$$A_z \cos(k_z h) = 0 \quad \Rightarrow \quad k_z = \frac{(2p+1)\pi}{2h}, \quad p = 0, 1, 2, 3\ldots \tag{2.40}$$

At $z = 0$, the presence of the ground plane required that the tangential electric field to be zero

$$E_\varrho/_{(z=0)} = 0 \qquad \Rightarrow \qquad B_z = 0 \tag{2.41}$$

Using 2.39–2.41, equation (2.10) can now be reduced to

$$\psi = A_{mnp} J_m(k_p \varrho) \cos(k_z z) \cos(k_\phi \phi) \tag{2.42}$$

where A_{mnp} is a normalization factor. Note that because of the orthogonality condition and the feed position at $\phi = 90^o$, only the $\cos(k_\phi \phi)$ term was chosen. Equation (2.8) can be also written as

$$k = \sqrt{\left(\frac{x'_{mn}}{a}\right)^2 + \left(\frac{\pi(2p+1)}{2h}\right)^2} \tag{2.43}$$

In this form, m indexes the azimuthal modes, n the radial modes and p the longitudinal modes. Then using (2.8), the resonant frequencies for the TM_{mnp} mode of the dielectric resonator becomes,

$$f_{mnp} = \frac{1}{2\pi\sqrt{\varepsilon\mu}} \sqrt{\left(\frac{x'_{mn}}{a}\right)^2 + \left(\frac{\pi(2p+1)}{2h}\right)^2} \tag{2.44}$$

The dominant mode is the one which has the lowest resonant frequency and also which can be supported by the slot on the ground plane of the microstrip line. As mentioned before, this is the $HEM_{11\delta}$ mode. Since $x'_{11} = 1.84118$ is the lowest value zero of the derivative of the Bessel function J'_1, the resonant frequency for the $HEM_{11\delta}$ mode using the cavity model is given by

$$f_{110} = \frac{1}{2\pi\sqrt{\varepsilon\mu}} \sqrt{\left(\frac{x'_{11}}{a}\right)^2 + \left(\frac{\pi}{2h}\right)^2} \tag{2.45}$$

where, $\varepsilon = \varepsilon_0 \varepsilon_{r_{DR}}$. In this nomenclature, the δ in the index is used rather than $p = 0$ to match the notation adopted when analyzing DR using numerical techniques or using dielec-

tric waveguide model for the DR. As mentioned in section 1.3 of Chapter 1, the two methods adopt the nomenclature notation to take into account the decays of the field outside DR along its axis of symmetry. All fields that correspond to this dominant mode inside the dielectric resonator cavity are obtained using (2.42) and (2.11)–(2.16), and they are given below as

$$E_\varrho = -\frac{1}{\hat{y}} k_p \; k_z \; J'_1(k_p \; \varrho) \cos(\phi) \sin(k_z z) \tag{2.46}$$

$$E_\phi = \frac{1}{\hat{y}\varrho} \; k_z \; J_1(k_\varrho \; \varrho) \sin(\phi) \sin(k_z z) \tag{2.47}$$

$$E_z = \frac{1}{\hat{y}} k_p^2 \; J_1(k_p \; \varrho) cos(\phi) \cos(k_z z) \tag{2.48}$$

$$H_\varrho = -\frac{1}{\varrho} J_1(k_p \; \varrho) \sin(\phi) \cos(k_z \; z) \tag{2.49}$$

$$H_\phi = -k_p \; J'_1(k_p \; \varrho) \cos(\phi) \cos(k_z \; z) \tag{2.50}$$

$$H_z = 0 \tag{2.51}$$

where $\left(\hat{y} = j\omega\varepsilon_0\varepsilon_{r_{DR}} \; , \; k_z = \frac{\pi}{2\,h} \text{ and } k_p = \frac{x'_{11}}{a} \right)$

Using this model, the surfaces of the DR are assumed to be perfect magnetic conductors. Therefore, the leakage fields outside the DR were not taken into consideration. This will result in an inaccurate determination of the characteristics of this antenna, especially when using dielectric resonators that have moderate values of permittivity, such as the one used in this thesis ($\epsilon_{r_{DR}} = 10.5$).

2.2.4 The Dual Dielectric Waveguide Model (DWM)

In this model, the dielectric resonator (DR) is assumed to be a truncated section of an infinite waveguide with the same dimensions as those of the DR. The fields in the radial direction inside the DR vary in the same fashion as those in an infinite dielectric waveguide, having the same radius a and dielectric constant $\epsilon_{r_{DR}}$ as that of the resonator. Furthermore,

the fields have a standing wave pattern in the axial direction similar to that of an infinite radial slab guide of the same height and dielectric constant as that of the resonator. This method was first developed by Marcatili [29] for analyzing the propagation characteristics of a rectangular dielectric waveguide and later by Itoh and Rudokas [30] for finding the resonant frequency of a cylindrical dielectric resonator excited in the $TE_{01\delta}$ mode (Note that in the $TE_{01\delta}$ mode, the electric and magnetic fields have no circumferential variation). Also, this method was used in conjunction with an the effective dielectric constant (EDC) by Mongia and Bhartia [31] for obtaining a more accurate result for the resonant frequency of the $TE_{01\delta}$ mode in cylindrical dielectric resonators. In this chapter the DWM method is extended to obtain the resonant frequency, the near field, the far field, and the radiated quality factor Q_{rad} of cylindrical dielectric resonators that are excited in the $HEM_{11\delta}$ mode.

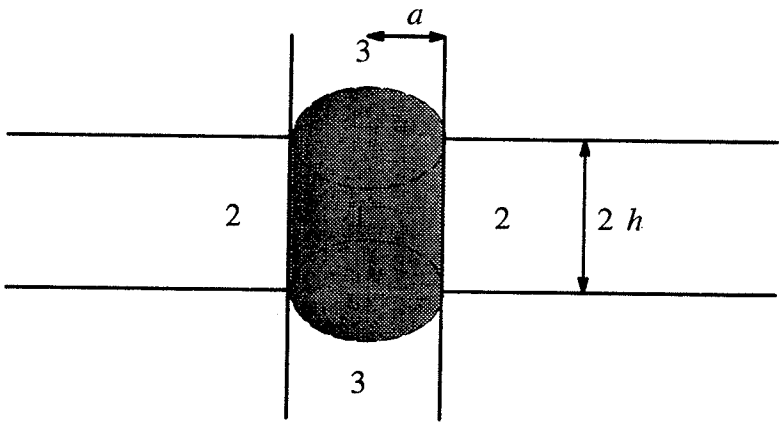

Figure 2.6 The regions of interest for analyzing the fields of DR using DWM

Fig. 2.6, shows the three regions of the dielectric resonator structure where the fields of interest will be determined. Region (1), which contains most of the electromagnetic energy has a standing wave pattern for its fields and regions (2) and (3) have fields that decay exponentially in the ρ and z directions, respectively. Using the same technique as for the case of the cavity model for the DR in the previous section, the scalar wave equation ψ in region (1), (2) and (3) are given by,

$$\psi = \begin{cases} A_1 J_1(k_p \varrho) \cos(k_z z) \cos(\phi) & \text{region (1)} \\ A_3 K_1(k_{p_o} \varrho) \cos(k_z z) \cos(\phi) & \text{region (2)} \\ A_2 J_1(k_p \varrho) e^{(-k_{z_o} z)} \cos(\phi) & \text{region (3)} \end{cases} \quad (2.52)$$

k_p, k_z, k_{p_o}, and k_{z_o} are related to each other by the following characteristics equation,

$$k^2 = k_z^2 + k_p^2 \quad (2.53)$$

$$k_{p_o}^2 = k_z^2 - k_o^2 \quad (2.54)$$

$$k_p^2 = k_{z_0}^2 + k_o^2 \quad (2.55)$$

where $$k_o = \omega_o \sqrt{(\mu_o \epsilon_o)}$$

J_1 and K_1 are the Bessel and the modified Hankel function of order one, respectively, ω_o is the angular resonant frequency. Using equations (2.11)–(2.16), all the fields components of regions (1)–(3) can be derived. Note that, the fields of region 1 (inside the DR) have the same form as those found using the cavity model, but with a different wave number. The new value of k is specified by the values of k_p and k_z , which must be determined.

The problem of determining the resonant frequency, the fields, and the radiated quality factor of the $HEM_{11\delta}$ mode in a cylindrical dielectric resonators is now reduced to the problem of finding the values of the radial and axial wave numbers k_p and k_z , which satisfy the characteristics equation (2.53). These wavenumbers will be solved for using a dual dielectric waveguide model as will be formulated next. In this model the continuity of fields at the interface between the resonator region (1) and region (2) and at interface between region (1) and (3) are used to form a set of equations that can be used to solve for k_p and k_z . The only approximation to the model is the discontinuity of fields in the region outside of (1), (2), and (3).

2.2.4.1 Radial Wave Number k_p estimate

The radial wave number k_p of the $HEM_{11\delta}$ mode in a cylindrical dielectric resonator will be determined by assuming that it is the same as that of HEM_{11} mode in an infinitely cylindrical dielectric waveguide of radius a and of dielectric constant $\epsilon_{r_{DR}}$ as shown in Fig. 2.7.

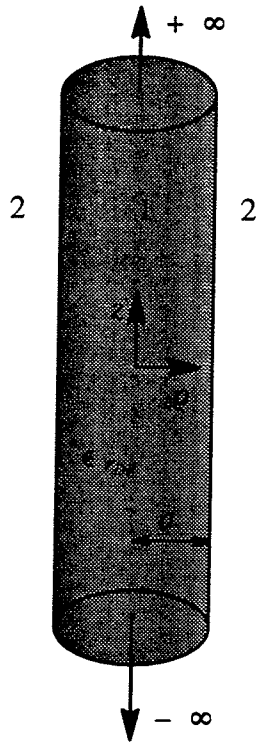

Figure 2.7 Infinite cylindrical waveguide model

The fields of the HEM_{11} mode in an infinite cylindrical dielectric waveguide are the sum of the TE_{11} fields and of the TM_{11} fields in the same waveguide.The scalar wave function ψ for TE_{11} and TM_{11} modes of the waveguide shown in Fig. 2.7 can be derived using the steps outlined in section (2.2.1). For this case, an electromagnetic wave propagating in the positive z direction of the infinite cylindrical dielectric waveguide will have a standing wave pattern inside the waveguide, while decaying outside in the ϱ direction. The scalar wave functions ψ^m and ψ^e will have the following forms in regions 1 and 2.

Inside the waveguide, region 1 ($\varrho \leq a$)

$$\psi_i^m = A_1 \, J_1(\, k_p \, \varrho \,) \cos(\, \phi \,) \, e^{(-j k_z z)} \tag{2.56}$$

$$\psi_i^e = A_2 \, J_1(\, k_p \, \varrho \,) \sin(\, \phi \,) \, e^{(-j k_z z)} \tag{2.57}$$

where,
$$k^2 = k_z^2 + k_p^2 \, . \tag{2.58}$$

Outside the waveguide, region 2 ($\varrho \geq a$)

$$\psi_o^m = B_1 \, K_1(\, k_{p_o} \, \varrho \,) \cos(\, \phi \,) \, e^{(-j k_z z)} \tag{2.59}$$

$$\psi_o^e = B_2 \, K_1(\, k_{p_o} \, \varrho \,) \sin(\, \phi \,) \, e^{(-j k_z z)} \tag{2.60}$$

where,
$$k_{p_o}^2 = k_{z_0}^2 + k_0^2 \, . \tag{2.61}$$

Substituting (2.56)–(2.57) into (2.17)–(2.22) for the TE_{11} mode and into (2.11)–(2.16) for TM_{11} mode, and then adding the corresponding fields components, the following HEM_{11} fields components inside the waveguide ($\varrho \leq a$) are obtained:

$$E_{z_i} = \frac{A_1 \, k_p^2}{\hat{y}} \, J_1(\, k_p \, \varrho) \cos(\phi) \, e^{(-j k_z z)} \tag{2.62}$$

$$E_{\varrho_i} = \left(\frac{(-jk_z k_p A_1)}{\hat{y}} J_1'(k_p \, \varrho) - \frac{A_2}{\varrho} \, J_1(k_p \, \varrho) \right) \cos(\phi) e^{(-jk_z z)} \tag{2.63}$$

$$E_{\phi_i} = \left(\frac{jk_z A_1}{\hat{y} \, \varrho} J_1(k_p \varrho) + (k_p A_2) J_1'(k_p \, \varrho) \right) \, sin(\phi) e^{(-jk_z z)} \tag{2.64}$$

$$H_{z_i} = \frac{A_2 \, k_p^2}{\hat{z}} \, J_1(\, k_p \, \varrho) \sin(\phi) \, e^{(-j k_z z)} \tag{2.65}$$

$$H_{\varrho_i} = \left(-\frac{A_1}{\varrho} J_1(k_p \, \varrho) - \frac{(\, jk_z k_p A_2)}{\hat{z}} \, J_1'(k_p \, \varrho) \right) \, sin(\phi) \, e^{(-jk_z z)} \tag{2.66}$$

$$H_{\phi_i} = \left(-A_1 k_p \, J_1'(k_p \varrho) - \frac{(jk_z A_2)}{\varrho \hat{z}} \, J_1(k_p \, \varrho) \right) \cos(\phi) e^{(-jk_z z)} \tag{2.67}$$

Outside the waveguide region 2 ($\varrho \geq a$) the following field components are obtained:

$$E_{z_o} = \frac{-B_1 \; k_{p_o}^2}{\hat{y}} \; K_1(\; k_{p_o} \varrho) \cos(\phi) \; e^{(-j\, k_z\, z)} \tag{2.68}$$

$$E_{\varrho_o} = \left(\frac{(-jk_z k_{p_o} B_1)}{\hat{y_o}} K_1'(k_{p_o}\varrho) - \frac{B_2}{\varrho} \; K_1(k_{p_o}\; \varrho) \right) \cos(\phi) \; e^{(-jk_z\, z)} \tag{2.69}$$

$$E_{\phi_o} = \left(\frac{jk_z B_1}{\hat{y}\; \varrho} K_1(k_{p_o}\; \varrho) + (k_{p_o} B_2) K_1'(k_{p_o}\; \varrho) \right) sin(\phi) \; e^{(-jk_z z)} \tag{2.70}$$

$$H_{z_o} = \frac{-B_2 \; k_{p_o}^2}{\hat{z_o}} \; K_1(\; k_{p_o} \varrho) \sin(\phi) \; e^{(-j\, k_z\, z)} \tag{2.71}$$

$$H_{\varrho_o} = \left(-\frac{B_1}{\varrho} K_1(k_{p_o}\; \varrho) - \frac{(\; jk_z k_{p_o} B_2)}{\hat{z}} \; K_1'(k_{p_o}\; \varrho) \right) sin(\phi) \; e^{(-j\, k_z\, z)} \tag{2.72}$$

$$H_{\phi_o} = \left(-A_1 k_{p_o} \; K_1'(k_{p_o}\varrho) - \frac{(jk_z B_2)}{\varrho \; \hat{z}} K_1(k_{p_o}\; \varrho) \right) \cos(\phi) \; e^{(-jk_z\, z)} \tag{2.73}$$

where, $\hat{z} = \hat{z}_0 = j\omega\mu_0$, $\hat{y} = j\omega\epsilon_0 \varepsilon_{r_{DR}}$ and $\hat{y}_0 = j\omega\epsilon_0$. By enforcing the tangential components of the fields to be continuous across the surfaces of the waveguide at $\varrho = a$,

$$E_{z_i} = E_{z_o} \tag{2.74}$$

$$H_{z_i} = H_{z_o} \tag{2.75}$$

$$E_{\phi_i} = E_{\phi_o} \tag{2.76}$$

$$H_{\phi_i} = H_{\phi_o} \; . \tag{2.77}$$

Finally, by substituting (2.62)–(2.67) and (2.68)–(2.70) into (2.74)–(2.77), the following system of equations is obtained

$$\begin{cases} A_1 k_p^2 J_1(k_p a) + B_1 \varepsilon_{r_{DR}} \; k_{p_o}^2 \; K_1(\; k_{p_0} a \;) = 0 \\ \\ A_2 k_p^2 J_1(k_p a) + \; B_2 k_{p_o}^2 K_1(k_{p_0} a \;) = 0 \\ \\ \dfrac{A_1 k_z}{a\omega\epsilon} J_1(k_p a) + A_2 k_p \; J_1'(k_p a) - \dfrac{B_1 k_z}{\omega\varepsilon_o a} K_1(k_{p_o}\; a) - B_2 k_{p_o} \; K_1'(k_{p_o}\; a) = 0 \\ \\ A_1 k_p J_1'(k_p a) + \dfrac{A_2 k_z}{\omega\mu a} J_1(k_p a) - B_1 k_{p_o} K_1'(k_{p_o} a) - \dfrac{B_2 k_z}{\omega\mu a} K_1(k_{p_o}\; a) = 0 \end{cases} \tag{2.78}$$

Equation (2.81) can also be written in matrix form as,

$$\underline{A}\ \underline{X} = \underline{0} \tag{2.79}$$

where,

$$\underline{A} = \begin{bmatrix} k_p^2 J_1(k_p a) & 0 & \varepsilon_{r_{DR}} k_{p_o}^2 K_1(k_{p_o} a) & 0 \\ 0 & k_p^2 J_1(k_p a) & 0 & k_{p_o}^2 K_1(k_{p_o} a) \\ \frac{k_z}{a\omega\epsilon} J_1(k_p a) & k_p J_1'(k_p a) & \frac{-k_z}{\omega \epsilon_o a} K_1(k_{p_o} a) & -k_{p_o} K_1'(k_{p_o} a) \\ k_p J_1'(k_p a) & \frac{k_z}{\omega \mu a} J_1(k_p a) & -k_{p_o} K_1'(k_{p_o} a) & \frac{-k_z}{\omega \mu a} K_1(k_{p_o} a) \end{bmatrix}$$

and,

$$\underline{X} = \begin{bmatrix} A_1 \\ A_2 \\ B_1 \\ B_2 \end{bmatrix}$$

The matrix equation (2.79) has a nontrivial solution if and only if the determinant of its matrix is equal to zero.

$$\det(\underline{A}) = 0 \tag{2.80}$$

thus yield a mode equation in terms of k_p and k_z. By expanding the determinant of the matrix A in term of the element of its first row, equation (2.80) can be written as

$$\left(k_p^2\, J_1(k_p\, a)\right)^2 \left(\frac{k_z^2}{(\omega\ a)^2\ \mu\ \epsilon_o}\ K_1^2(k_{p_o}a) - k_{p_o}^2\ K_1'^2(\ k_{p_o}a) \right)$$

$$+ \left(k_p^2\ k_{p_o}^2 J_1(k_p a) K_1(k_{p_o}a)\right)\left(- k_p k_{p_o} J_1'(k_p a)\ K_1'(k_{p_o}a) + \frac{k_z^2}{(\omega\ a)^2\ \mu\epsilon_{\ o}} J_1(k_p a)\ K_1(k_{p_o}a) \right)$$

$$- \left(\frac{\varepsilon_{r_{DR}}\ k_z\ k_{p_o}^2}{a\ \omega\ \epsilon}\ J_1(k_p a)\ K_1(k_{p_o}a) \right) \left(\frac{-k_p^2\ k_z}{\omega\mu a} J_1(k_p a)\ K_1(k_{p_o}a) - \frac{k_{p_o}^2\ k_z}{\omega\ a\ \mu} J_1(k_p a)\ K_1(k_{p_o}a) \right)$$

$$+ \left(\varepsilon_{r_{DR}}\ k_p k_{p_o}^2 J_1'(k_p a) K_1(k_{p_o}a)\right)\left(- k_p^2 k_{p_o} J_1(k_p a) K'_1(k_{p_o}a) - k_{p_o}^2 k_p J'_1(k_p a) K_1(k_{p_o}a) \right) = 0\ . \quad (2.81)$$

2.2.4.2 Axial Wave Number k_z estimate

The axial wave number k_z of the $HEM_{11\delta}$ mode in the cylindrical dielectric resonator is calculated by assuming that it is same as that of the TM_{01} mode in a dielectric slab waveguide. For this case the dielectric slab is of height $2\ h$ and of permittivity $\epsilon_{\ r_{DR}}$ as shown in Fig. 2.8.

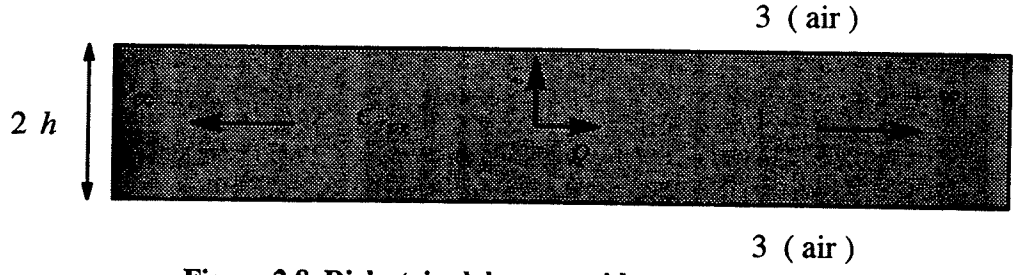

Figure 2.8 Dielectric slab waveguide

Again, using the steps outlined in section (2.2.1), the scalar wave function ψ^m of the TM_{01} mode for an electromagnetic wave propagating in ϱ direction in a dielectric slab waveguide is of the following forms in region 1 and 3.

In the dielectric region ($1 - h \leq z \leq h$) :

$$\psi_i^m = A \cos(k_z z) e^{(-j k_p \varrho)} \tag{2.82}$$

where,

$$k^2 = k_z^2 + k_p^2 \tag{2.83}$$

In air region 3 $| z | \geq h$:

$$\psi_o^m = B e^{-k_{z_0}|z|} e^{(-j k_p \varrho)} \tag{2.84}$$

where,

$$k_p^2 = k_{z_0}^2 + k_0^2 \tag{2.85}$$

Thus, using(2.11) and (2.16), the fields components inside the dielectric slab guide $-h \leq z \leq h$ are given by

$$H_{\phi_i} = j A k_p \cos(k_z z) e^{(-j k_p \varrho)} \tag{2.86}$$

$$E_{\varrho_i} = j \frac{A k_z k_p}{j\omega\epsilon} \sin(k_z z) e^{(-j k_p \varrho)} \tag{2.87}$$

$$E_{z_i} = A \frac{k_p^2}{j\omega\epsilon} \cos(k_z z) e^{(-j k_\varrho \varrho)} \tag{2.88}$$

whereas, those outside the dielectric waveguide ($z \geq h$ or $z \leq -h$) are given by

$$H_{\phi_o} = jBk_p e^{-k_{z_0}|z|} e^{(-j k_\varrho \varrho)} \tag{2.89}$$

$$E_{\varrho_o} = j sgn B \frac{k_{z_o} k_p}{j\omega\epsilon} e^{-k_{z_0}|z|} e^{(-j k_\varrho \varrho)} \tag{2.90}$$

$$E_{z_o} = B sgn \frac{k_{p_o}^2}{j\omega\epsilon} e^{-k_{z_0}|z|} e^{(-j k_\varrho \varrho)} \tag{2.91}$$

where,

$$sgn = \begin{cases} 1 & z > h \\ -1 & z < -h \end{cases} .$$

At $z = \pm\ h$, continuity of the tangential field components E_ϱ and H_ϕ requires that

$$A\ k_z\ \sin(\ k_z\ h\ ) = \epsilon_{r_{DR}}\ k_{z_0}\ B\ e^{(-k_{z_0} h)} \tag{2.92}$$

$$A\ \cos(\ k_z\ h\ ) = B\ e^{(-k_{z_0} h)}\ . \tag{2.93}$$

By taking the ratio of (2.92) and (2.93) a mode equation in term of k_z is determined.

$$\tan(\ k_z\ h\ ) = \frac{k_{z_0}\ \epsilon_{r_{DR}}}{k_z} \tag{2.94}$$

The waves numbers k_z, k_p and k_0 of the dielectric resonator excited in $HEM_{11\delta}$ can now be determined by solving the system of equations consisting of (2.53), (2.81), and (2.94). This can be accomplished numerically by first approximating the values of the wave numbers using the values obtained from the cavity model. Then, by employing a suitable iterative procedure that solves for non–linear equations, such as Newton's method, to determine these wave numbers using DWM model fo the DR.

2.3 Numerical Computation of Dielectric Resonator Properties

The resonant frequency, near– and far– fields and the radiated quality factor of an isolated (DR), as shown in Fig. 2.2, can be found numerically using the surface Integral equation formulation and the method of moments solution technique [20,21]. The feed structure for the DR antenna under investigation is usually modelled by a magnetic dipole inside the DR whose orientation is along the direction of the slot. In this section we will mainly concentrate on determining the resonant frequencies of the DR structure. The surface integral equation is used to formulate the problem by writing the unknown surface current in an integral equation in terms of the known quantities such as the tangential fields at the boundary surfaces of the DR. The method of moment [37] transforms the obtained integral equation into a matrix equation that can be solved using a digital computer. This technique is discussed briefly in this section. The obtained matrix equation has the following general form,

$$T_n \cdot I_n = V_n \quad ; \quad n = 0 , \pm 1 , \pm 2 , \ldots . \qquad (2.95)$$

T_n is the square matrix that represents the moment matrix and it depends only on the geometry of the DR, frequency, and the dielectric constant of the DR.

I_n is the column for the unknown expansion coefficient of the electric and magnetic surface currents.

V_n is the excitation vector that depends only on the equivalent magnetic dipole.

The resonant frequencies are defined as the frequencies for which the system can have a response with no excitation, therefore, equation (2.95) becomes

$$T_n \cdot I_n = 0 \quad ; \quad n = 0 , \pm 1 , \pm 2 , \ldots . \qquad (2.96)$$

The resonant frequencies of the dielectric resonator are then obtained by finding the zeros of the determinant of the matrix T_n in the complex frequency plane

$$\det\left(T_n \right) = 0 \qquad (2.97)$$

The solution of equation (2.97) is given by

$$r_{mn} = -\sigma_{mn} \pm j\omega_{mn} \qquad (2.98)$$

where ω_{mn} is the resonant frequency of the mode $\left(m , n\right)$ and σ_{mn} is the decay time constant

of the same mode$(m\ ,n)$. Kishk et. al. [21] used this technique to find the resonant frequencies of dielectric resonator with dielectric constant $\varepsilon_{r_{DR}} = 38$. The DR was excited by $HEM_{11\delta}$ mode for various ratios of the radius to the height $\frac{a}{h}$. with a curve fitting procedure applied to the numerical results, they obtained an expression for the resonant frequency for $\varepsilon_{r_{DR}} = 38$ as

$$k_0\ a = 0.27 + 0.36\left(\frac{a}{h}\right) + 0.02\left(\frac{a}{h}\right)^2 . \tag{2.99}$$

The resonant frequency f can then calculated using

$$f = \frac{k_0\ c}{2\pi} \tag{2.100}$$

2.3.1 Empirical Resonant Frequency Formula

Building on the numerical results of Kishk [21], Mongia developed a general formula for the DR resonant frequency valid for a wide range of $\varepsilon_{r_{DR}}$ [26].

For a dielectric resonator with a high permittivity $\varepsilon_{r_{DR}} \gtrsim 100$, the resonant frequency is proportional to the square roots of the the dielectric constant $\epsilon_{r_{DR}}$ [33] as,

$$f \propto \frac{1}{\sqrt{\varepsilon_{r_{DR}}}} \tag{2.101}$$

For moderate values of $\varepsilon_{r_{DR}}$ the resonant frequency is reported to be proportional approximately to the square root of $(\varepsilon_{r_{DR}} + X)$ [26]

$$f \propto \frac{1}{\sqrt{\varepsilon_{r_{DR}} + X}} \tag{2.102}$$

The value of X depends on the mode of excitation for the DR with $X = 2$ for the $HEM_{11\delta}$ mode. By combining the accurate numerical equation (2.99) of the resonant frequency for $\varepsilon_{r_{DR}} = 38$ and the approximate equation (2.102), Mongia [26] proposed the following equation for the resonant frequency in term of the ratio $\frac{a}{h}$ and $\epsilon_{r_{DR}}$:

$$k_0\, a = \frac{2\pi f_o\, a}{c} = \frac{6.324}{\sqrt{\varepsilon_{r_{DR}} + 2}} \left(0.27 + \left(0.18\, \frac{a}{h} \right) + 0.005 \left(\frac{a}{h} \right)^2 \right) \qquad (2.103)$$

This equation is valid only for a moderate values of $\epsilon_{r_{DR}}$ and in the range of $0.4 \leq \frac{a}{h} \leq 5$.

Using this method, the resonant frequency of the $HEM_{11\delta}$ mode can then be obtained directly using (2.100).

2.3.2 Comparison of Resonant Frequency Models

In this section the computed results for the resonant frequency of a dielectric resonator antenna excited in the $HEM_{11\delta}$ mode using the dual dielectric waveguide model for the DR are compared to the results using equation (2.103) and also to the results using the magnetic wall model for the same DR.

Table 2.1 Resonant frequency of $HEM_{11\delta}$ mode of an isolated DR versus a / h

h = 0.46 cm , $\epsilon_{r_{DR}} = 38$

a / h	Resonant Frequency (GHz)		
	Waveguide Model (DWM)	Mongia formula	Cavity Model (MWM)
0.6	6.679	6.565	5.800
1.0	4.503	4.719	4.072
1.4	3.694	3.939	3.447
1.6	3.468	3.700	3.276
1.8	3.302	3.516	3.154
2.2	3.098	3.253	2.994
2.4	3.000	3.158	2.941
2.8	2.883	3.012	2.865
3.0	2.838	2.955	2.837
3.4	2.766	2.866	2.795

Table 2.1 shows the calculated resonant frequencies for a DR with $\varepsilon_{r_{DR}} = 38$, $h = 0.46\ cm$ and with various diameter using the cavity model (section (2.2.3)) , the proposed dual dielectric waveguide model (section (2.2.4)), and Mongia's formula (2.103). Note that in the case of $\epsilon_{r_{DR}} = 38$ Mongia's formula is same as the numerical formulas (2.99). Table 2.2 shows the same for a DR with $\epsilon_{r_{DR}} = 22$. By examining both tables, it can be seen that for most cases, the results of the resonant frequency using DWM differs only 4–6 % from Mongia's formula while the results of the MWM differ by about 10–12%. Results for the computed resonant frequency of the DR, with $\epsilon_{r_{DR}} = 38$ and 22 are also plotted respectively in Fig. 2.9 and 2.10.

Table 2.2 Resonant frequency of $HEM_{11\delta}$ mode of an isolated DR versus a / h
h = 0.46 cm , $\epsilon_{r_{DR}} = 22$

	Resonant Frequency (GHZ)		
a / h	Waveguide Model (DWM)	Mongia formula	Cavity Model (MWM)
0.6	8.601	8.475	7.623
1.0	5.849	6.092	5.352
1.4	4.802	5.080	4.530
1.6	4.504	4.776	4.306
2.0	4.113	4.351	4.026
2.4	3.898	4.077	3.865
3.0	3.738	3.816	3.729
3.4	3.587	3.701	3.674

The dual waveguide model developed in this thesis performs much better than the cavity model and yields reasonable agreement to the numerical method.

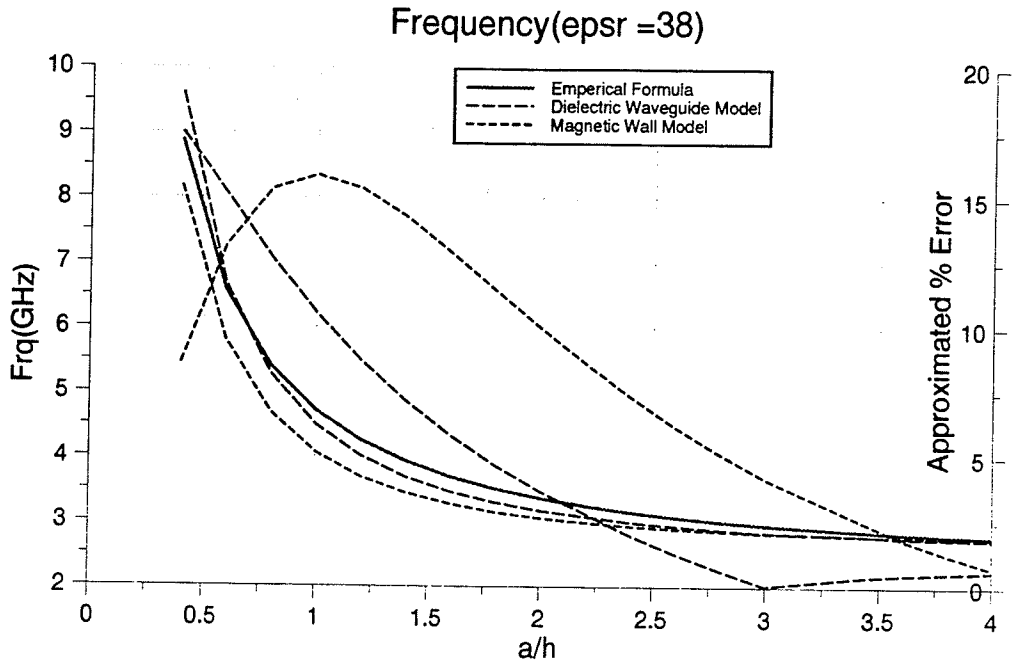

Figure 2.9 **Resonant frequency of $HEM_{11\delta}$ mode of an isolated DR versus a / h**
h = 0.46 cm , $\epsilon_{r_{DR}} = 38$

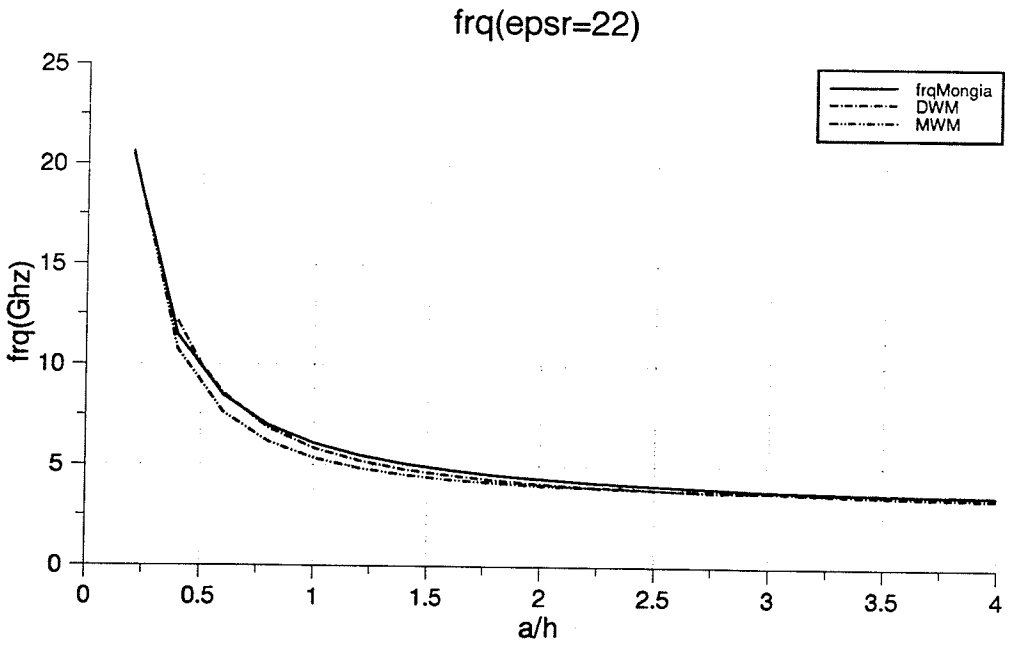

Figure 2.10 **Resonant frequency of $HEM_{11\delta}$ mode of an isolated DR versus a / h**
h = 0.46 cm , $\epsilon_{r_{DR}} = 22$

2.4 Field Computation for a Dielectric Resonator excited in its Dominant Mode

The calculation of the near and far fields for the dielectric resonator antenna excited in the dominant $HEM_{11\delta}$ mode will be based on applying the field equivalence principle [28]. The equivalence principle equates the fields at the surface of the DR with its equivalent electric J_s and magnetic $M_s$surface currents. The fields at the surface of the DR are calculated from the field expressions inside the DR. Once the equivalents sources J_s M_s are determined, they are in turn used to calculate the fields outside the DR at any observation location.With the cavity model, S.A.Lang [11] used this method to find the radiation pattern of a DR antenna positioned on a ground plane and excited by an electric probe. In this theses, the equivalent principle method will be used to find the near field and the far field of an isolated dielectric resonator, which is modelled first by the cavity model and then by the dielectric waveguide model.

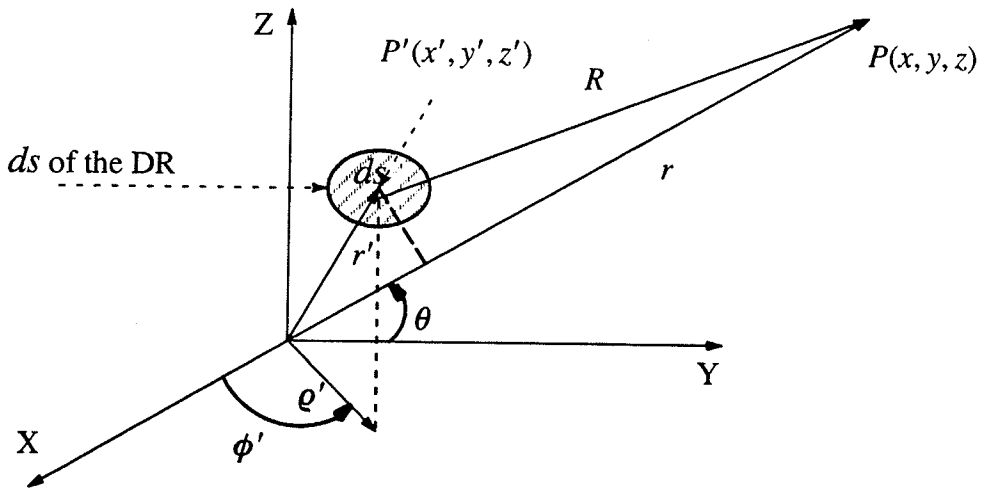

Figure 2.11 Coordinates system for the calculated fields

Referring to Fig. 2.11, the total electric $\vec{E_T}$ and magnetic $\vec{H_T}$ fields at point in free space $P(x, y, z)$ can be formulated in terms of the surface electric $\vec{J_s}$ and magnetic currents $\vec{M_s}$on the DR surface dS are by the following [28]

$$\vec{E_T} = \vec{E}_F + \vec{E}_A = -j\omega\vec{A} - \frac{j}{\omega\mu\varepsilon}\nabla(\nabla \cdot \vec{A}) - \frac{1}{\epsilon}\nabla \times \vec{F} \tag{2.104}$$

$$\vec{H_T} = \vec{H}_F + \vec{H}_A = -j\omega\vec{F} - \frac{j}{\omega\mu\varepsilon}\nabla(\nabla \cdot \vec{F}) + \frac{1}{\mu}\nabla \times \vec{A} \tag{2.105}$$

Here,

$$\vec{F} = \frac{\varepsilon_o}{4\pi}\int\int \vec{M}_s\, G(R/R')\, dS \tag{2.106}$$

$$\vec{A} = \frac{\mu_o}{4\pi}\int\int \vec{J}_s\, G(R/R')\, dS \tag{2.107}$$

are the vector electric and magnetic potentials, respectively.

$G(R/R')$ is the Green's function for free space and is defined by

$$G(R/R') = \frac{e^{-j k_0 R}}{R} \tag{2.108}$$

where R is the distance between an observation point $P(x, y, z)$ in free space and a source point $P'(x', y', z')$ located on the surface of the dielectric resonator as in Fig. 2.11. The distance R is given by

$$R = \left| r - r' \right| = \sqrt{(x-x')^2 + (y-y')^2 + (z-z')^2}\ . \tag{2.109}$$

2.4.1 Formulation of Equivalent Surface Currents :

The equivalent electric $\vec{J}_s$ and magnetic $\vec{M}_s$ surface currents are determined from the field expressions that were developed using the cavity model or the waveguide model. Once the fields just at the surface of the resonator are known, the surface currents densities are given by [28]

$$\vec{M} = \vec{E} \times \vec{n} \tag{2.110}$$

$$\vec{J} = \vec{n} \times \vec{H} \tag{2.111}$$

Here $\vec{n}$ is the unit normal vector pointing out of the surface of the dielectric cylindrical resonator, and $\vec{E}$ and $\vec{H}$ are the electric and magnetic fields, respectively, at the surface of the DR.

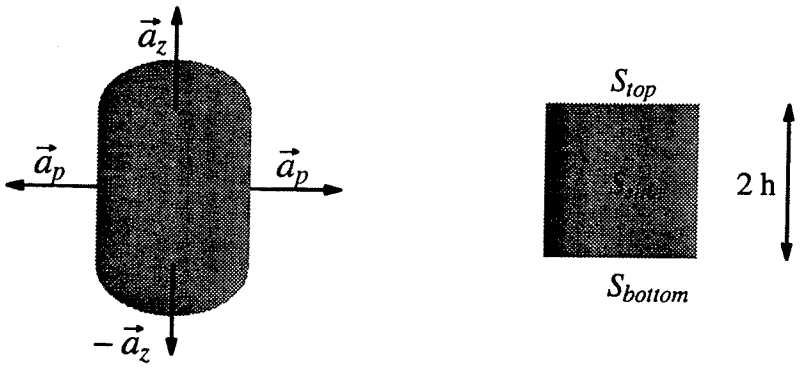

Figure (2.12) Surfaces of the DR and their corresponding normal vectors

As shown in Fig. 2.12, the surface of the dielectric resonator is divided into three sections; the top section, the bottom section, and the side section. By using equations (2.110) and (2.111) the surface currents for each section of the DR are formulated as below.

At the surface side $\varrho = a$ with $\vec{n} = \vec{a}_p$, equations (2.110) and (2.111) become

$$\vec{M} = \vec{E} \times \vec{a}_p = \left(E_p\ \vec{a}_p + E_\phi\ \vec{a}_\phi + E_z\ \vec{a}_z\right) \times \vec{a}_p = -E_\phi\ \vec{a}_z + E_z\ \vec{a}_\phi \qquad (2.112)$$

$$\vec{J} = \vec{a}_p \times \vec{H} = \vec{a}_p \times \left(H_p\ \vec{a}_p + H_\phi\ \vec{a}_\phi + H_z\ \vec{a}_z\right) = H_\phi\ \vec{a}_z - H_z\ \vec{a}_\phi\ . \qquad (2.113)$$

Substituting (2.46) –(2.51) into (2.112)–(2.113), the following is then obtained

$$M_p = 0 \qquad (2.114)$$

$$M_\phi = E_z = \frac{1}{\hat{y}} k_p^2\ J_1(k_p\ a) cos(\phi) \cos(k_z z) \qquad (2.115)$$

$$M_z = -E_\phi = -\frac{1}{\hat{y}\varrho}\ k_z\ J_1(k_\varrho\ a) \sin(\phi) \sin(k_z z) \qquad (2.116)$$

$$J_p = 0 \qquad (2.117)$$

$$J_\phi = -H_z\ = 0 \qquad (2.118)$$

$$J_z = H_\phi = -k_p\ J'_1(k_p\ a) \cos(\phi) \cos\left(k_z\ z\right) \qquad (2.119)$$

At the top–bottom surfaces of the DR, $z = \pm\ h$ with $\vec{n} = \pm\ \vec{a}_z$ (Note the (+) sign is for the top of the DR while the (–) sign is for the bottom side of the DR) equations (2.110) and (2.111) become

$$\vec{M} = \vec{E} \times \pm\, \vec{a}_z = \left(E_p\, \vec{a}_p + E_\phi\, \vec{a}_\phi + E_z\, \vec{a}_z\right) \times \pm\, \vec{a}_z$$

$$= \pm \left(-E_p\, \vec{a}_\phi + E_\phi\, \vec{a}_p\right) \tag{2.120}$$

$$\vec{J} = \pm\, \vec{a}_z \times \vec{H} = \pm\, \vec{a}_z \times \left(H_p\, \vec{a}_p + H_\phi\, \vec{a}_\phi + H_z\, \vec{a}_z\right)$$

$$= \pm \left(H_p\, \vec{a}_\phi - H_\phi\, \vec{a}_p\right) \tag{2.121}$$

Substituting (2.46)–(2.51) into (2.120)–(2.121), the following is then obtained

$$M_z = 0 \tag{2.122}$$

$$M_p = E_\phi = \frac{1}{\hat{y}\varrho}\; k_z\; J_1(k_\varrho\; a) \sin(\phi) \sin(k_z z) \tag{2.123}$$

$$M_\phi = -E_\varrho = \frac{1}{\hat{y}} k_p\; k_z\; J'_1(k_p\; \varrho) \cos(\phi) \sin(k_z z) \tag{2.124}$$

$$J_z = 0 \tag{2.125}$$

$$J_p = \pm\; -H_\phi = \pm\; k_p J'_1(k_p\; \varrho) \cos(\phi) \cos\left(k_z\; z\right) \tag{2.126}$$

$$J_\phi = \pm\; H_\varrho = \pm\; -\frac{1}{\varrho} J_1(k_p\; \varrho) \sin(\phi) \cos\left(k_z\; z\right) \tag{2.127}$$

Now that the surface currents are specified, the near and far fields can be determined using (2.104 – 2.107).

2.4.2 Calculation of the Far Field

Having calculated all the equivalent surfaces currents components for the DR, the radiated far fields can be found using 2.104 and 2.105 along with an expression for the approximated expression for the free space Green's function. In the far region, the magnitude of the distance R in the Green's function expression (2.108) is approximated by $r = \left|\vec{r}\right|$, whereas the phase term is given by $R \simeq r - \vec{r} \cdot \vec{r'}$

In cylindrical coordinates

$$\vec{r} \cdot \vec{r'} = \varrho' \sin(\theta) \cos(\phi - \phi') + z' \cos(\theta) \tag{2.128}$$

Therefore, in the far field ($|\vec{r}| \gg |\vec{r}\,'|$) the Green's function in free space becomes

$$G(R/R') \simeq \frac{e^{-j k_0 r}}{r} e^{j k_0 \left(\varrho' \sin(\theta) \cos(\phi - \phi') + z' \cos(\theta)\right)} \tag{2.129}$$

In the far field, the radiated vector fields $\vec{E}$ and $\vec{H}$, in a spherical coordinate system, have only θ and ϕ components, which are expressed as

$$E_\theta = -j \mu \omega A_\theta - j k_0 F_\phi \tag{2.130}$$

$$E_\phi = -j \mu \omega A_\phi + j k_0 F_\theta \tag{2.131}$$

$$H_\theta = -\frac{E_\phi}{\eta_0} \tag{2.132}$$

$$H_\phi = \frac{E_\theta}{\eta_0} \tag{2.133}$$

where η_0 the intrinsic impedance of the free space, $\eta_0 = \sqrt{\frac{\mu_0}{\epsilon_0}} \cong 377$ (ohms).

A_θ, A_ϕ, F_θ and F_ϕ are the θ and ϕ spherical components of the electric and magnetic vector potentials, respectively, and are obtained from equations (2.106) and (2.107).

Using the developed equation's for the calculation of the far field, two computer codes were developed in Fortran 77 to find the radiated far field in the two principal planes (E–plan and H–plane) of an isolated dielectric resonator. One program uses the surface fields generated using the magnetic wall model (MWM) for the DR, while the other uses the dual dielectric waveguide model (DWM). The E–plane pattern is obtained by fixing the angle $\phi = 0^o$ and calculating E_θ as a function of θ. The H–plane pattern is obtained by fixing the angle $\phi = 90^o$ while calculating E_ϕ as a function of θ.

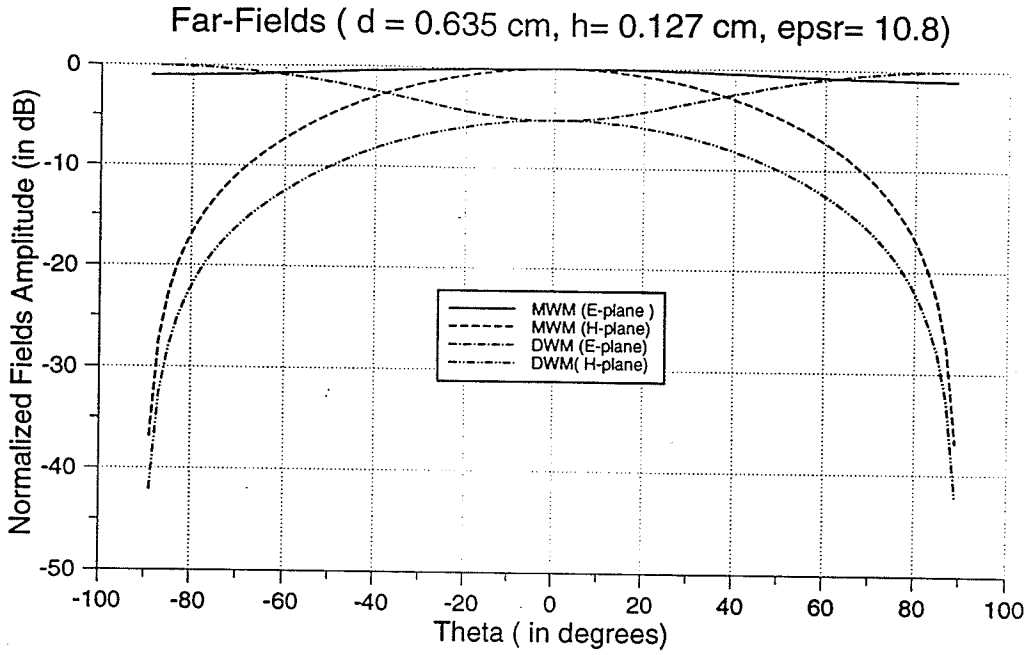

Figure 2.13 Radiated pattern of the $HEM_{11\delta}$ mode of a DR using MWM and DWM

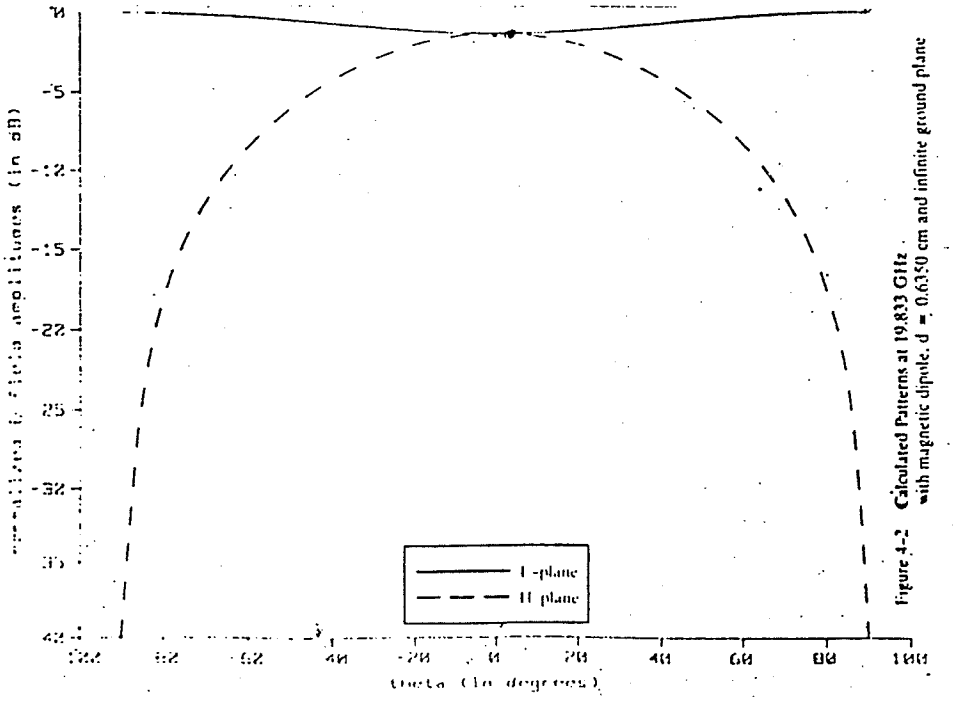

Figure 2.14 Radiated pattern of the $HEM_{11\delta}$ mode of a DR using the Moment Method [23]

In Fig. 2.13, the radiation patterns are shown in both the E–plane and H–plane while using both the MWM and DWM models for the DR. The computed far fields in this Fig. 2.13 are for a dielectric resonator of dielectric constant $\varepsilon_{r_{DR}} = 10.8$, of height $h = 0.127\ cm$ and of diameter $d = 2a = 0.635\ cm$. For each model of the DR, the computed data was normalized to the maximum of E_θ and E_ϕ. Fig. 2.14 was taken from [23] and displays the radiated fields of the same antenna as the one used in Fig. 2.13. The computed fields in this figure were calculated using a numerical program which is based on the integro–differential equations for the equivalent electrics and magnetic surface currents and the moment method solution [23] as described in section (2.3). By examining the two figures, we can see that the radiation pattern of the DR using DWM is similar to the one obtained from the numerical program, with a dip in the E– plane fields at $\theta = 0^o$. The radiation pattern in the E–plane using the MWM model differs from the radiation pattern using the DWM model and from the pattern using the numerical program. It has a maximum in the E–plane at $\theta = 0^o$ while the others have a maximum at $\theta = 90^o$.

The dip in the E–plane pattern at $\theta = 0^o$ was thought previously to be due to higher order modes generated in the DR [11]. However, since the DWM model exhibits a similar behavior, and only a single mode is assumed in the model, the dip is due to the transverse variation in the current distribution on the DR surface.

To examine the far field variation as a function of the dimensions of the dielectric resonator, a height of $h = 0.127\ cm$ and a dielectric constant of $\varepsilon_{r_{DR}} = 10.5$ was chosen. The normalized (to 0 dB) field patterns for values of radius to height ratios (a/h) of 0.6, 1, 1.5, and of 3 are shown in Fig. (2.15a), for the E–plane pattern and in Fig. (2.15b) for the H–plane pattern. As was expected, the field patterns for all cases are fairly broad. This characterizes the dielectric resonator antenna as radiating similar to a horizontal magnetic dipole. In the E–plane, the fields are omnidirectional for a DR with a smaller a/h ratio. As the a/h ratio increases, a dip begins to appear along the direction normal to the plane of the radiator. In the

H–plane, the field patterns are relatively unchanged for all ratios (a/h) of the DR.

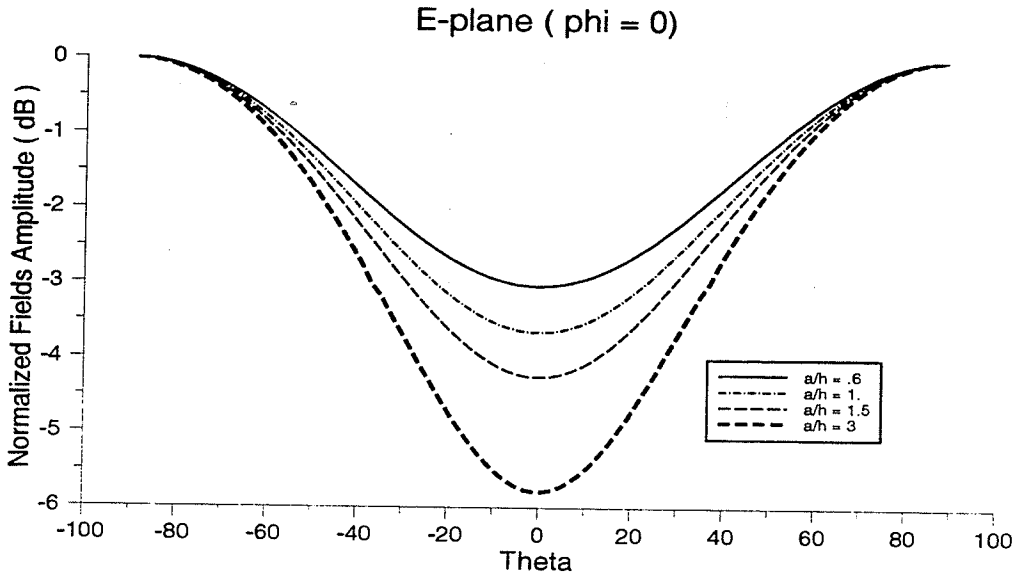

Figure 2.15a DWM radiated pattern for the $HEM_{11\delta}$ mode for a DR with various a/h

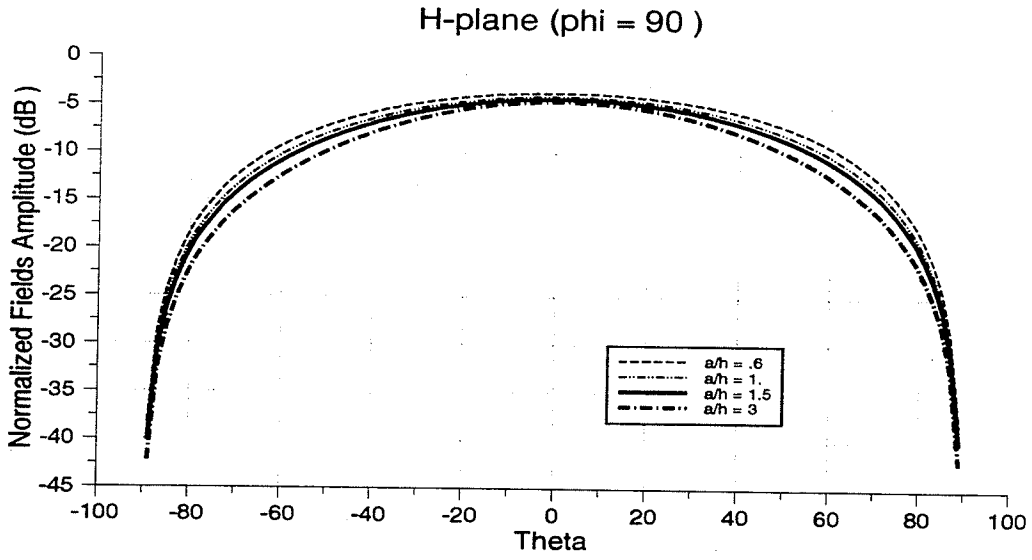

Figure 2.15b DWM radiated pattern for the $HEM_{11\delta}$ mode for a DR with various a/h

2.4.3 Calculation of Near Fields

To calculate the mutual coupling of two neighboring dielectric resonators, the near field of a single DR must be known. Using equations (2.106), (2.107), (2.114)–(2.119) and (2.122)–(2.127), a computer program was developed to calculate for the near fields of an isolated dielectric resonator.This DR, which was modelled using the dielectric waveguide model DWM, was assumed to be excited in its dominant mode $HEM_{11\delta}$. Figs. (2.16a)–(2.16d) and (2.17a)–(2.17d) show, respectively, E– and H– plane plots of the near fields of a dielectric resonator of height $h = 0.3175\ cm$, diameter $d = 2a = 1.0\ cm$ and of dielectric constant of $\varepsilon_{r_{DR}} = 10.5$. The near fields are plotted on these figures for various distances (r) from the resonator. Also shown in these figures are the corresponding far field results for the same antenna in both planes of interest. As can be seen from these figures E–plane and the H–plane fields coincide with the far fields in the same plane as the distance increases. This was expected since the formulation of the near field becomes similar to the far field at distant far from the resonator ($r \geq 4\lambda_o$).

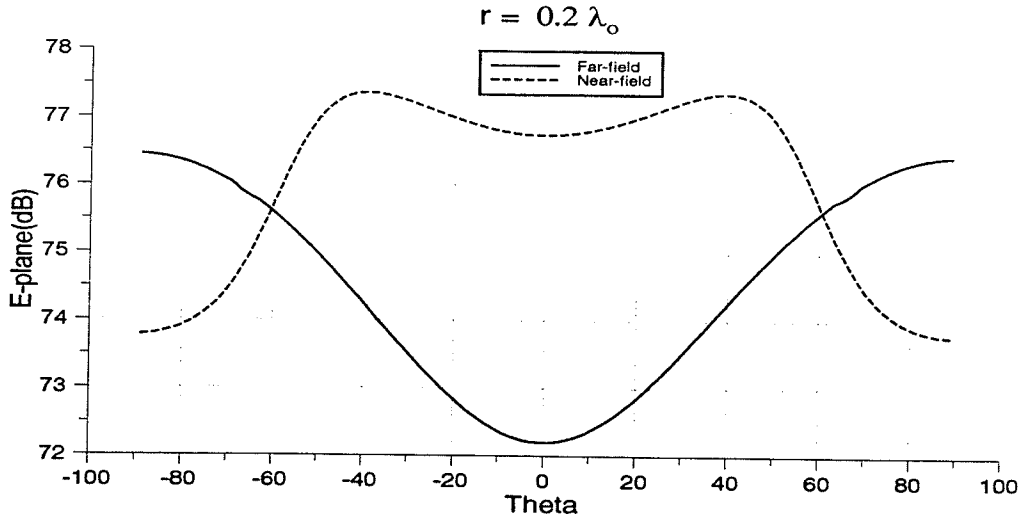

(a)

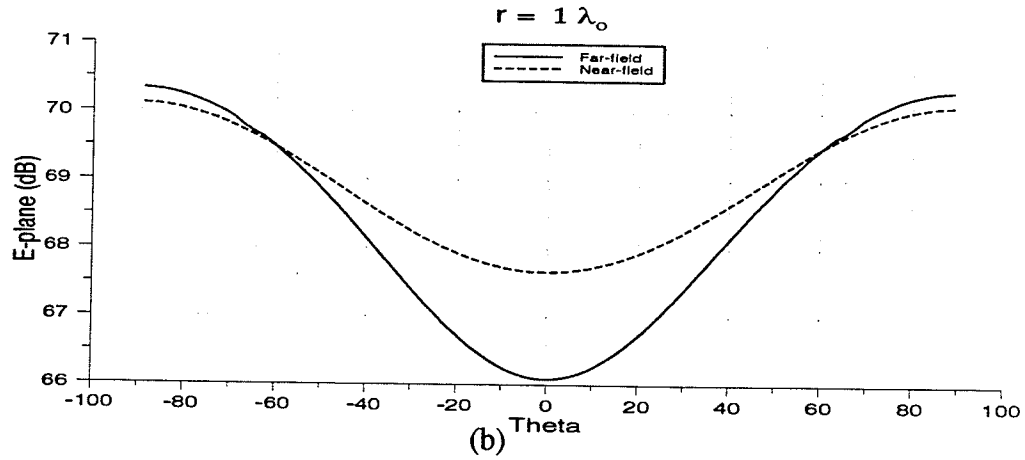

(b)

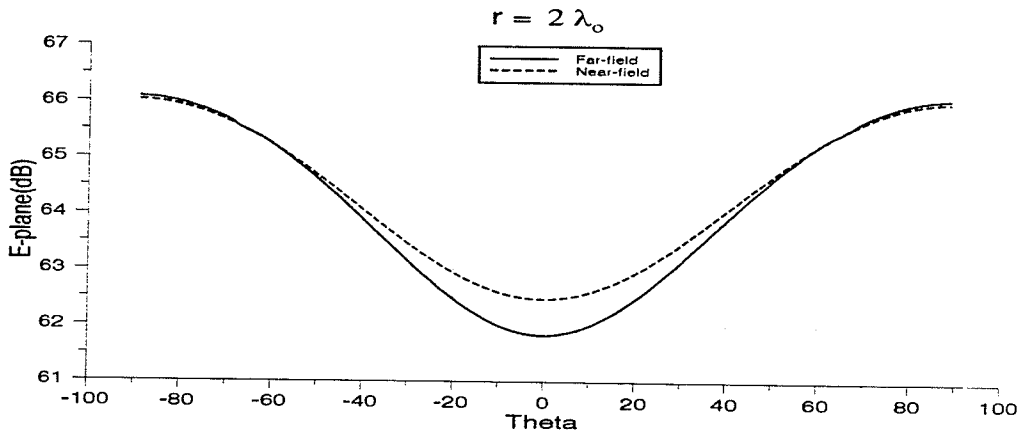

(c)

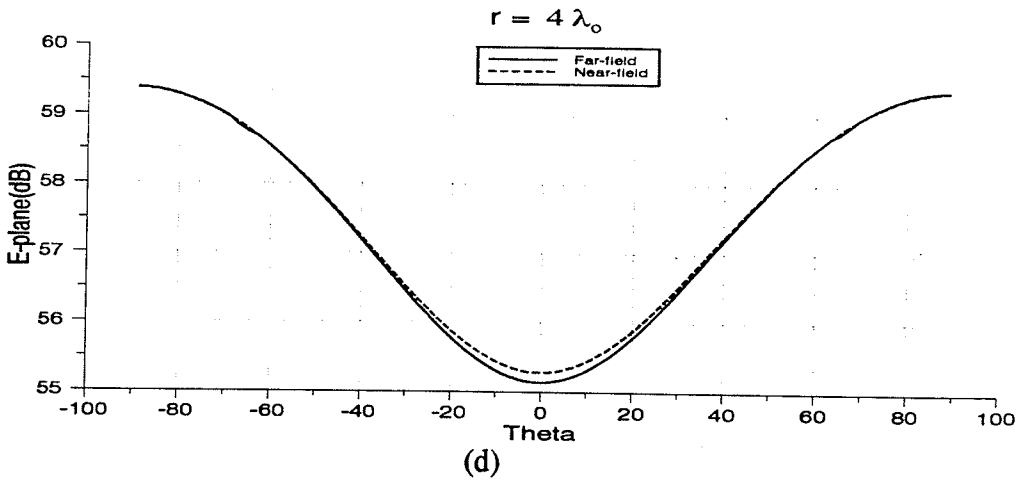

(d)

Figure 2.16 DWM E_θ field for the $HEM_{11\delta}$ mode for a DR for various r (a) $r = 0.2\ \lambda_o$
(b) $r = 1.0\lambda_o$
(c) $r = 2.0\ \lambda_o$
(d) $r = 4.0\ \lambda_o$

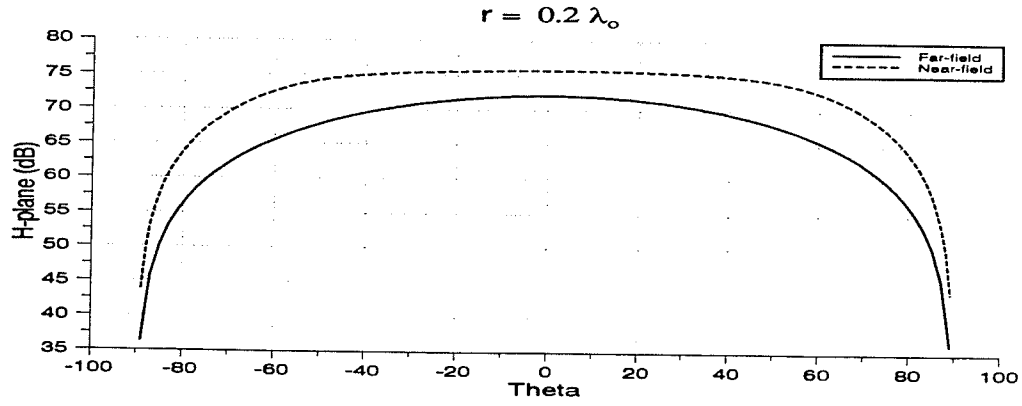

(a)

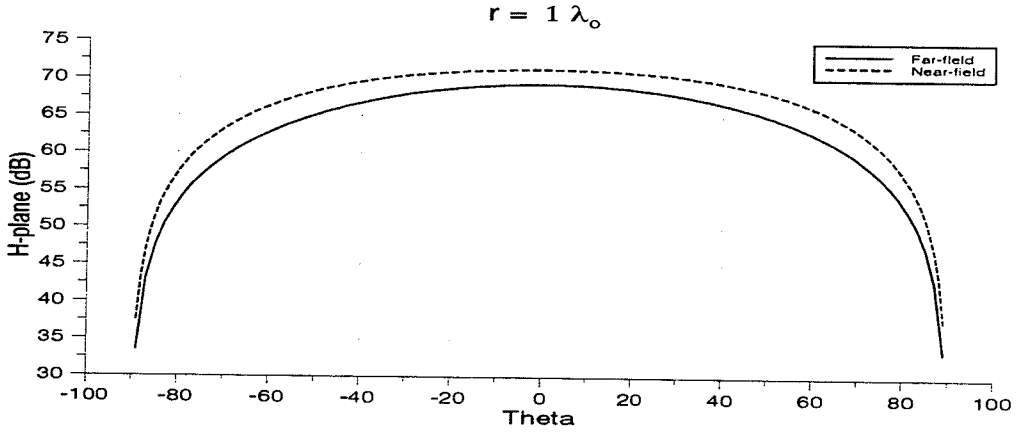

(b)

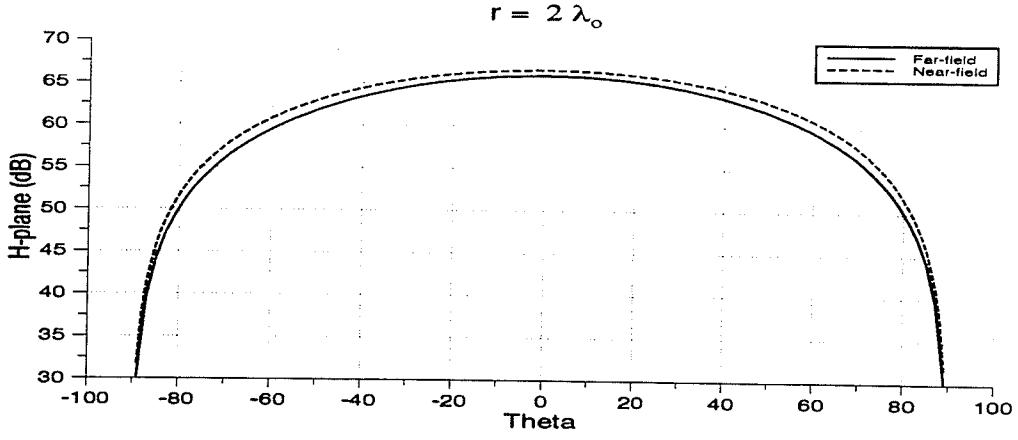

(c)

Figure 2.17 DWM E_ϕ field of $HEM_{11\delta}$ mode for a DR for various r (a) $r = 0.2\ \lambda_o$ (b) $r = 1.0\ \lambda_o$ (c) $r = 2.0\ \lambda_o$ (d) $r = 4.0\ \lambda_o$

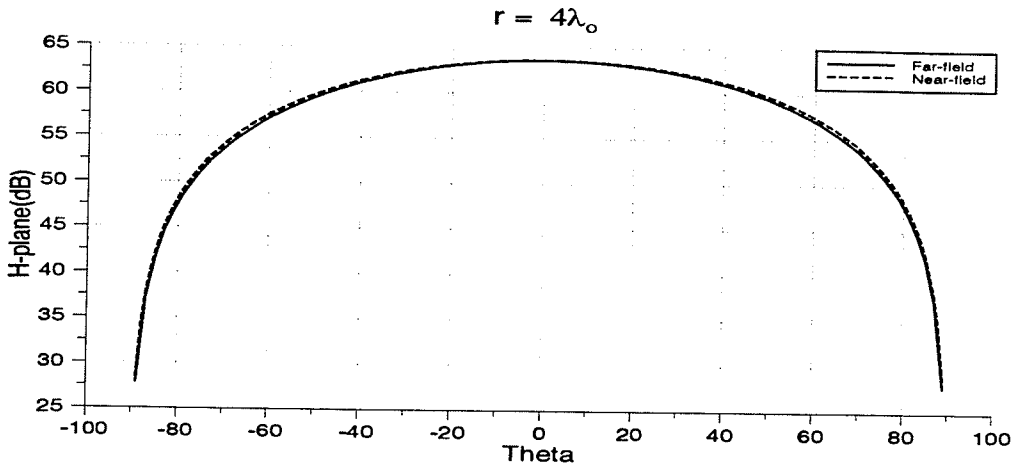

(d)

Figure 2.17 DWM E_ϕ field of $HEM_{11\delta}$ mode for a DR for various r (a) $r = 0.2\ \lambda_o$ (b) $r = 1.0\ \lambda_o$ (c) $r = 2.0\ \lambda_o$ (d) $r = 4.0\ \lambda_o$

2.5 The Radiated Quality Factor

The quality factor Q of an antenna is a measure of the energy loss per cycle as compared to the energy stored in the fields inside the resonator. Knowledge of the quality factor yields an indication of the radiation efficiency of the antenna and is inverse proportional to the bandwidth of the antenna. The quality factor is defined mathematically as

$$Q = \omega_o \frac{W_T}{P_T} \tag{2.134}$$

where ω_o is the angular resonant frequency, W_T is the total average stored energy and P_T is the dissipated power. The stored energy is the sum of the stored electric W_e and magnetic W_m energies which are defined by

$$W_e = \frac{\varepsilon}{4} \int_v \left| E \right|^2 \, dv \tag{2.135}$$

$$W_m = \frac{\mu}{4} \int_v \left| H \right|^2 \, dv \tag{2.136}$$

where v is a volume including all the reactive fields inside and outside the DR.

The total dissipated power P_T in a DR is due to dielectric loss, radiation loss, and any losses due to the coupling of a DR to an external device. This is given as

$$P_T = P_d + P_{rad} + P_{ex} \tag{2.137}$$

P_{rad} is the power loss due to radiation, which can be determined for the $HEM_{11\delta}$ mode as

$$P_{rad} = \int_0^{2\pi} \int_0^{\pi} U \sin(\theta) d\theta d\phi \ . \tag{2.138}$$

here U is the radiation intensity given by [36]

$$U = \frac{r^2}{2\eta} \left(\left| E_\theta \ (\theta, \phi) \right|^2 + \left| E_\phi \ (\theta, \phi) \right|^2 \right), \tag{2.139}$$

with E_θ and E_ϕ the far fields of the antenna. P_d is the power loss in the dielectric material and is given by

$$P_d = \frac{\sigma}{2} \int_{v_{DR}} \left| E \right|^2 \ dv \tag{2.140}$$

where v_{DR} is the DR volume. Using v_{DR} instead of v assumes almost all energy is inside the DR, which is reasonable for high constant materials. The term P_{ex} is extremely difficult to determine and will be neglected here. From the above definitions, the unloaded quality factor Q_u, which excludes external coupling, is defined as

$$Q_u = \omega_o \frac{W_T}{P_r + P_d} \tag{2.141}$$

By rearranging (2.141), the following is obtained

$$\frac{1}{Q_u} = \frac{1}{Q_d} + \frac{1}{Q_r} \tag{2.142}$$

where Q_r is the radiated quality factor as defined by

$$Q_r = \omega_o \frac{W_T}{P_r}, \tag{2.143}$$

and Q_d is the dielectric quality factor as defined by

$$Q_d = \omega_o \frac{W_T}{P_d}. \tag{2.144}$$

Using (2.135) and (2.140), and assuming, $v \approx v_{DR}$ equation(2.144) becomes

$$Q_d = \frac{\omega_0 \epsilon}{\sigma} = \frac{1}{\tan(\delta)} \tag{2.145}$$

For dielectric resonators that are fabricated out of low loss material $\tan(\delta) \approx 10^{-4}$ which is small compared to loss due to radiation. Therefore, in antenna applications where the DR is placed in an open environment, the unloaded quality factor Q_u will be approximately equal to Q_r. Finally, the radiated quality factor Q_r of a DR depends only on its dielectric constant and its dimension. Thus, with a proper choice of these parameters, one can control the Q–factor and therefore, control the operating bandwidth of the antenna under consideration.

2.5.1 Numerical Computed Radiated Quality Factor

It has been shown [9] that for a DR fabricated from low loss material, the radiated quality factor of the dielectric resonator can be calculated by

$$Q_r = \frac{\omega_{mn}}{2\ \sigma_{mn}} \tag{2.146}$$

where ω_{mn} and σ_{mn} are the resonant frequency and the decay time constant, respectively, of a specific mode $(m\ ,n)$. These two parameters can be obtained numerically using equation (2.98). With the use of a curve fitting procedure for the calculated numerical results Kishk et. al. [21] obtained an expression for the radiated quality factor of a DR with $\epsilon_{r_{DR}} = 38$ .This expression is similar to the one obtained for the resonant frequency of the same DR and it is given for by,

$$Q_r = 2.28 \frac{a}{h}\left(1. + 100\ e^{-2.05\left(\frac{a}{h} - 0.05\ (\frac{a}{h})^2\right)}\right) \tag{2.147}$$

2.5.2 Empirical Radiated Quality Factor Formula

The radiated quality factor for a dielectric resonator with a very high permittivity ($\varepsilon_{r_{DR}} \gtrsim 100$) was shown to vary with respect to the resonator permittivity as [33]

$$Q_r \propto \left(\varepsilon_{r_{DR}}\right)^p \tag{2.148}$$

where p = 1.3 for the mode that radiates as a magnetic dipole (such as $HEM_{11\delta}$). Using the equations (2.147) and (2.148), a general formula [26] for the radiated quality factor with respect to DR's permittivity and its aspect ratio (a/h) was obtained as

$$Q_r = 0.01007\ \varepsilon_{r_{DR}}^{1.3}\ \frac{a}{h}\left(1 + 100\ e^{-2.05\left(\frac{a}{2h} - 0.05\ (\frac{a}{2h})^2\right)}\right). \tag{2.149}$$

This expression is valid in the range $0.4 \leq \frac{a}{h} \leq 5$.

2.5.3 Comparison of Various Models

In this section, the computed results for the quality factor of a dielectric resonator antenna excited in the $HEM_{11\delta}$ mode using dual dielectric waveguide model are compared to the one using (2.149) and also to the one using the magnetic wall model for the same antenna.

Table 2.3 and Fig. 2.18 compare the radiated quality factor of the $HEM_{11\delta}$ mode computed using the DWM model for the DR to both, the numerically obtained formulas (2.147) and that found using the MWM model. In this comparison, the DR is of permittivity $\epsilon_{r_{DR}} = 38$, height $h = 0.46\ cm$ and with various ratios (a/h). The comparison shows that the DWM offers better results than the MWM over the entire (a/h) range when they are compared to the numerical result. Also, the results of DWM is very accurate in the range of $0.8 < \frac{a}{h} < 3.4$ since it deviates by only 1.75 to 7% from the obtained using (2.147).

Table 2.4 and Fig. 2.26 shows the computed results for the radiated quality factor using the DWM, MWM and Empirical formula (2.149) for a DR with $\epsilon_{r_{DR}} = 22, h = 0.46\ cm$ and for

Table 2.3 Quality factor of $HEM_{11\delta}$ mode of an isolated DR versus a / h

h = 0.46 cm , $\epsilon_{r_{DR}} = 38$

a / h	Radiated Quality factor		
	Mongia Formula	Dielectric Model (DWM)	Cavity Model (MWM)
0.4	26.830	29.140	62.784
0.6	33.010	38.149	76.767
1.0	37.425	44.867	79.275
1.4	36.191	41.441	66.882
1.8	32.667	35.100	53.192
2.2	28.516	29.025	42.013
2.6	24.517	24.026	33.570
3.0	20.990	20.104	27.293
3.4	18.025	17.063	22.601
3.8	15.609	14.699	19.046

Table 2.4 Quality factor of $HEM_{11\delta}$ mode of an isolated DR versus a / h

h = 0.46 cm , $\epsilon_{r_{DR}} = 22$

a / h	Radiated Quality factor		
	Mongia Formula	Cavity Model (MWM)	Cavity Model (MWM)
0.4	15.156	19.146	29.997
0.6	18.676	22.777	36.108
1.0	21.181	24.935	37.081
1.4	20.420	22.308	31.357
2.0	17.100	16.859	22.341
2.2	15.863	15.481	19.948
2.4	14.657	13.978	17.873
3.0	11.456	10.725	13.218
3.4	9.756	9.289	11.080
3.6	9.036	8.664	10.218

various ratios (a/h). When $\frac{a}{h} > 1$, a good agreement was obtained between the results of DWM and of the formula (2.149).

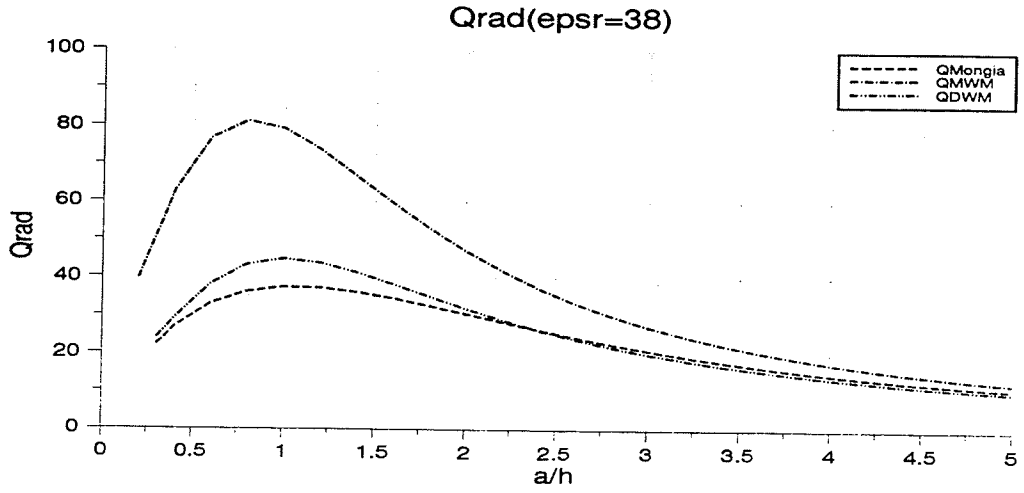

Figure 2.18 Quality factor of $HEM_{11\delta}$ mode of an isolated DR versus a / h
$h = 0.46\ cm,\ \varepsilon_{r_{DR}} = 38$

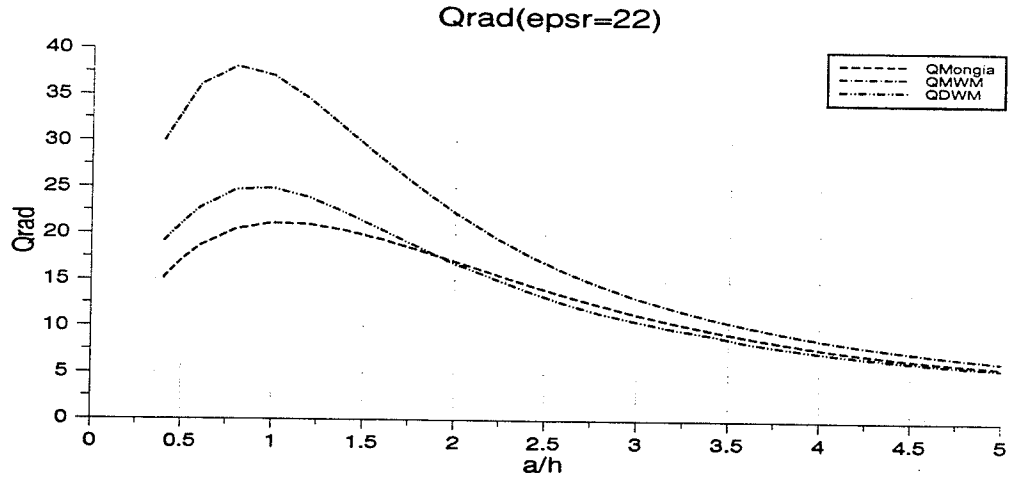

Figure 2.19 Quality factor of $HEM_{11\delta}$ mode of an isolated DR versus a / h
$h = 0.46\ cm,\ \varepsilon_{r_{DR}} = 22$

Fairly good results are obtained when computing the quality factor of a dielectric resonator antenna using the dual dielectric waveguide model for the DR. This is demonstrated by comparison with the numerical results.

2.6 Aperture Coupling Model

The aperture coupling method of providing the electromagnetic energy from a microstrip feed line to a radiating element was introduced by Pozar [24]. He used it to feed a microstrip patch antenna that operated around 2.14 GHz. Later, due to its enormous advantages in MIC technology (see Chapter 1) many other research groups have studied and used the technique as a coupling tool for both the patch antenna and the dielectric resonator antenna [24], [27], [18], [19], and [20]. The material presented in this section will follow the formulation for aperture coupling as described in [23] and [27].

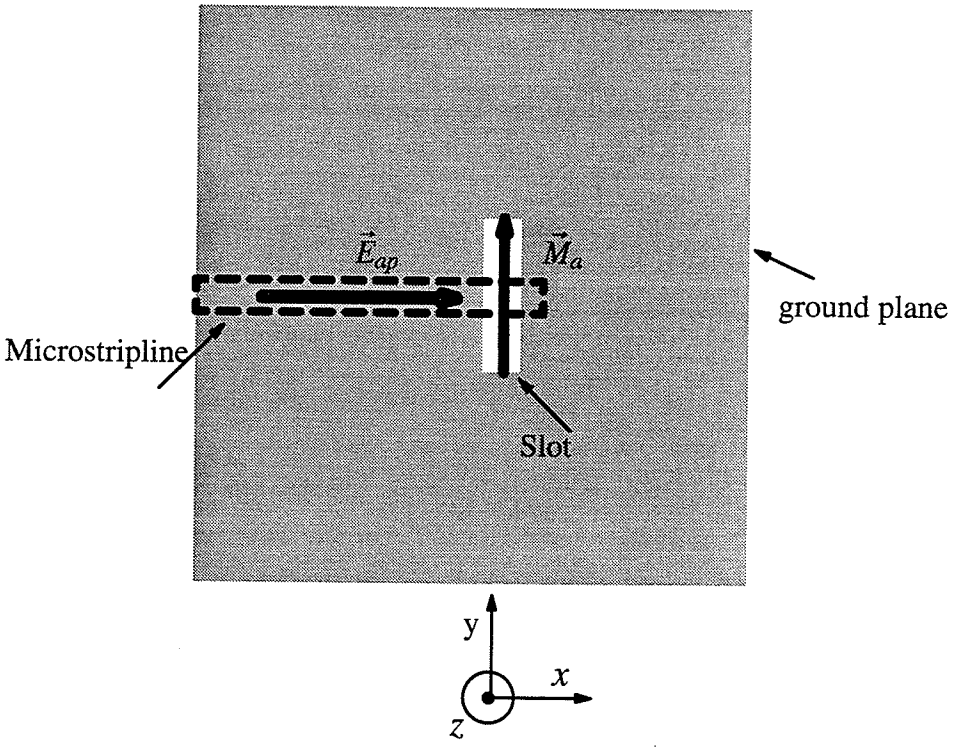

Figure 2.20 The equivalent magnetic current for the slot

As illustrate in the Fig. 2.20, for a microstrip fed slot, the electric field in the aperture $\vec{E}_{ap}$ is along the x direction, which is the direction of propagation along the microstrip feed line. The dimensions of the slot are chosen so that it can be modeled by magnetic equivalent currents $\vec{M}_a$ whose direction and magnitude are determined by the electric field $\vec{E}_{ap}$ inside the aperture. The magnetic equivalent currents $\vec{M}_a$ can be found as [28]

$$\vec{M}_a = \vec{E}_{ap} \times \vec{n} \tag{2.150}$$

where $\vec{n}$ is the unit normal vector pointing out of the slot and coincides with the unit normal $\vec{a}_z$. Since the aperture electric field lies in the x direction, the following result is obtained

$$\vec{M}_a = E_{ap}\ \vec{a}_x \times \vec{a}_z = E_{ap}\ \vec{a}_y\ . \tag{2.151}$$

Equation (2.151) can also be written as,

$$\vec{M}_a = M_y\ \vec{a}_y \quad ; \qquad M_y = E_{ap} \tag{2.152}$$

The aperture field $\vec{E}_{ap}$ can be approximated by a single piecewise sinusoidal (PWS) mode describing the aperture electric field [25], as follow,

$$\vec{E}_{ap} = V\ f(y)\ \vec{a}_x \tag{2.153}$$

where V is the voltage at the center of the slot and,

$$f(y) = \begin{cases} \dfrac{1}{W_{ap}} & -\dfrac{W_e}{2} \le y \le \dfrac{W_e}{2} \\ \dfrac{1}{W_s}\ \dfrac{\sin k_s\left(\frac{L_{ap}}{2} - |y|\right)}{\sin\frac{k_s}{2}\left(L_{ap} - W_e\right)} & \dfrac{W_e}{2} \le |y| \le \dfrac{L_{ap}}{2} \\ 0 & \text{Otherwise} \end{cases} \tag{2.154}$$

where, $k_s = k_0 \sqrt{\dfrac{\epsilon_{r_e} + \epsilon_{r_{DR}}}{2}}$

here ε_{r_e} is the effective dielectric constant of the feed substrate and $\varepsilon_{r_{DR}}$ is the dielectric constant of the dielectric resonator. In order to find the $\vec{H}$ field of the DR in terms of the magnetic surface current $\vec{M}_a$ in the aperture, the $\vec{H}$ field of the DR is expand in the following form,

$$\vec{H} = \sum_{m\,n\,l} \left(a_{mnl}\ \vec{H}_{mnl}\right) \tag{2.155}$$

where $\vec{H}_{mnl}$ is the set of the discrete orthogonal mode vectors for the DR and a_{mnl} is the corresponding coupling coefficient. Using Maxwell's equations [28], the relation between the DR fields and the equivalent magnetic current source can be expressed as

$$-\nabla \times \vec{E} = j\omega\mu \vec{H} + \vec{M}_a \tag{2.156}$$

$$\nabla \times \vec{H} = j\omega\epsilon \vec{E} \tag{2.157}$$

Taking the cross product $\nabla \times \nabla \times$ of both side of equation (2.157) and by using equations (2.156), the following equation is obtained,

$$\nabla \times \nabla \times \vec{H} = k^2 \vec{H} - j\,\omega\,\epsilon\,\vec{M}_a \tag{2.158}$$

Substituting (2.155) into (2.158) gives

$$\sum_{m\,m\,l} a_{mnl}\,\nabla \times \nabla \times \vec{H}_{mnl} = k^2 \sum_{m\,n\,l} a_{mnl}\,\vec{H}_{mnl} - j\,\omega\,\epsilon\,\vec{M}_a \tag{2.159}$$

Since the modal fields are in source free region

$$\nabla \times \nabla \times \vec{H}_{mnl} = k^2_{mnl}\,\vec{H}_{mnl} \quad . \tag{2.160}$$

By substituting (2.160) into (2.159),

$$\sum_{m\,m\,l} a_{mnl}\left(k^2 - k^2_{mnl}\right)\vec{H}_{mnl} = -j\,\omega\,\epsilon\,\vec{M}_a \tag{2.161}$$

Utilizing the orthogonality condition for the modal fields in the DR,

$$\iiint_v \mu\,\vec{H}_{mnl} \cdot \mu\,\vec{H}^*_{m'n'l'}\,dV = \begin{cases} 0\,; & mnl = m'n'l' \\ 1\,; & \text{Otherwise} \end{cases} \tag{2.162}$$

where $\vec{H}^*$ is the complex conjugate of $\vec{H}$, and then by taking the triple integral of both sides of equation (2.159),

$$\sum_{m\,m\,l} a_{mnl}\left(k^2 - k^2_{mnl}\right)\iiint_v \mu\vec{H}_{mnl} \cdot \mu\,\vec{H}_{m'n'l'} = -j\omega \sum_{m\,n\,l} \iint_{S_{ap}} \vec{M}_a \cdot \vec{H}^*_{mnl}\,ds_{ap} \tag{2.163}$$

Therefore using (2.163) and (2.162), the constants a_{mnl} can be obtained as

$$a_{mnl} = \frac{j\,\omega}{\omega^2 - \omega_{mnl}^2} \iint_{S_{ap}} \vec{M}_a \cdot \vec{H}^*_{mnl}\, dV \qquad (2.164)$$

and,

$$\vec{H} = \sum_{mnl} \frac{j\,\omega}{\omega^2 - \omega_{mnl}^2} \vec{H}_{mnl} \iint_{S_{ap}} \vec{M}_a \cdot \vec{H}^*_{mnl}\, dS_{ap} \qquad (2.165)$$

In this manner, equation (2.165) links the modal magnetic fields in DR to the slot magnetic currents.

2.7 The Feed Structure for the Antenna

The microstrip feed line of width W_s, substrate thickness T_s and of dielectric constant ϵ_r as inFig. 2.21, can be analyzed using the dynamic waveguide model [32]. This model assumes the microstrip line to be a waveguide of an effective permittivity ε_{r_e} with top and bottom electric walls of width W_e, and two magnetic side walls equal to the substrate thickness T_s as in Fig. 2.22. This model is used instead of a static planar waveguide to achieve a better description of the fields as it is has an upper frequency limit of 60 GHz, which is better suited for this thesis.

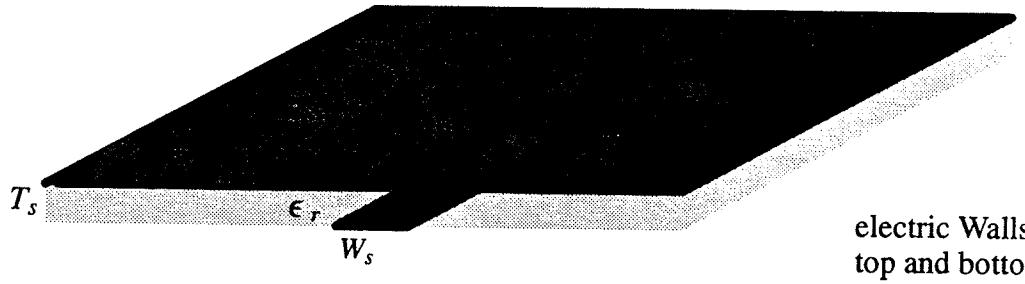

Figure 2.21 Microstrip feedline

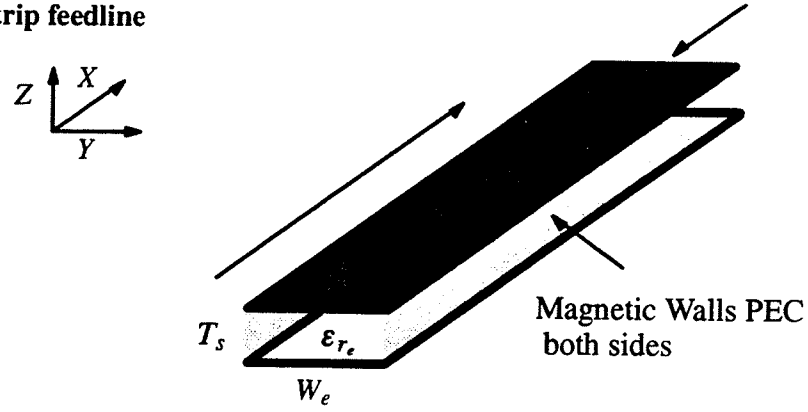

Figure 2.22 Equivalent model for the microstrip feedline

Coupling between the microstrip feedline and the DR antenna element is via a magnetic current in the y direction. Therefore, only the modal fields which are transverse electric to y (TE^y) are to be considered for analyzing the feedline. Here, the analysis follows the same steps as the cavity analysis and it is taken from [23] and [27]. The magnetic and electric vector potential for the feedline are given by

$$\vec{A} = \vec{0} \tag{2.166}$$

$$\vec{F} = \vec{y}\,\psi^{e} \tag{2.167}$$

where the scalar wave function is given by

$$\nabla^2\psi + k_e^2\,\psi = 0 \tag{2.168}$$

$$k_e = \sqrt{(\omega^2\mu\,\varepsilon)}\;; \quad \varepsilon = \varepsilon_o\,\varepsilon_{r_e} \tag{2.169}$$

Here ε_{r_e} is the dynamic effective dielectric constant of the feed line. Using similar steps that were outlined in section (2.2.1) and with a cartesian coordinate system, one can find the solution of equation (2.168) to be

$$\psi_f = F(x)\Big(A_y\,cos(k_y\,y) + B_y\,sin(k_y\,y)\Big)\Big(A_z\,\cos(k_z z) + B_z\,\sin(k_z z)\Big) \tag{2.170}$$

where

$$F(x) = A^{+}\,e^{-jk_x x} + A^{-}\,e^{jk_x x} \tag{2.171}$$

and

$$k_x^2 = k_e^2 - k_z^2 - k_y^2 \tag{2.172}$$

To determine the unknown coefficient $A's$ and $B's$ of equation (2.170), and the wave numbers k_x, k_y, and k_z the boundary condition must be applied to the surface of the planar waveguide wall. These boundary conditions, which are perfect electric walls at the top and bottom of the waveguide and perfect magnetic walls at the sides, require that the tangential electric field must be zero at $z = 0$ and $z = T_s$ and that the tangential magnetic fields must be also zero at $y = \pm W_e$. The application of these boundaries are clearly described in [23] and [27] and they are not repeated here. The final solution for the wave equa-

tion is

$$\psi_f = A\ F(x)\ cos(\ k_y\ y\ )\ \cos(\ k_z\ z\ )\ , \tag{2.173}$$

where $F(x)$ is given by (2.171) and the wave numbers are found to be:

$$k_z = \frac{m\ \pi}{T_s} \quad ; \quad m = 0\ ,1\ ,2\ ,\ \ldots \tag{2.174}$$

$$k_y = \frac{n\ \pi}{W_e} \quad ; \quad n = 0\ ,1\ ,2\ ,\ \ldots \tag{2.175}$$

The dominant mode and the cut–off frequencies of the different modes of this feed line can then be found using equations (2.169), (2.172), (2.174), and (2.175) as

$$\omega_{mn} = \frac{1}{\mu\ \epsilon}\sqrt{k_e^2 - \left(\frac{m\pi}{T_s}\right)^2 - \left(\frac{n\pi}{W_e}\right)^2} \tag{2.176}$$

As can be seen from the above equation the cut–off frequency occurs when $m = n = 0$. Thus the dominant mode of the feedline is purely transverse electromagnetic (TEM) with fields components H_y and E_z.

To determine all the actual fields that are due to the microstrip feed line and to link between them with those of the dielectric resonator (DR), the geometry of the feedline is first divided into two separate regions I and II as shown in Fig. 2.23. Region I is defined as the region where the microstripline passes underneath the resonator to the center of the aperture, while region II is defined as the region from the center of the aperture to the end of the stub.

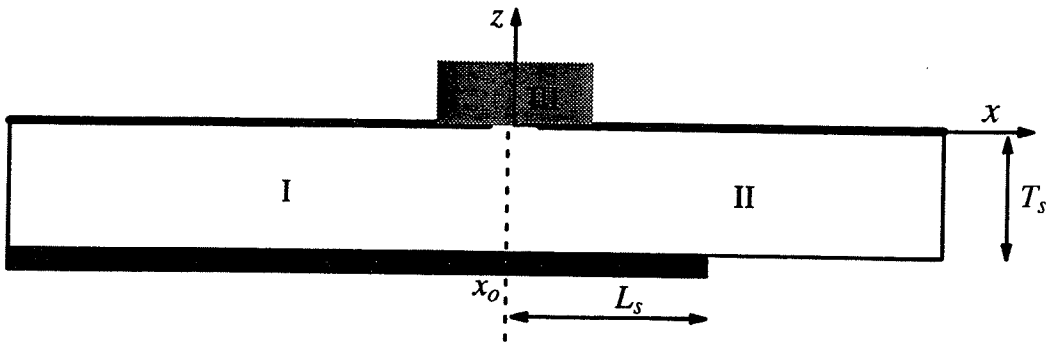

Figure 2.23 Chosen regions for the feedline

The analysis of the fields in these two region was outlined precisely in [23] and [27], and is only repeated briefly here. The scalar wave function, and the electric and magnetic fields are expressed as a summation of the dominant mode plus the higher order modes of the resonator. Using the coordinate system in Fig. 2.23, the scalar wave function in region I can be written as

$$\psi_f{}^{I} = A_I{}^{+} e^{-j k_x x} + A_I{}^{-} e^{j k_x x} + \sum_m \sum_n \left[A_{mnI}{}^{-} e^{\alpha_{mn} x} \cos\left(\frac{m\pi}{T_s} (z + T_s) \right) \cos\left(\frac{n\pi}{W_e} (y) \right) \right] \quad (2.177)$$

whereas, in region II

$$\psi_f{}^{II} = A_{II}{}^{+} e^{-j k_x x} + A_{II}{}^{-} e^{j k_x x} + \sum_m \sum_n \left[A_{mnII}{}^{+} e^{-\alpha_{mn} x} \cos\left(\frac{m\pi}{T_s} (z + T_s) \right) \cos\left(\frac{n\pi}{W_e} (y) \right) \right] \quad (2.178)$$

The unknown coefficients $A_I{}^{+}$, $A_I{}^{-}$ and $A_{mnI}{}^{-}$ for region I, and $A_{II}{}^{+}$, $A_{II}{}^{-}$ and $A_{mnII}{}^{+}$ for region II are to be determined by first using the boundary condition and then by applying the theorem of reciprocity. Using the waveguide boundary conditions, the unknown coefficients can be written in terms of each other. By enforcing the open circuit boundary condition (PMC) at $x = x_o + L_s$

$$A_{II}{}^{-} = A_{II}{}^{+} e^{-2j k_e (x_o + L_s)} \quad . \quad (2.179)$$

Also the continuity condition of the magnetic field at $x = x_o$ yields

$$A_{mnII}{}^{+} = -A_{mnI}{}^{-} e^{2 \alpha_{mn} (x_o)} \quad . \quad (2.180)$$

Next, the rest of the unknown coefficients of the feedline and those of the dielectric resonator are determined. These are accomplished by the use of the Lorentz reciprocity theorem.

2.8 Determination of the Field Components

As stated in the previous section the remaining unknown coefficients for the electric and magnetic fields of the feedline and of the dielectric resonator can be founded using the Lorentz reciprocity theorem. This relates the total field $\left(E_T\ , H_T\right)$ in a closed surface S to a Maxwellien test field $\left(E_{tst}\ , H_{tst}\right)$ by the following [22]

$$\iint_S \left(\vec{E}_{tst} \times \vec{H}_T - \vec{E}_T \times \vec{H}_{tst}\right) \cdot \vec{n}\ ds = 0 \qquad (2.181)$$

Thus,

$$\iint_S \left(\vec{E}_{tst} \times \vec{H}_T\right) \cdot \vec{n}\ ds = \iint_S \left(\vec{E}_T \times \vec{H}_{tst}\right) \cdot \vec{n}\ ds \qquad (2.182)$$

Where (S) is a closed surface of integration and $\vec{n}$ is the unit normal pointing out of the surface region (S). Equations (2.181) and (2.182) are for a closed surface in a free source region.

As shown in Fig. 2.24, the chosen volume for this method is a rectangular box which is formed by the slot cross sections between the slot and the plane of the microstrip line. The surface of integration can be expressed by six surfaces of integration as shown in Fig. 2.24.

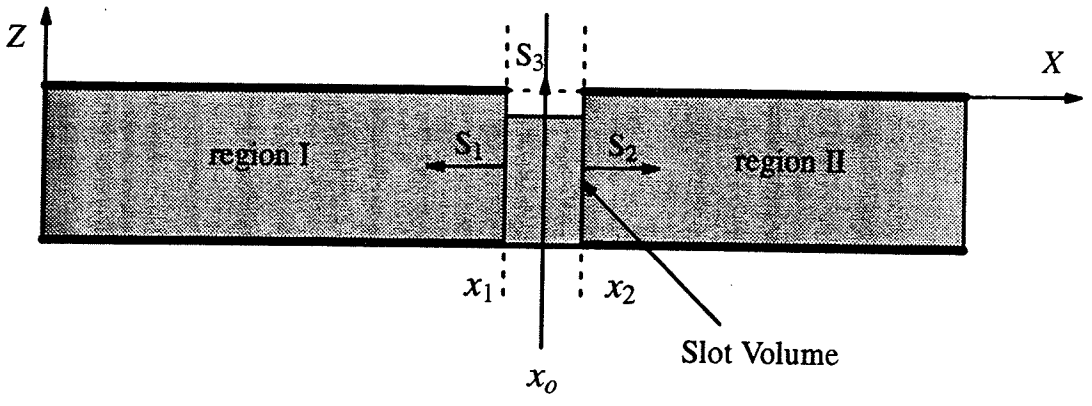

Figure 2.24 The surface of integration for the obtained reciprocity integrals

These surfaces are defined as :

S_1 : The surface across the plane that contained the feedline at the location x_1.

S_2 : The surface across the plane that contained the feedline at the location x_2.

S_3 : The surface across the aperture.

S_4 : The surface that is parallel to S_3 but along the bottom of the feedline.

S_5 : The surface along the the side of the feedline between S_1 and S_2.

S_6 : The parallel surface to S_5 but along the other side of the feedline.

The integration over the surfaces S_4 , S_5 and S_6 have no contribution because of the enforced PMC and PEC boundaries of the planar waveguide. Therefore, the left hand side of the equation (2.182) may be written in the following form

$$\iint_S \left(\vec{E}_{tst} \times \vec{H}_T\right) \cdot \vec{n}\, dS = \iint_{S_1} \vec{E}_{tst} \times \vec{H}_I \cdot -\vec{x}\, dS_1 + \iint_{S_{ap}} \vec{E}_{tst} \times \vec{H}_{ap} \cdot \vec{z}\, dS_{ap} + \iint_{S_2} \vec{E}_{tst} \times \vec{H}_{II} \cdot \vec{x}\, dS_2 \qquad (2.183)$$

and similarly the right hand side of (2.182) as

$$\iint_S \left(\vec{E}_T \times \vec{H}_{tst}\right) \cdot \vec{n}\, dS = \iint_{S_1} \vec{E}_I \times \vec{H}_{tst} \cdot -\vec{x}\, dS_1 + \iint_{S_{ap}} \vec{E}_{ap} \times \vec{H}_{tst} \cdot \vec{z}\, dS_{ap} + \iint_{S_2} \vec{E}_{II} \times \vec{H}_{tst} \cdot \vec{x}\, dS_2 \qquad (2.184)$$

where $\vec{E}_I$, $\vec{E}_{II}$, $\vec{H}_I$, and $\vec{H}_{II}$ are the total fields in region I and II, respectively, and are calculated using (2.177) and (2.178). $\vec{E}_{ap}$ and $\vec{H}_{ap}$ are the aperture fields and are obtained from (2.153) and (2.154). $\vec{E}_{tst}$, $\vec{H}_{tst}$ are the testing fields that can be chosen in any form as long as they satisfy Maxwell equations. Thus, for a simplicity, the testing fields are to be chosen so that they simplify the calculation for the above integral equations. A good choice for these

fields are ones that have a unit amplitude and have the same characteristic as the dominant feedline mode.

2.9 The Equivalent Circuit Model for the Dielectric Resonator Antenna and its Feeding Structure

As a result of the field analysis of the feedline and of the dielectric resonator, an equivalent circuit model for the whole system can be obtained along with the use of Pozar's technique for analyzing an aperture on a ground plane with the pointing vector theorem [28]. Pozar [25] has shown that a discontinuity introduced by a slot on the ground plane can be seen as a series impedance. This is shown in Fig. 2.25.

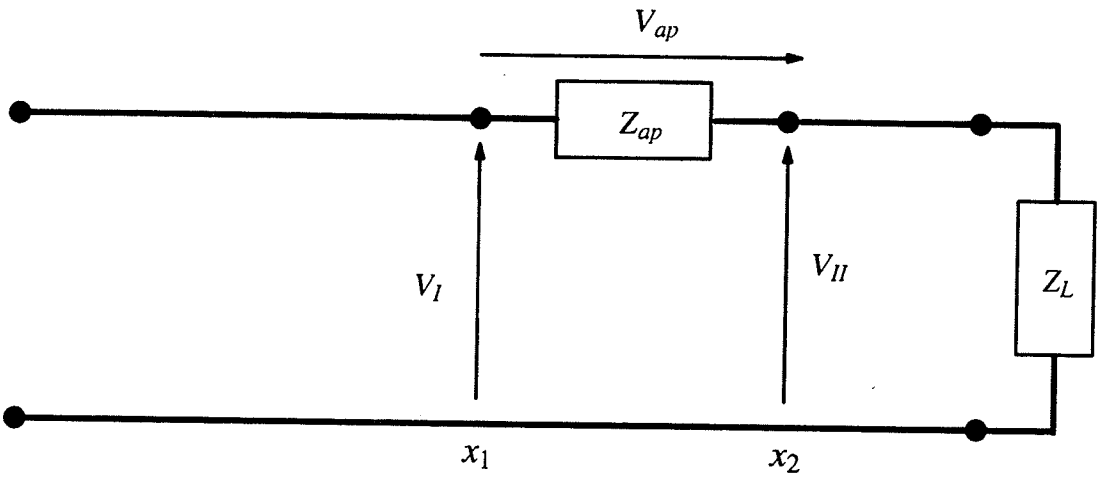

Figure 2.25 The equivalent circuit for representing impedance of the slot and the stub length and their corresponding voltages

The impedance of each section of the above circuit are given below,

Z_{ap} : The impedance of the loaded slot.

Z_L : The impedance of the Stub open circuit.

In order to find analytical formulas for the impedances of the stub open circuit Z_L and of the slot Z_{ap} ; the voltage is analyzed across each section of the circuit shown in Fig 2.25. Theses voltages are denoted by

V_I : The voltage across the feedline at the plane of the slot $x = x_1$

V_{II} : The voltage across the tuning stub at the plane of the slot $x = x_2$

V_{ap} : The voltage across the aperture

Since $\vec{E} = -\nabla V$, the voltages V_I , V_{II} and V_{ap} can be defined using the following

$$V_I = -\int_0^{T_s} E_z^I \, dz \tag{2.185}$$

$$V_{II} = -\int_0^{T_s} E_z^{II} \, dz \tag{2.186}$$

$$V_{ap} = V_{II} - V_I \tag{2.187}$$

where E_I and E_{II} are the fields in region I and II, respectively. Now, applying the pointing theorem to the slot volume of Fig. 2.24,

$$\frac{1}{2}\oint_S \left(\vec{E} \times \vec{H}\right) \cdot \vec{n} \, dS = -2j\omega \left[\frac{\mu}{4} \int\int\int_v \vec{H} \cdot \vec{H} \, dV - \frac{\epsilon}{4} \int\int\int_v \vec{E} \cdot \vec{E} \, dV \right] \tag{2.188}$$

The slot width (W_s) is considered to be very small, and therefore, the volume integral can be neglected. Hence,

$$\frac{1}{2}\oint_S \left(\vec{E} \times \vec{H}\right) \cdot \vec{n} \, dS = 0 \tag{2.189}$$

and equation (2.188) becomes

$$\frac{1}{2}\int_{S_1} \left(\vec{E}_I \times \vec{H}_I\right) \cdot \vec{a}_x \, dS_1 = \frac{1}{2} \int_{S_{II}} \left(\vec{E}_{II} \times \vec{H}_{II}\right) \cdot \vec{a}_x \, dS_2 + \frac{1}{2} \int_{S_a} E_{ap} \, H_y \, dS_{ap} \tag{2.190}$$

where H_y is the y–component of the $\vec{H}$ field in the DR and $\vec{E}_{ap}$ is the aperture field given by (2.153). Substituting the fields of region I and II into equation (2.190) and through the algebraic manipulation outlined in [27], the following is obtained

$$y_{in} \, V^2_I = y_L \, V^2_{II} + y_s \, V^2_{ap} \tag{2.191}$$

V_I , V_{II} and V_{ap} can be found using equation (2.185), (2.186), and (2.187), respectively and they are given by [27] as

$$V_I = j\,k\,A_I^{+}\,T_s\left(1-\frac{A_I^{-}}{A_I^{+}}\,e^{2jkx_o}\right)e^{-jkx_0} \tag{2.192}$$

$$V_{II} = j\,k\,A_{II}^{+}\,T_s\left(1+e^{-2jkx_o}\right)e^{-jkx_0} \tag{2.193}$$

Here y_{in} is the input admittance as seen by the microstrip line at the plane central to the slot, y_L is the admittance of the matching stub at the slot, and y_s is the total admittance comprising the admittance of the higher order modes inside the guide as well as the admittance of the DR. y_s is given by [27]

$$y_s = y_e + N^2\,y_{DR} \tag{2.194}$$

where N is the turn ratio of DR–slot transformer and may be approximated by the use of expressions for stripline as given in [27].

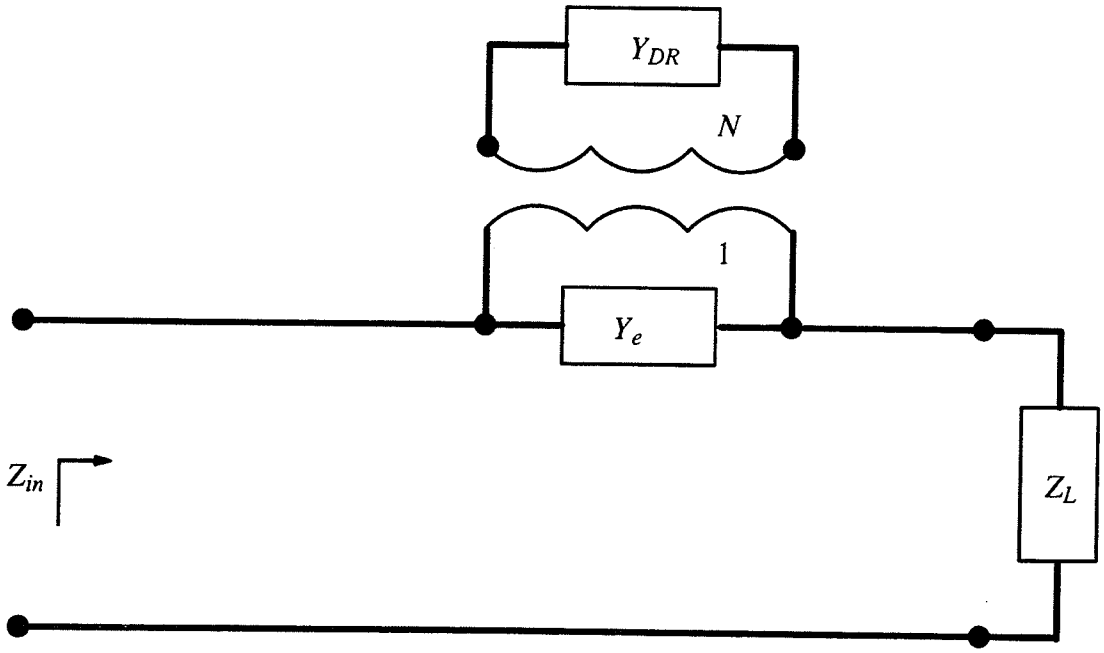

2.26 The final circuit configuration for the aperture–couped DR

The equivalent circuit shown in Fig. 2.26, along with equations (2.185)–(2.193) can then provide a means for evaluating the input impedance of the aperture coupled DR antenna in term of the slot dimensions, DR dimensions, DR permittivity and the tuning stub length.

CHAPTER 3

ANTENNA DESIGN AND EXPERIMENTAL RESULTS

3.1 Introduction

This chapter examines the design and the construction of an aperture coupled cylindrical dielectric resonator antenna. As can be seen from Fig. 2.1, this antenna is composed of three parts, namely; a dielectric resonator, an aperture, and a microstrip feedline. The parameters of the different parts of this antenna, such as their dimension and associated dielectric constant, defines the characteristics of this antenna.

3.2 Dielectric Resonator Design

The dielectric resonators (DRs) dimension primarily determines the operating frequency of the DR antenna. Two different sets of cylindrical shaped DRs are used in this experiment. They are constructed from the microwave laminated substrate RT/Duroid 6010 with the upper and the bottom copper layers etched locally using "Anhydrous Etchant Powder". The first set was constructed from RT/Duroid 6010 with a thickness of $h = 0.3175\ cm$ and a permittivity of $\varepsilon_{r_{DR}} = 10.5$, while the second set was constructed from RT/Duroid 6010 with a thickness of $h = 0.1905\ cm$ and a permittivity of $\varepsilon_{r_{DR}} = 10.2$. The diameter of the dielectric resonators were chosen so that the designed antennas can operate at frequencies of 5.5 Ghz, 7.5 Ghz and 9.4 Ghz. Table 3.1 shows the measured diameter $d(cm)$, height $h(cm)$ and the dielectric constant $\epsilon_{r_{DR}}$ of the constructed DRs and the corresponding frequencies that were calculated using the dielectric waveguide model.

Table 3.1 The dimension of the constructed DR and their corresponding calculated frequency using the DWM theory

Samples	d (cm)	h (cm)	$\epsilon_{r_{DR}}$	Frequency (Ghz)
DR_1	0.804	0.316	10.5	10.32
DR_2	0.92	0.314	10.5	9.59
DR_3	0.996	0.314	10.5	9.2
DR_4	1.0	0.268	10.2	10.21
DR_5	1.2	0.315	10.5	8.47
DR_7	1.597	0.642	10.5	5.15
DR_8	1.697	0.314	10.5	7.42
DR_9	2.0	0.316	10.5	7.0

3.3 Feedline Design

The antenna was designed for a characteristic impedance of 50 ohms. The parameters that determine the feedline width for a given substrate are the dielectric constant, the substrate thickness and the operating frequency. The design equations that were used to calculate the width of the microstrip line, taking into account the dependance on frequency, are given by Getsinger [35] and are valid up to 60 Ghz.These equations are accurate for $\frac{T_s}{\lambda_o} \leq 0.04$, where λ_o is the free space wavelength and are specified as,

$$\epsilon_{r,eff}\left(f\right) = \epsilon_r - \left[\frac{\epsilon_r - \epsilon_{r,eff,stat}}{1 + G\left(\frac{f}{f_p}\right)^2}\right] \tag{3.1}$$

$$f_p = \frac{15.66\ Z_{L,stat}}{T_s} \tag{3.2}$$

$$G = 0.6 + 0.009\ Z_{L,stat} \tag{3.3}$$

$$W_{s,eff}\left(f\right) = W_s + \frac{W_{s,eff,stat} - W_s}{1 + (f/f_{p_1})} \tag{3.4}$$

$$f_{p_1} = \frac{c_0}{2\ W_s \sqrt{\epsilon_r}} \tag{3.5}$$

Where the static parameters required for the above are given by [34] and [35] and are given below. The static parameter results are valid for $0.01 \leq \epsilon_r \leq 100$ and $0.01 \leq \frac{W_s}{T_s} \leq 100$ and are:

$$Z_{LO} = \frac{\eta_0}{2\pi} \ln\left[\frac{F_1 T_s}{W_s} + \sqrt{1 + \left(\frac{2 T_s}{W_s}\right)^2}\right] \tag{3.6}$$

$$F_1 = 6 + (2\pi - 6)\exp\left(-\frac{30.666\, T_s}{W_s}\right)^{0.7528} \tag{3.7}$$

$$\epsilon_{r,eff,stat} = \frac{\epsilon_r + 1}{2} + \frac{\epsilon_r - 1}{2}\left[1 + \left(10\frac{T_s}{W_s}\right)\right]^{-ab} \tag{3.8}$$

$$a = 1 + \frac{1}{49}\ln\left[\frac{\left(\frac{W_s}{T_s}\right)^4 + \left(\frac{W_s}{52} T_s\right)^2}{\left(\frac{W_s}{T_s}\right)^4 + 0.432}\right] + \frac{1}{18.7}\ln\left[1 + \left(\frac{W_s}{18.1\, T_s}\right)^3\right] \tag{3.9}$$

$$b = 0.564\left(\frac{\epsilon_r - 0.9}{\epsilon_r + 3}\right)^{0.053} \tag{3.10}$$

$$W_{s,eff,stat} = \frac{\eta_0 T_s}{Z_{Lo}} \tag{3.11}$$

$$Z_{L,stat} = \frac{Z_L}{\sqrt{\epsilon_{r,eff,stat}}} \tag{3.12}$$

$$Z_L = \frac{\eta_0 T_s}{W_{s,eff}\sqrt{\epsilon_{r,eff}}} \tag{3.13}$$

$$\eta_0 = \sqrt{\frac{\mu_0}{\epsilon_0}} \tag{3.14}$$

ϵ_r : the substrate dielectric constant

W_s : the physical width of the microstrip line (mil)

T_s : the physical width of the microstrip line (mil)

$W_{s,\,eff,\,stat}$: the static width of the microstrip line

$\epsilon_{r,\,eff,\,stat}$: the static dielectric constant

c_o : the free space velocity constant

$Z_{L,\,stat}$: the static microstrip feedline impedance

A computer program was developed to find the width of the substrate, the microstrip feedline's guided wavelength, and the frequency dependance of the dielectric constant at a given substrate of known thickness, permittivity, operating frequency and characteristic impedance. The calculated values of the width and the guided wavelength for a substrate with $\epsilon_r = 2.5$ and $T_s = 0.0625\ cm$ are shown in table 3.2

Table 3.2 The calculated dimension of the microstrip feed line

frequency (Ghz)	w_s (cm)	$\lambda_{eff}\ (cm)$
5.5	.4343	3.781
9.4	.4367	2.212

3.4 Stub length Design

The stub length L_s is defined as the distance from the center of the aperture to the end of the microstrip feed line. It was chosen to be one–quarter of a wavelength long so that it tunes out the reactive component of the aperture. The stub length is then given by,
The Calculated values for the L_s are shown in table 3.3

$$L_s = \frac{\lambda_{eff}}{4} \tag{3.6}$$

where,

$$\lambda_{eff} = \frac{\lambda_o}{\sqrt{\epsilon_{eff}}}$$

3.5 The Aperture Design

The aperture width w_{ap} was chosen to be significantly smaller than the microstrip feedline's guided wavelength $\lambda_{eff}(f)$ so that it can be modeled by a magnetic current. Throughout this experiment, the aperture was chosen to be approximately

$$w_{ap} \simeq \frac{\lambda_{eff}}{20} \tag{3.7}$$

The aperture length, denoted by L_{ap}, was chosen to be smaller than the diameter of the resonator and larger than the microstrip feedline width $w_s \leq L_{ap} \leq d$. A number of aperture lengths were tested and their values are given in table 3.3.

Table 3.3 The calculated dimension of the aperture

frequency (Ghz)	w_{ap}(cm)	L_{ap}(cm)	L_s(cm)
9.4	.1143	0.56	0.6096
5.5	.188	0.686	1.016

3.6 Measured Resonant Frequency and Input Impedance of the DRA

The frequency and the input impedance of the DRA were measured using a Wiltron 360 Network Analyzer. Before each measurement, the network analyzer was calibrated to a 50 ohm standard to ensure the accuracy of the measurements. Since the fabricated antennas are one port devices only the return loss measurement S_{11}, both in phase and magnitude, was performed on the network analyzer. The magnitude measurement of S_{11}, giving information

about the resonant frequency and the bandwidth of the designed antennas, was performed over a range of frequencies of interest and was displayed on the network analyzer in logarithmic–to–linear rectangular format. The phase measurement of the return loss, giving information about the input impedance of the antenna, was done for a selected range of frequencies and was displayed on the network analyzer in a Smith chart format. The resonant frequency can be taken to be the point of minimum return loss or the average of the frequencies that are near the resonance and at a 10 dB return loss. The minimum return loss measurement was used for comparing results.

Several antenna measurements were performed and the first set of measurement of the return loss were taken in the range of 9.4 GHz using a slot of width 0.1143 *cm* and of length 0.56 *cm*. The second set of measurement were taken in the range of 5.5 GHz using a slot of width 0.188 *cm* and length of 0.686 *cm*. The results of these measurements are shown respectively, in Figs. 3.3 to 3.13 and in Figs 3.15 to 3.16. Fig 3.1 and Fig 3.2 shows the resonance frequency of both slots that were designed for the DRA. These slots resonates respectively, at 11.42 GHz and 10.56 GHz. Their results frequency was greater than the resonant frequencies of the DRs measured. Measurements were taken both with and without a glue to fix the DR to the ground plane. This is specified in the figure captions. A Silicon GE–glue was used.

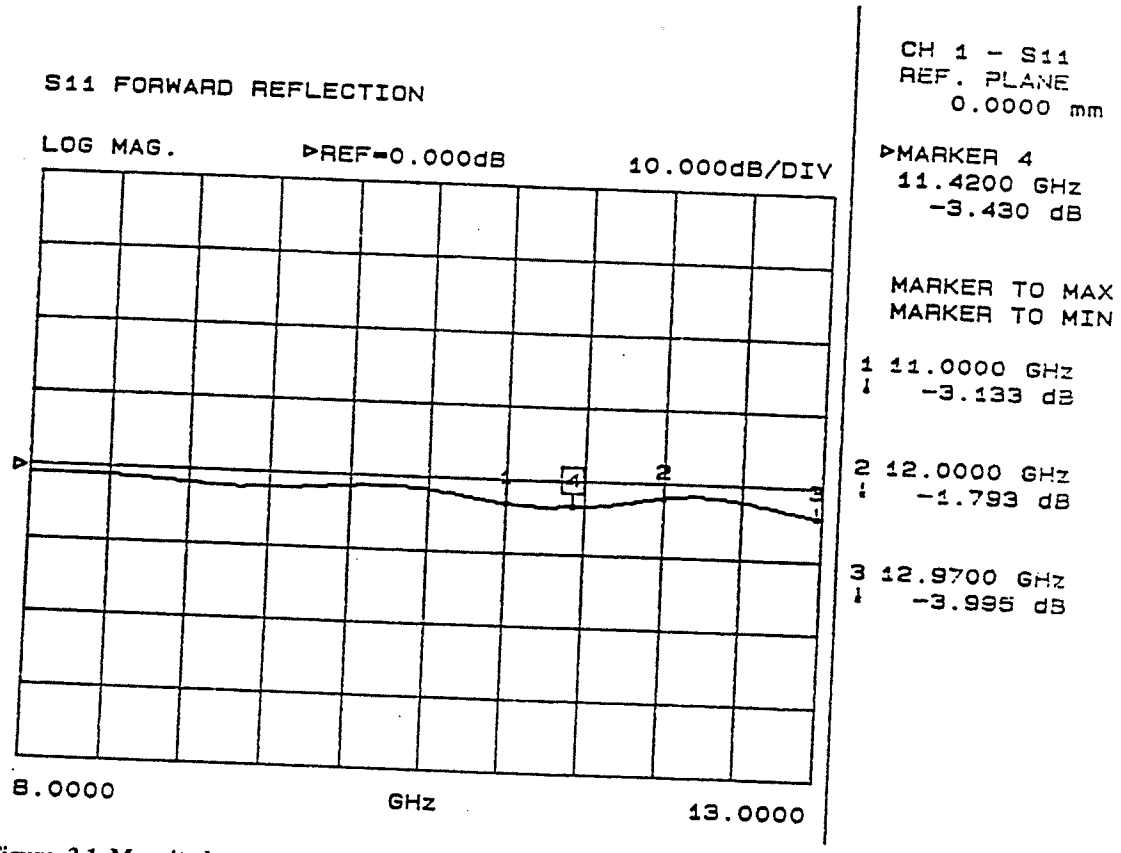

Figure 3.1 Magnitude measurement of reflection coefficient of the slot (without a DR) of
$w_{ap} = 0.1143cm$ $L_{ap} = 0.56cm$ $L_s = 0.6cm$

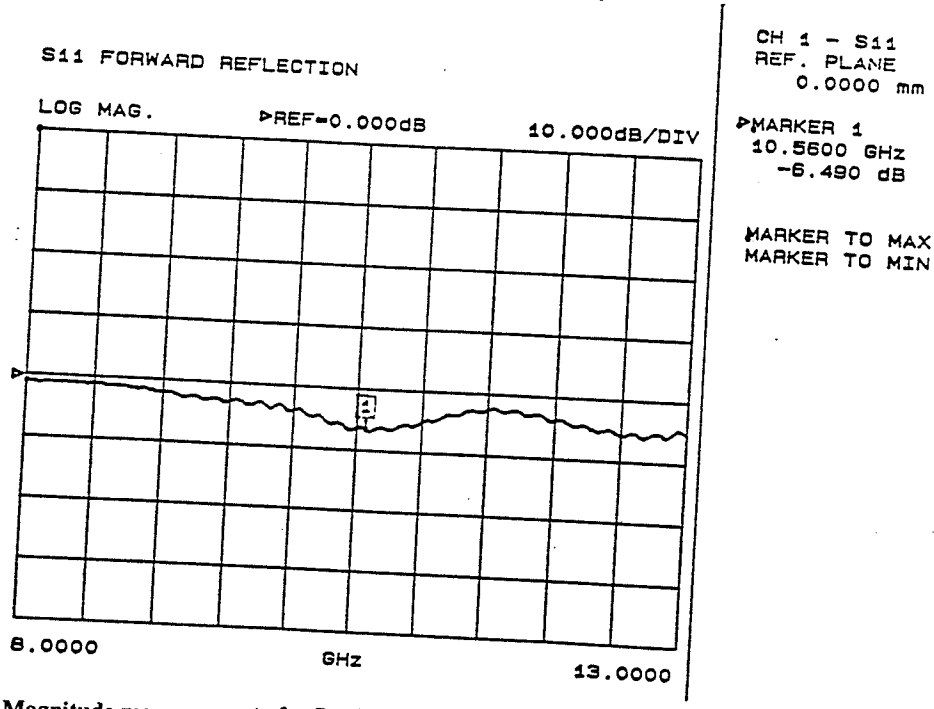

Figure 3.2 Magnitude measurement of reflection coefficient of the slot (without a DR) of
$w_{ap} = 0.188cm$ $L_{ap} = 0.686cm$ $L_s = 1.016cm$

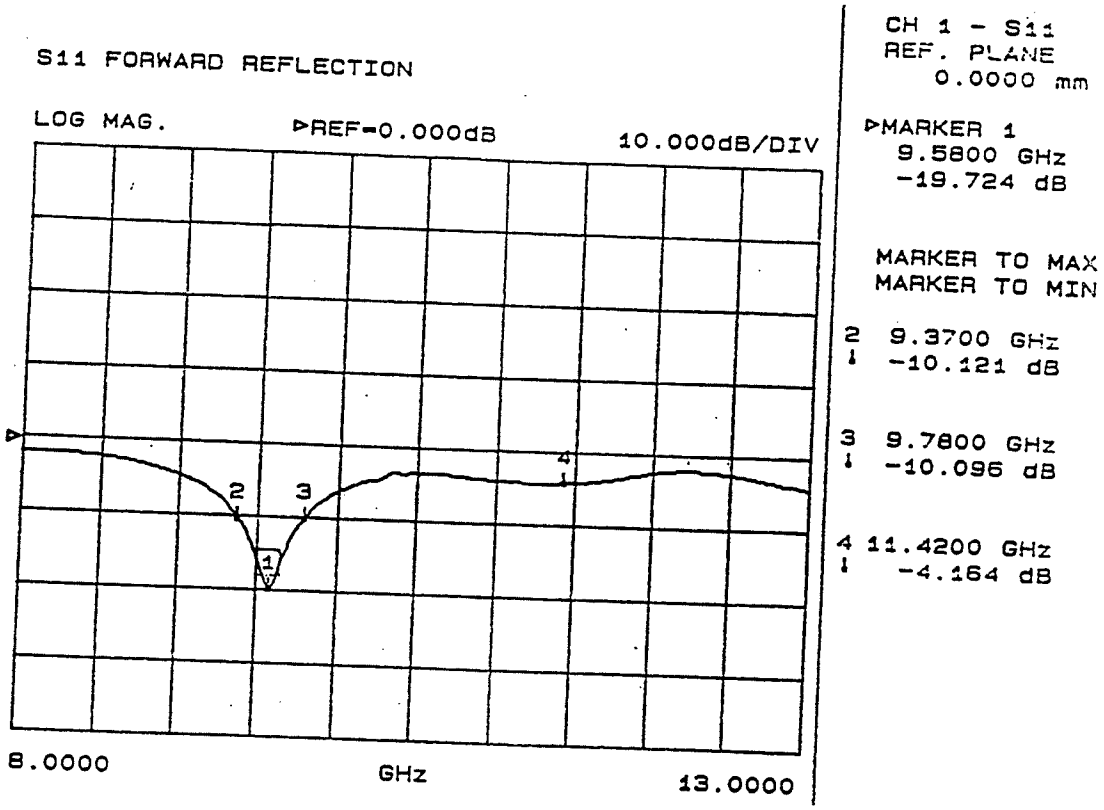

Figure 3.3 Magnitude measurement of reflection coefficient DRA (without glue)

$d = .804cm$, $h = .316cm$, $\varepsilon_{r_{DR}} = 10.5$, $w_{ap} = 0.1143cm$, $L_{ap} = 0.56cm$, $L_s = 0.6cm$

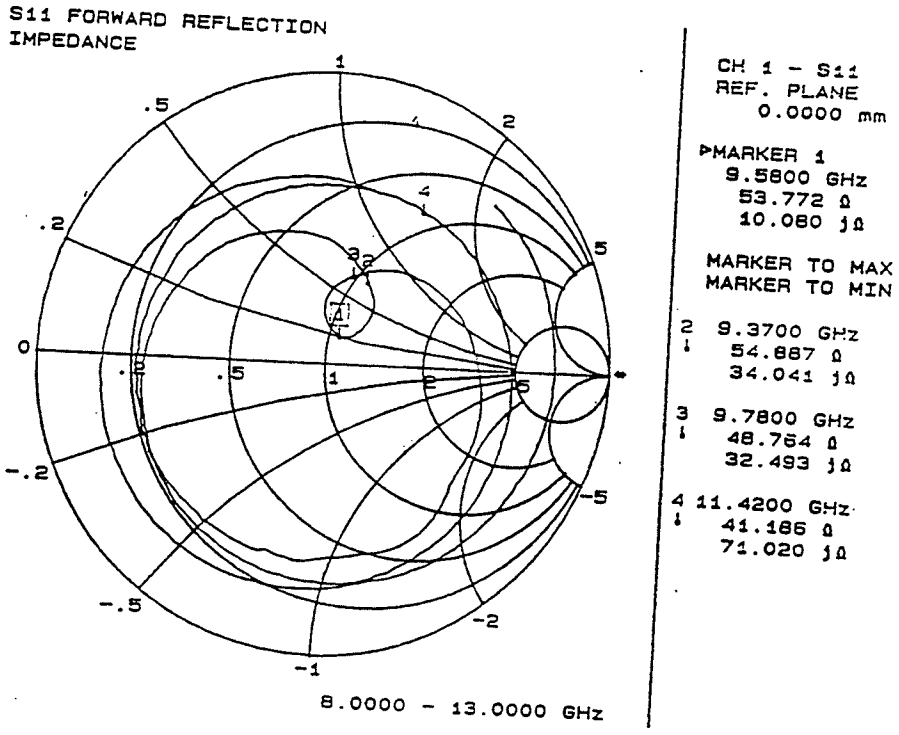

Figure 3.4 Phase measurement of reflection coefficient of DRA (without glue)

$d = .804cm$, $h = .316cm$, $\varepsilon_{r_{DR}} = 10.5$, $w_{ap} = 0.1143cm$, $L_{ap} = 0.56cm$, $L_s = 0.6cm$

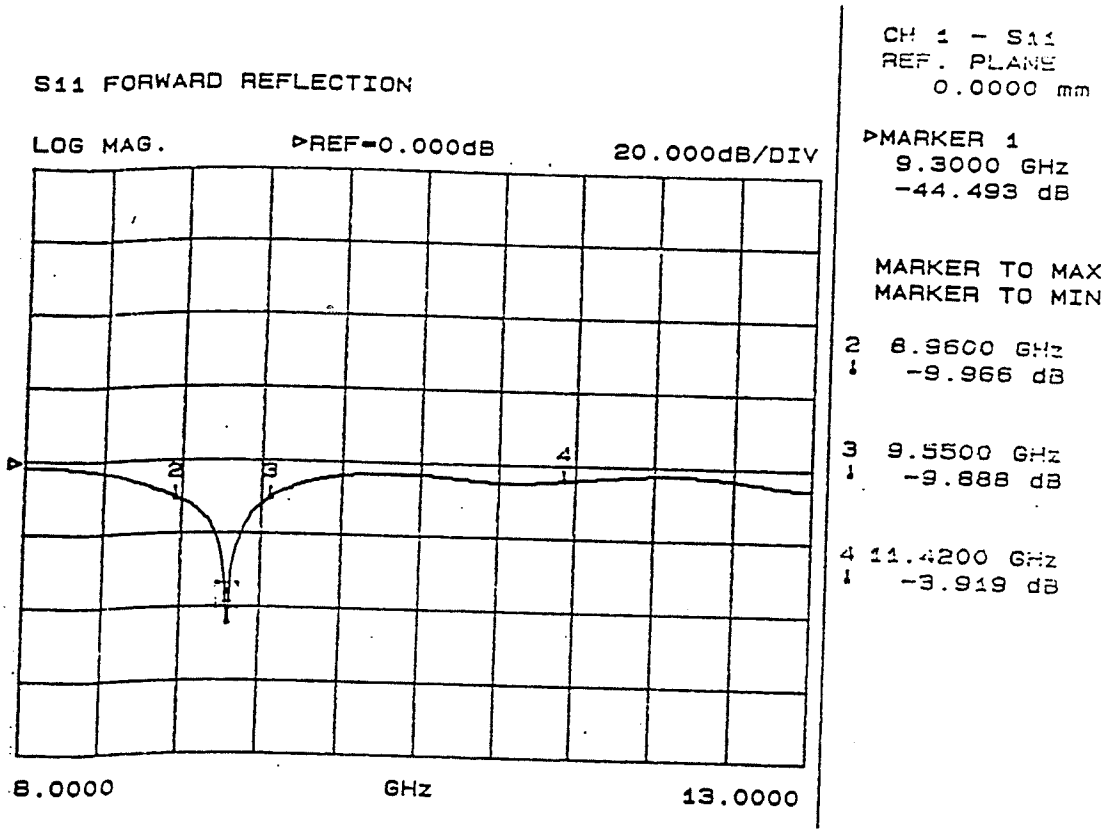

Figure 3.5 Magnitude measurement of reflection coefficient DRA (with a glue)

$d = .804cm$, $h = .316cm$, $\varepsilon_{r_{DR}} = 10.5$, $w_{ap} = 0.1143cm$, $L_{ap} = 0.56cm$, $L_s = 0.6cm$

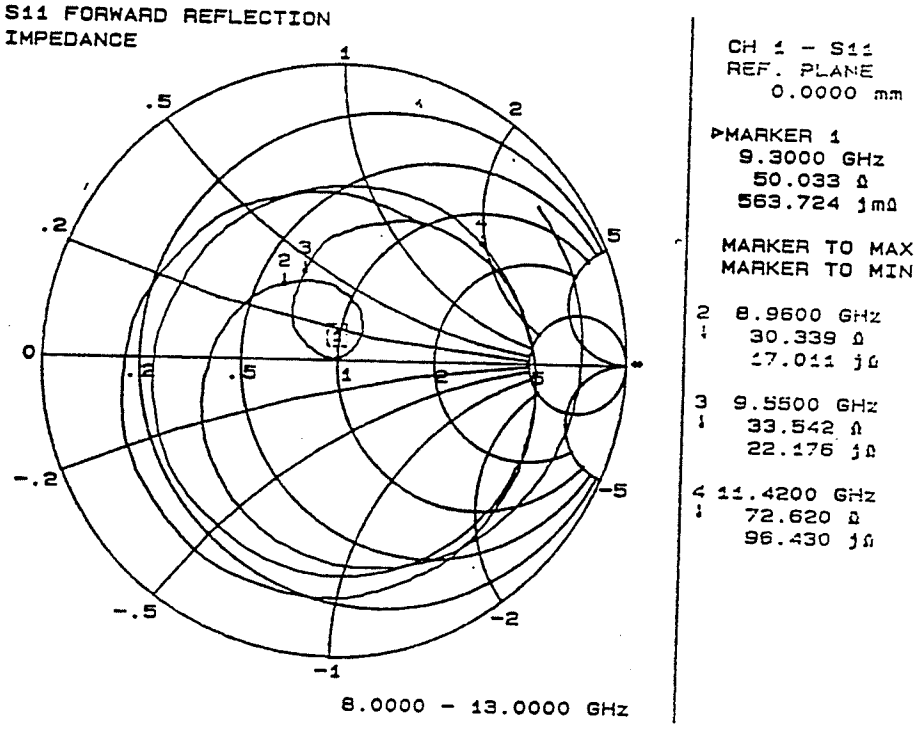

Figure 3.6 Phase measurement of reflection coefficient of DRA (with a glue)

$d = .804cm$, $h = .316cm$, $\varepsilon_{r_{DR}} = 10.5$, $w_{ap} = 0.1143cm$, $L_{ap} = 0.56cm$, $L_s = 0.6cm$

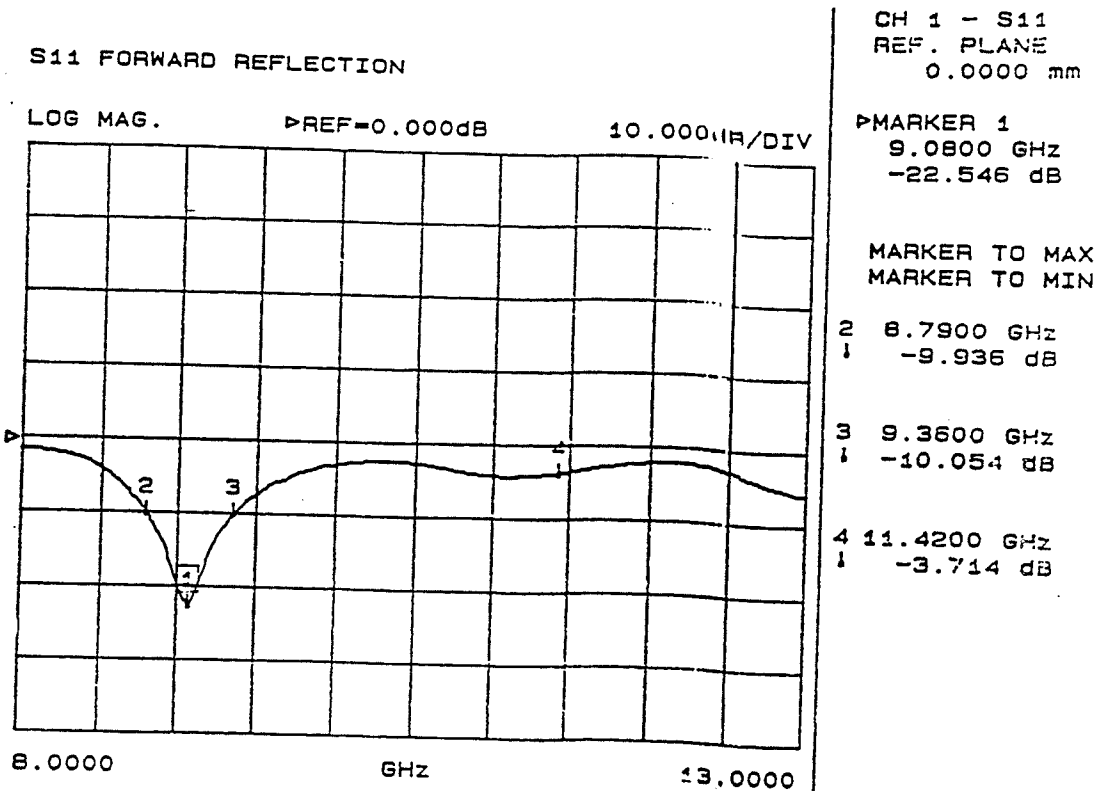

Figure 3.7 Magnitude measurement of reflection coefficient DRA (without glue)

$d = .92cm,\quad h = .314cm,\quad \varepsilon_{r_{DR}} = 10.5,\quad w_{ap} = 0.1143cm,\quad L_{ap} = 0.56cm,\quad L_s = 0.6cm$

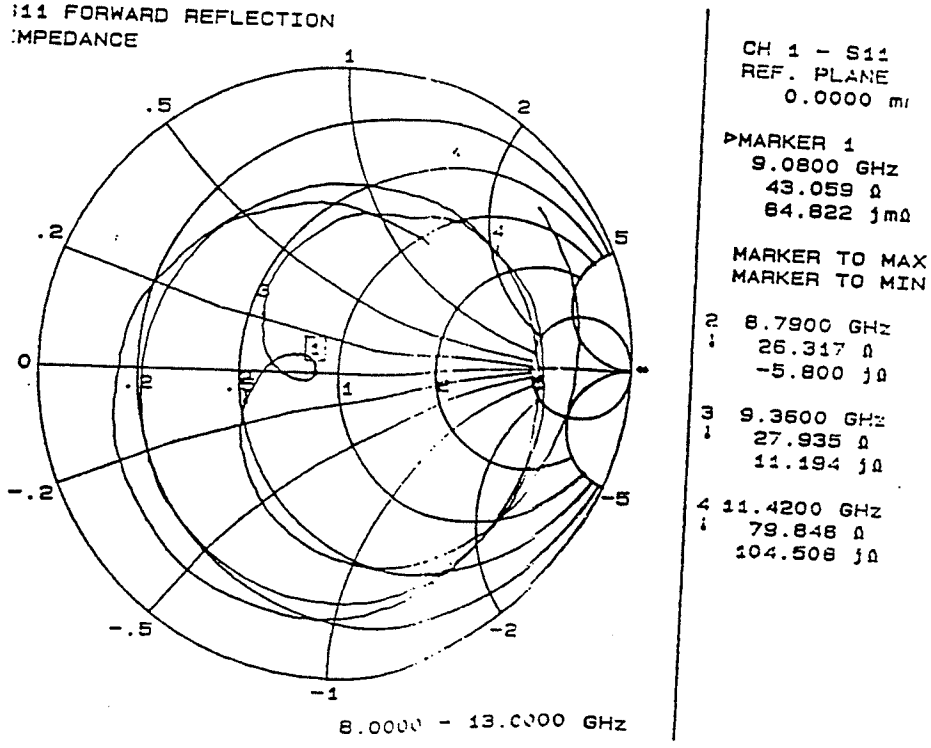

Figure 3.8 Phase measurement of reflection coefficient of DRA (without glue)

$d = .92cm,\quad h = .314cm,\quad \varepsilon_{r_{DR}} = 10.5,\quad w_{ap} = 0.1143cm,\quad L_{ap} = 0.56cm,\quad L_s = 0.6cm$

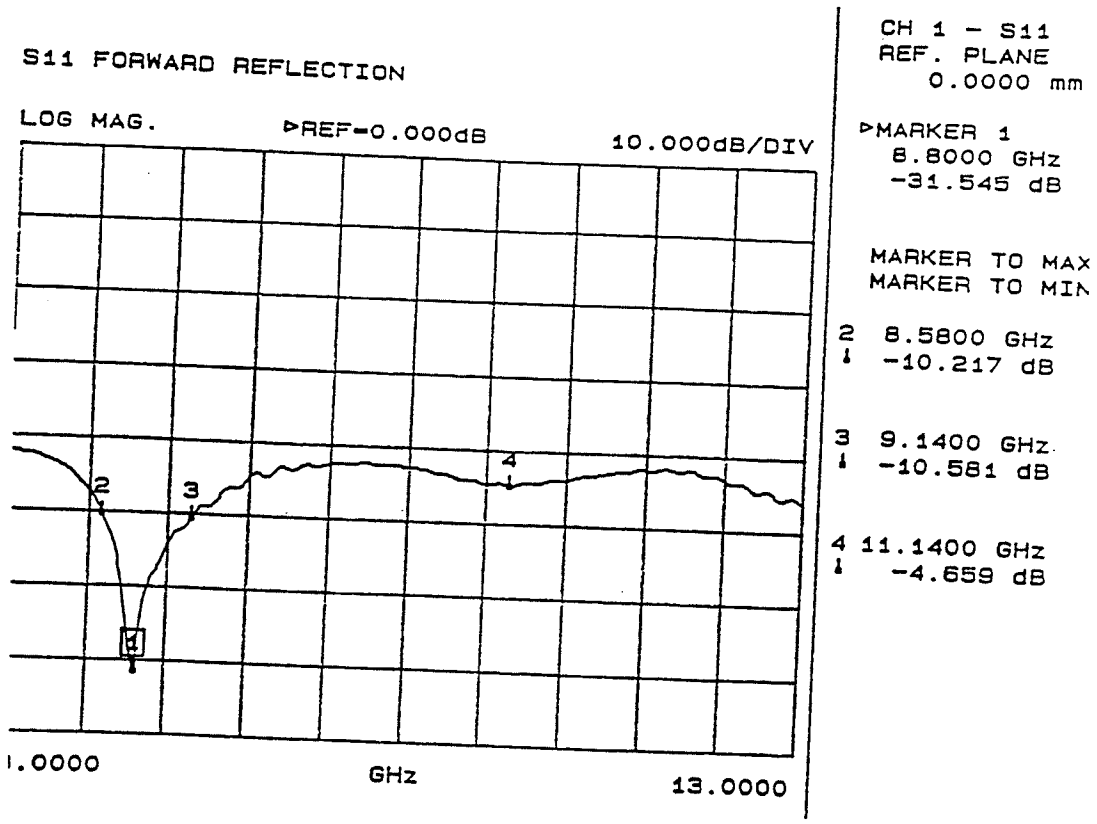

Figure 3.9 **Magnitude measurement of reflection coefficient DRA (with a glue)**
$d = .92cm,\quad h = .314cm,\quad \varepsilon_{r_{DR}} = 10.5,\quad w_{ap} = 0.1143cm,\quad L_{ap} = 0.56cm,\quad L_s = 0.6cm$

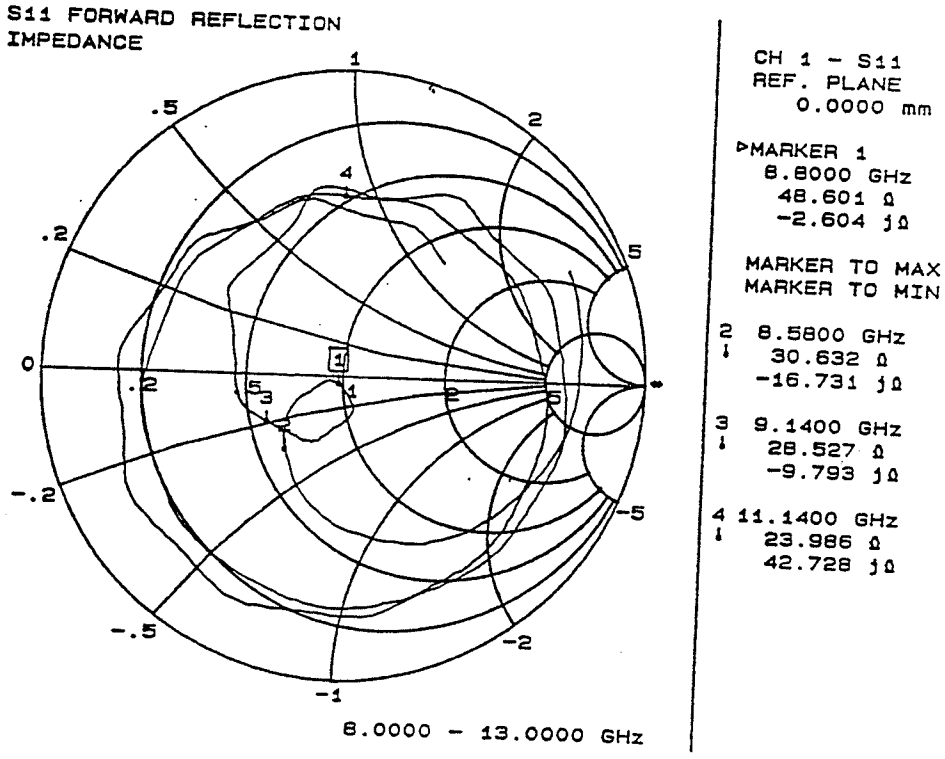

Figure 3.10 **Phase measurement of reflection coefficient of DRA (with a glue)**
$d = .92cm,\quad h = .314cm,\quad \varepsilon_{r_{DR}} = 10.5,\quad w_{ap} = 0.1143cm,\quad L_{ap} = 0.56cm,\quad L_s = 0.6cm$

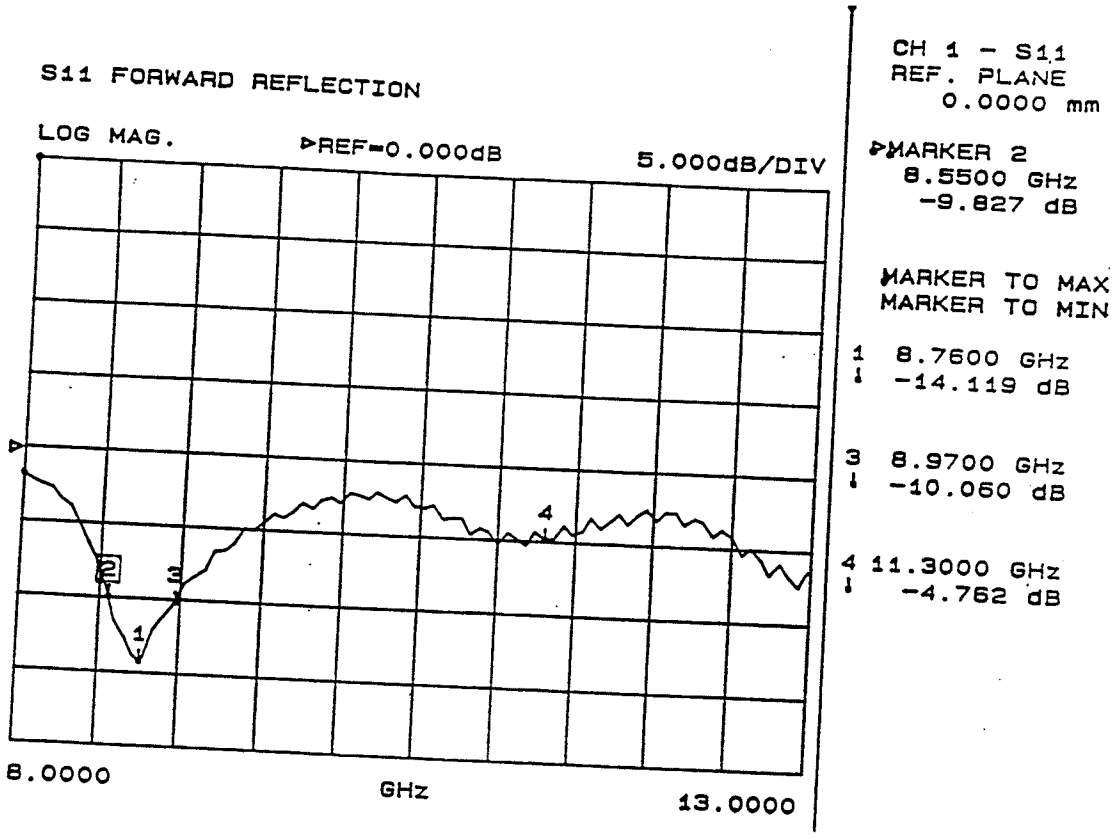

Figure 3.11 **Magnitude measurement of reflection coefficient DRA (without glue)**

$d = 1.cm,\ h = .314cm,\ \varepsilon_{r_{DR}} = 10.5,\ w_{ap} = 0.1143cm, L_{ap} = 0.56cm,\ L_s = 0.6cm$

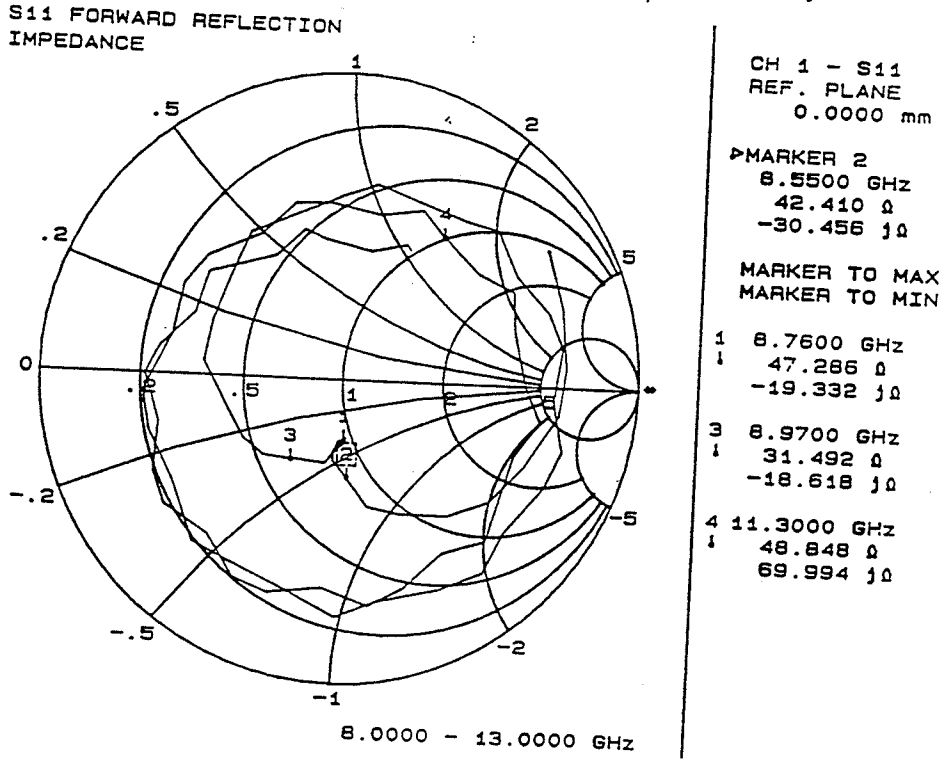

Figure 3.12 **Phase measurement of reflection coefficient of DRA (without glue)**

$d = 1.cm,\ h = .314cm,\ \varepsilon_{r_{DR}} = 10.5,\ w_{ap} = 0.1143cm, L_{ap} = 0.56cm,\ L_s = 0.6cm$

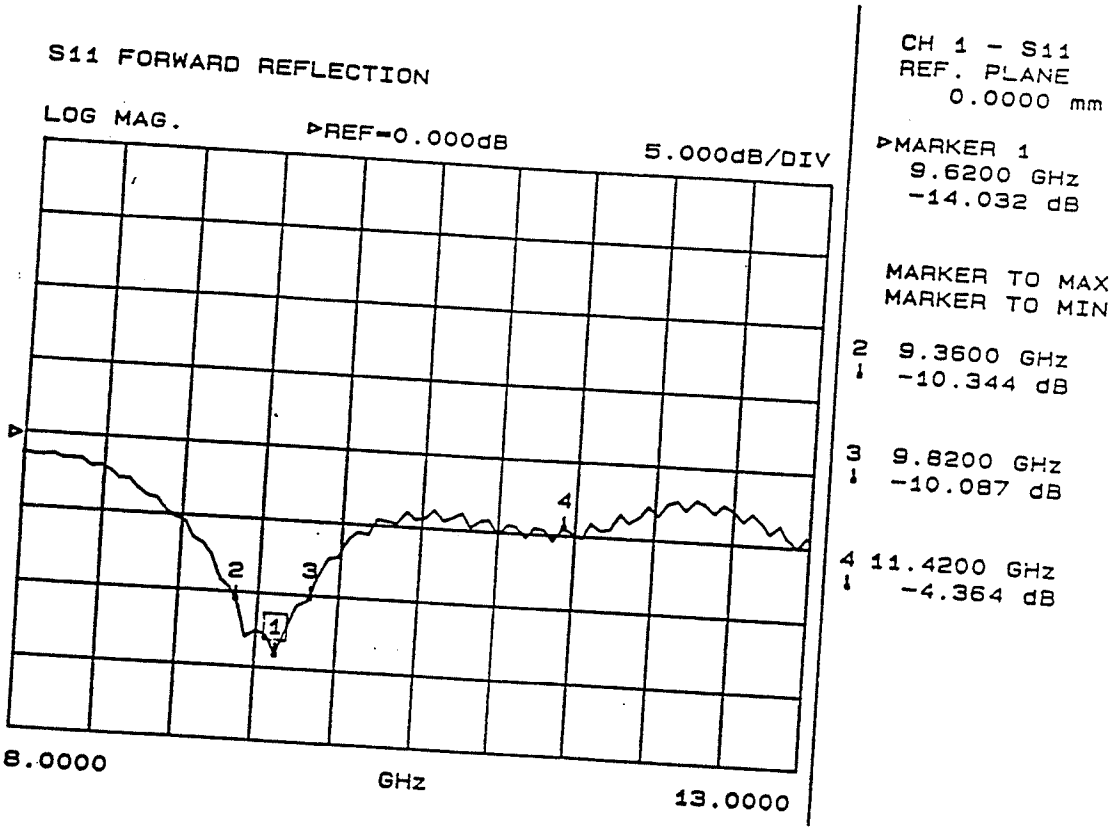

Figure 3.13 Magnitude measurement of reflection coefficient DRA (with a glue)

$d = 1.cm,\ h = .268cm,\ \varepsilon_{r_{DR}} = 10.2,\ w_{ap} = 0.1143cm, L_{ap} = 0.56cm,\ L_s = 0.6cm$

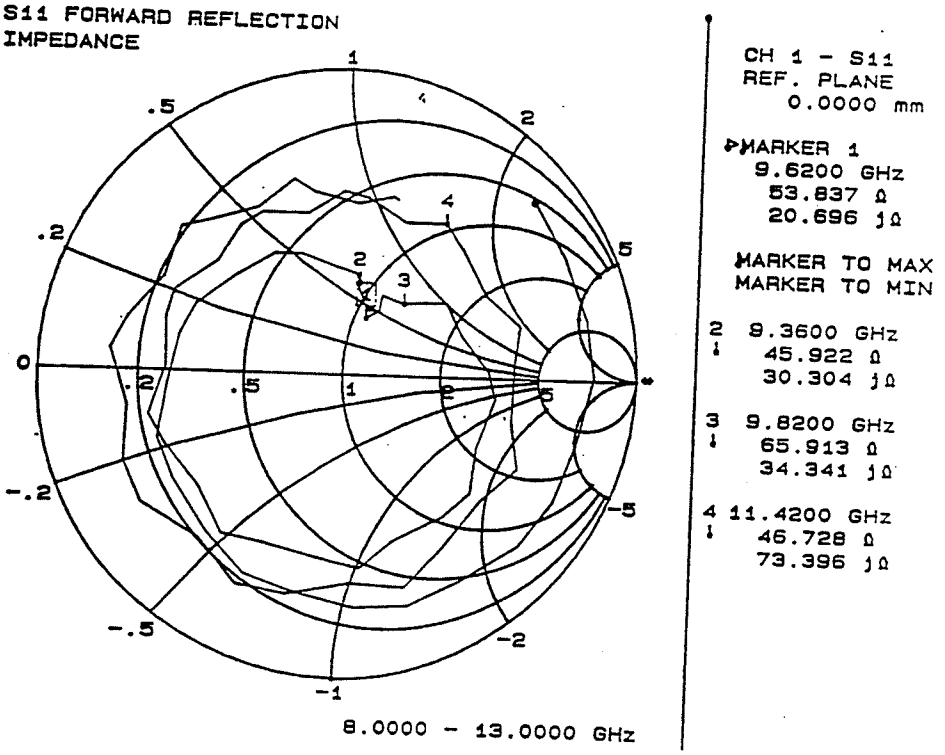

Figure 3.14 Phase measurement of reflection coefficient of DRA (with a glue)

$d = 1.cm,\quad h = .268cm,\ \varepsilon_{r_{DR}} = 10.2,\ w_{ap} = 0.1143cm,\ L_{ap} = 0.56cm,\ L_s = 0.6cm$

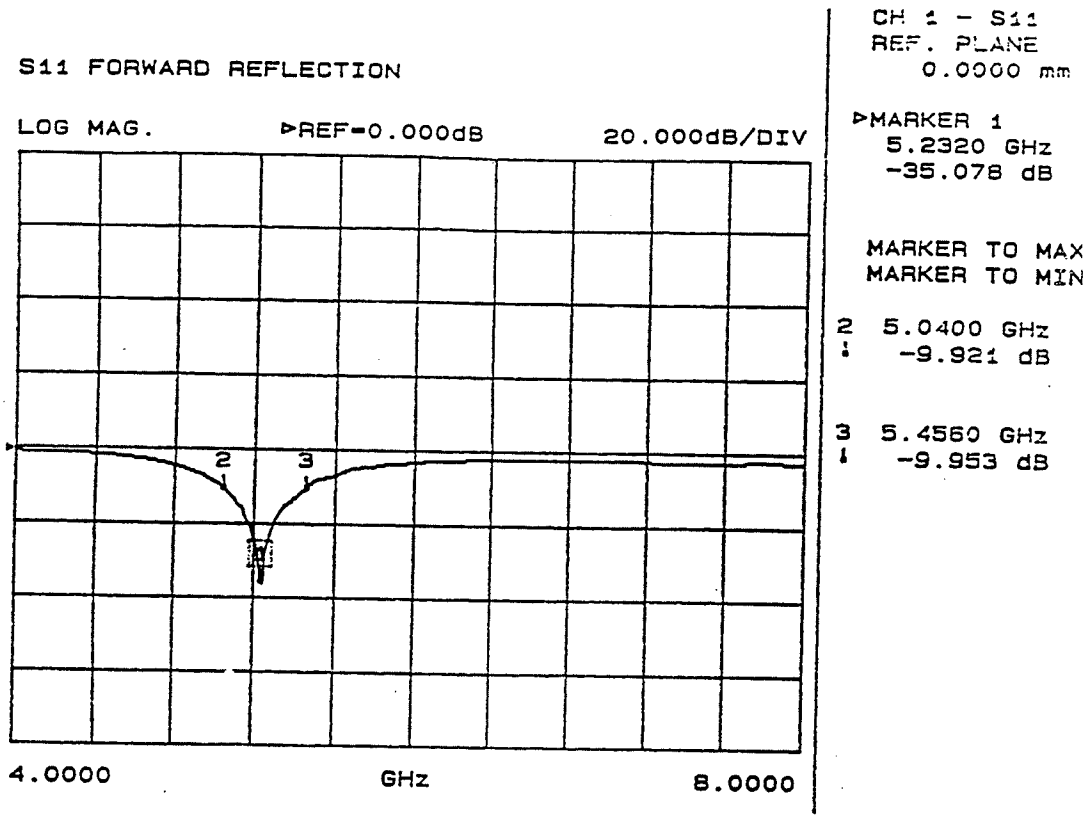

Figure 3.15 **Magnitude measurement of reflection coefficient of DRA (with a glue)**

$d = 1.6cm$, $h = .642cm$, $\epsilon_r = 10.5$, $w_{ap} = 0.188cm$, $L_{ap} = 0.686cm$, $L_s = 1.016cm$

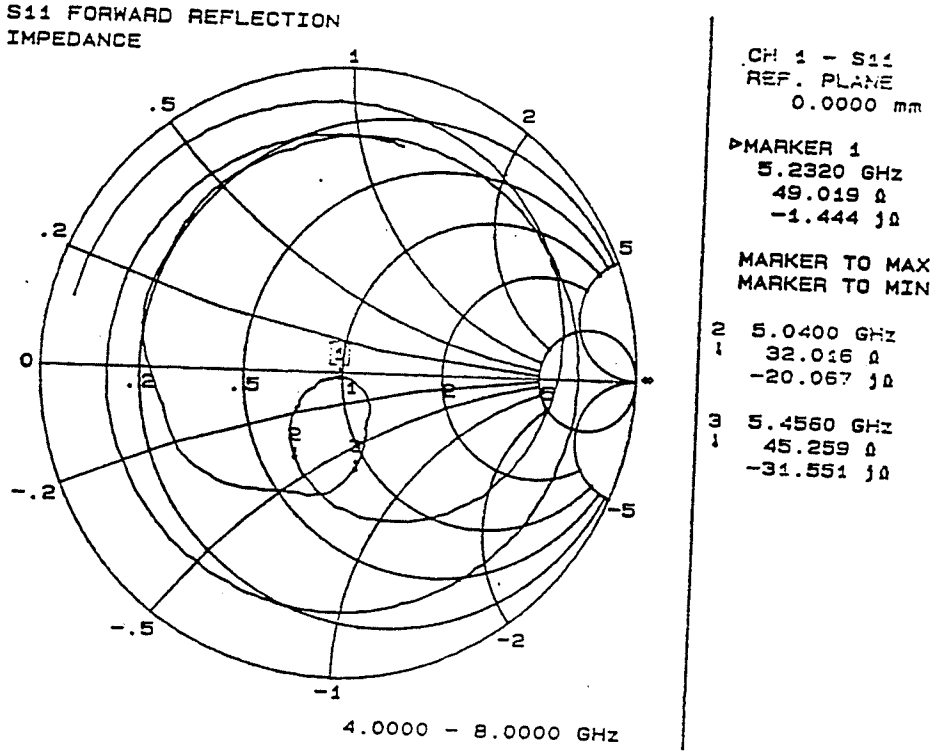

Figure 3.16 **Phase measurement of reflection coefficient of DRA (with a glue)**

$d = 1.6cm$, $h = .642cm$, $\epsilon_r = 10.5$, $w_{ap} = 0.188cm$, $L_{ap} = 0.686cm$, $L_s = 1.016cm$

Table 3.4 The measured and computed resonant frequency for various DRA

d (cm)	h (cm)	$\varepsilon_{r_{DR}}$	Frequency (Ghz) Mongia Formulas	Frequency (Ghz) DWM	Frequency (Ghz) Measured
0.804	0.316	10.5	10.77	10.02	9.58
0.92	0.314	10.5	10.10	9.59	9.08
0.996	0.314	10.5	9.75	9.2	8.76
1.2	0.315	10.5	8.97	8.47	7.712
1.0	0.268	10.2	10.81	10.21	9.62

Table 3.4 tabulates the results of Figs. 3.3, 3.7, 3.11 and 3.13. As it can be seen from Fig. 3.1 to Fig 3.13 and Table 3.4. The value of the resonant frequency found experimentally is less than the ones predicted theoretically. The theoretical results which are based on the dual dielectric waveguide model for the DR are found to be 4.3% to 5.8% higher than the experimental results. This is as expected due to the following reasons:

1– The calculated resonant frequency does not take into consideration the losses, namely, the dielectric loss inside the DR, the conduction loss in the ground plane, and the radiation loss through the dielectric/air interference. These losses have the effect of lowering the resonant frequency of the antenna.

2– The calculated resonance frequency was obtained for in isolated DR and not for a DR sitting on a ground plane and is loaded slightly by the slot. This would have the effect of lowering the experimental value of the resonant frequency as compared to the theoreti–cal value.

3– Another factor that may cause a change in the resonant frequency is the existence of the air gap between the DR and the ground plane, which will cause an increase in the value of the resonant frequency.

4– An important factor is the tuning stub length of the feedline. If it is not exactly equal to one fourth of the microstrip guided wavelength it pulls the resonant frequency down. This occurs because of the unmatching condition.

Table 3.5 Measured resonant frequency, bandwith, return loss and the Input Impedance for various DRA

	Samples	d (cm)	h (cm)	ϵ_{rDR}	Frequency Ghz	Bandwidth %	Return Loss dB	Input Impedance Ω
without the Glue	DR_1	0.804	0.316	10.5	9.58	4.3	–19.724	53.77 + j10.08
with the Glue	DR_1	0.804	0.316	10.5	9.30	6.34	–44.49	50.033 + j0.56
without the Glue	DR_2	0.92	0.314	10.5	9.08	6.28	–22.546	43.059 + j0.84
with the Glue	DR_2	0.92	0.314	10.5	8.80	6.36	–31.545	48.601–j2.604
with out the Glue	DR_3	0.996	0.314	10.5	8.76	4.79	–14.119	42.4 – j30.45
with the Glue	DR_4	1.0	0.268	10.2	9.62	4.78	–14.032	53.8 + j 20.696

Table 3.5 tabulates the experimental results for the input impedance, the bandwidth for a level at 10 dB, the magnitude of the return loss of the designed DRAs. Also, this table shows the effect of using glue to affix the DR to the ground plane on the parameters of the DRA. The dielectric resonator antennas DR_1 and DR_2 have an input impedance that is near 50 Ω. This was expected since the dimension and the dielectric constant of these two resonators (Table 3.1 and Table 3.3) yields a resonance frequency that is close to the one chosen for the stub length of the feedline (9.4 GHz). For the radiation pattern measurement, the DR has to be affixed to the ground plane. As can be observed from table 3.5, the glue provides a better coupling of the feedline to the DR and shifts the resonant frequency of the antenna to a 3% lower value. This may be due to the partial elimination of the air gap that existed between the DR and the ground plane when they were not affixed and also due to the slight change of the height of the DR when putting the glue on its surface.

The bandwidth of an antenna is defined as the frequency range in which the reflected power is below a specified level. As shown in Table 3.5, the bandwith of each different DRA

is much wider then the bandwith of a microstrip antenna which is (1% to 2%).

Two identical cylindrical DRs made of $\varepsilon_{r_{DR}} = 10.5$ with dimension $h = 0.3175\ cm$ and $d = 1.592\ cm$ were stacked on top of each other to provide an aperture coupled DR antenna that resonates near 5.5 GHz. The experimental results for the resonant frequency and for the input impedance of this antenna are shown in Fig.3.15 and Fig. 3.16, respectively. The measured resonant frequency of this antenna is found to be 3.91% higher than the one predicted using the dielectric waveguide model. This is in contrast to the result obtained previously in table 3.4, where the experimented resonant frequency was expected to be lower than the theoretical one for the reasons mentioned in the previous section. Here, the increase in resonant frequency is due to the fabrication process of this stacked DR, namely the air gap and the glue that exists between the two element of the DR, which may perturb the resonance of the DR. One important feature of this antenna is its bandwidth which was found to be 8.0 %. This was higher than those obtained using a single DR.

3.7 Radiation Pattern Measurement of DRA

This section examines experimentally the radiation pattern of an aperture coupled dielectric resonator, and compares the experimental results to those predicted theoretically using the dual dielectric waveguide model (DWM) and the magnetic wall model (MWM). Pattern measurements were performed on the samples which provide the best matching conditions that were available as from Table 3.4. The constructed antennas had initial rectangular ground plane of dimensions of 10 cm by 10 cm, however, for radiation pattern measurements these antennas were placed on top of a circular ground plane extender of diameter 34 cm. All the measured radiation patterns were performed in an anechoic chamber. The anechoic chamber was first calibrated in the X band range (8 Ghz to 12 Ghz) using a standard horn antenna. The measured radiation patterns were obtained in both planes of interest, namely the E–plane and the H–plane which were defined previously in Chapter 2.

Fig. 3.17, shows the measured radiation patterns in both the E–plane and H–planes for a dielectric resonator antenna of dielectric constant $\varepsilon_{r_{DR}} = 10.5$, height $h = 0.316\ cm$ and diameter $d = 0.804\ cm$. This was DR_1 in tables 3.1 and 3.5. This DR is fed by an aperture of length $L_{ap} = 0.56\ cm$ and width of $w_{ap} = 0.12\ cm$. The measured resonant frequency of this configuration was 9.3 GHz. Also plotted in the figure are the theoretical radiation patterns using the MWM and DWM models for the same DR antenna. Fig. 3.18 shows the measured radiation patterns at a frequency of 9.42 GHz. Plots for the measured pattern at different frequencies are shown in Appendix A. By examining Fig.17, the theoretical and the experimental results compares quite well, given the fact that the theory assumes the presence of an infinite ground plane and thus does not take into consideration the edge effects of the finite size ground plane. The ground plane edge effects is shown to be strong for this type of antenna especially near $\theta = 90^{o}$. This effect is described in [36], and is due to the diffraction at the discontinuity of the ground plane edge where surface currents will be formed and interfere with the main antenna radiation pattern causing some scalloping and roll–off of the measured pattern.

The experimental and theoretical radiation patterns for another dielectric resonator of dielectric constant $\varepsilon_{r_{DR}} = 10.5$, height $h = 0.316\ cm$ and diameter $d = 0.92\ cm$, which was fed by an aperture of the same dimension as the one used for the previous DR are plotted in Fig. 3.19. This corresponds to DR_2 in tables 3.1 and 3.5. Again, by taking into consideration the effect of ground plane, good agreement between the computed and the measured data is observed. The effect of the edge diffraction is also present in this measurement. Fig. 3.20 shows the measured radiation pattern of this antenna for a frequency 8.86 GHz. Other plots of the measured pattern of this antenna at different frequencies are shown in Appendix A.

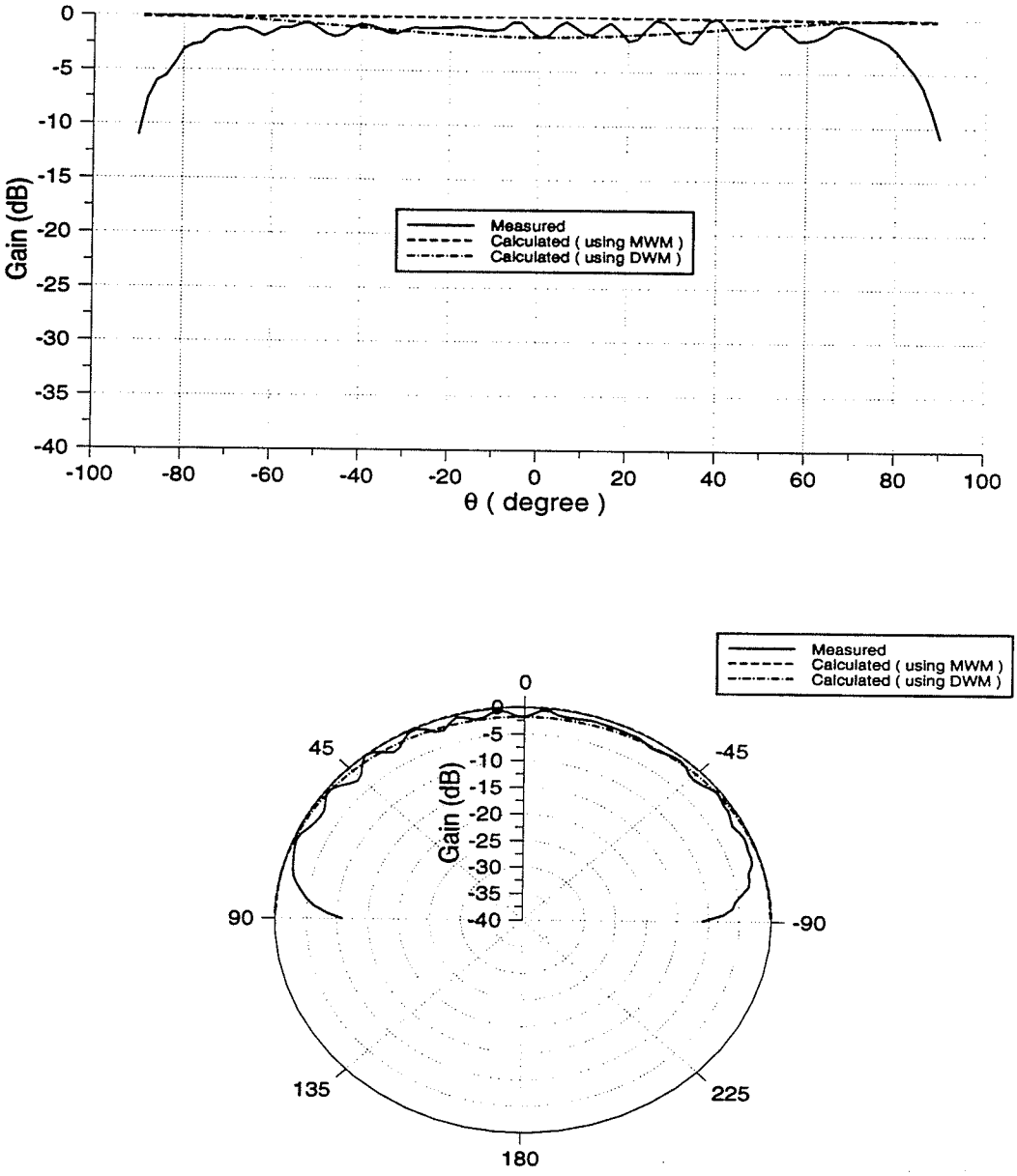

(a)

Figure 3.17 Theoretical and experimental radiation pattern for DRA (a) E–plane., (b) H–plane.
$d = .804cm$, $h = .316cm$, $\varepsilon_{r_{DR}} = 10.5$, $w_{ap} = 0.12cm$, $L_{ap} = 0.56cm$, $L_s = 0.6cm$

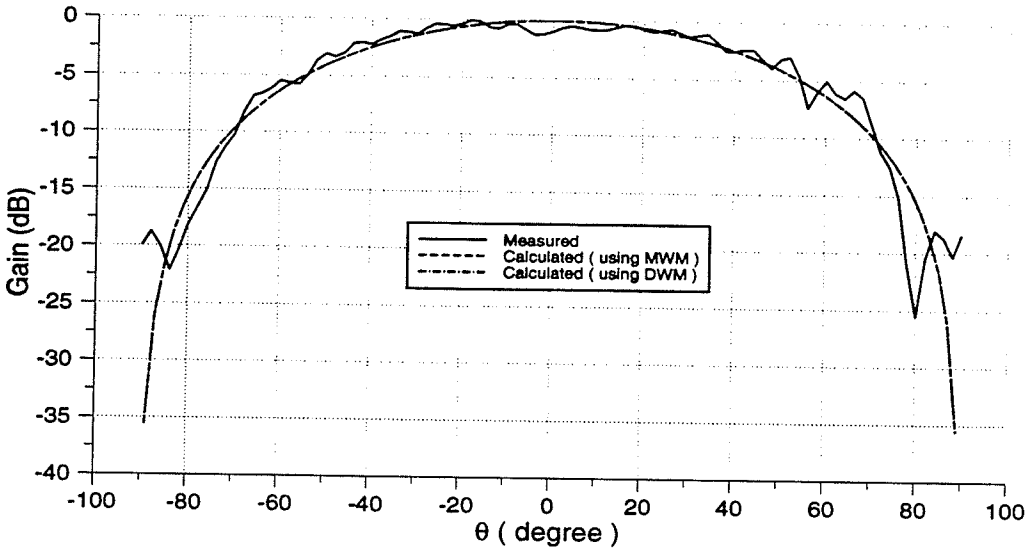

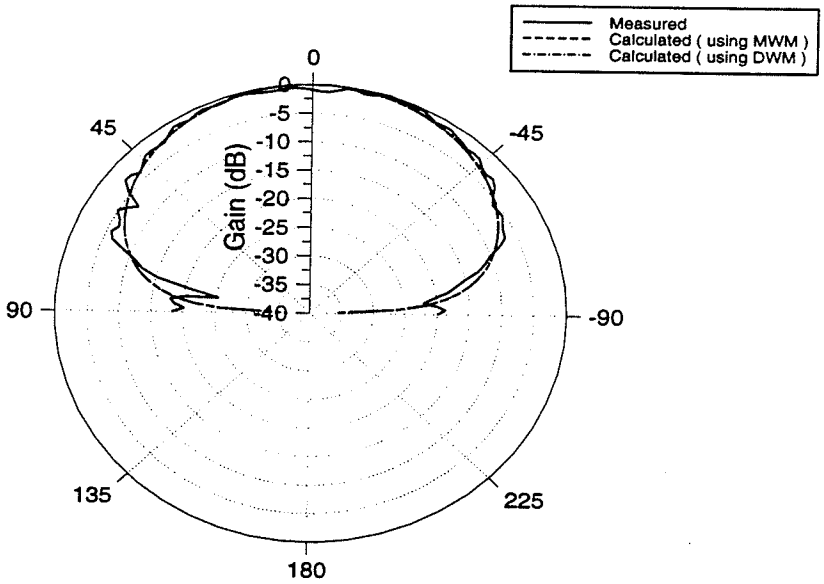

(b)

Figure 3.17 Theoretical and experimental radiation pattern for DRA (a) E–plane, (b) H–plane.
$d = .804cm,\ h = .316cm,\ \varepsilon_{r_{DR}} = 10.5,\ w_{ap} = 0.12cm,\ L_{ap} = 0.56cm,\ L_s = 0.6cm$

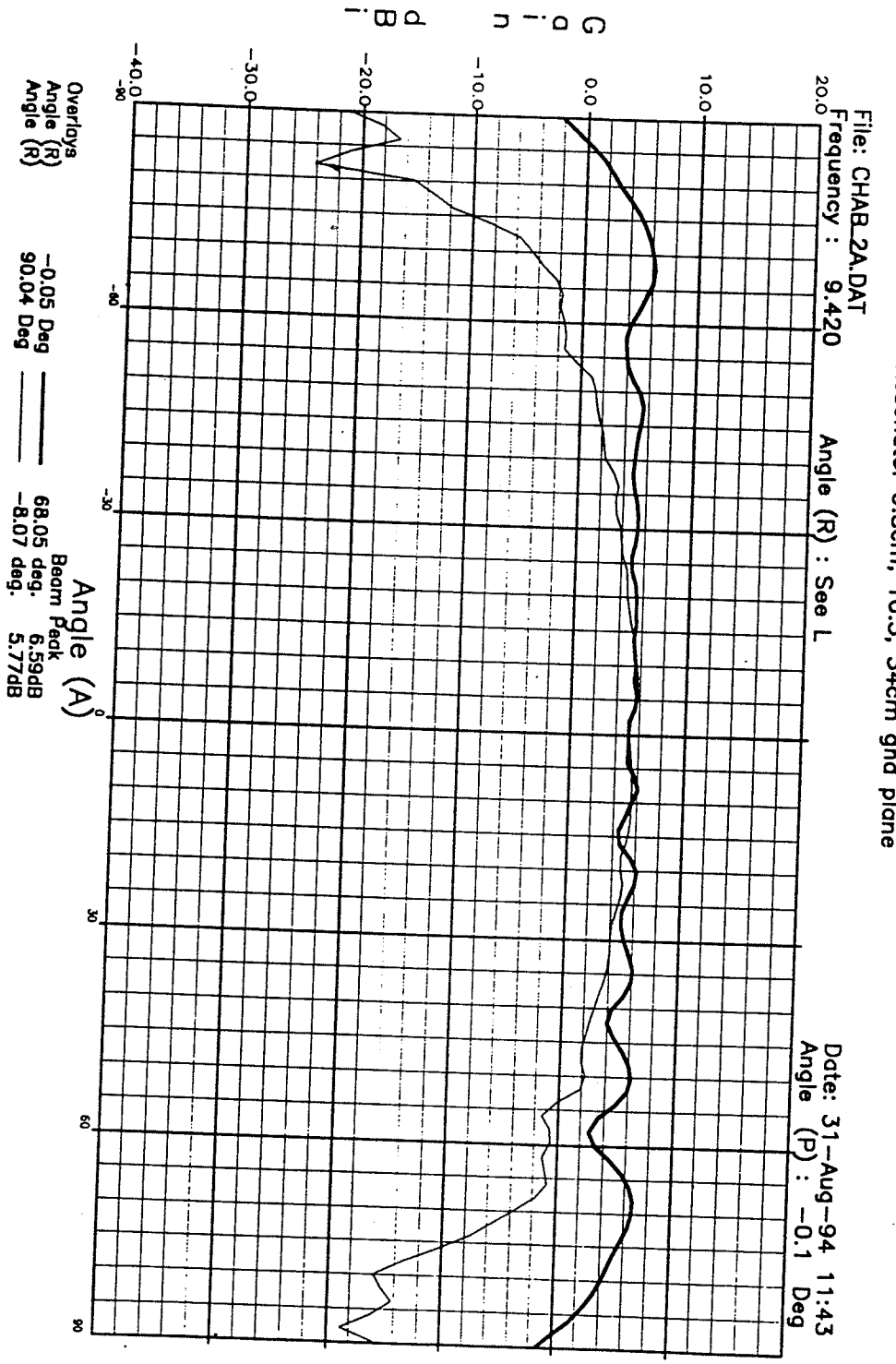

Figure 3.18 Measured radiation pattern for DRA at frequency 9.4 Ghz.
$d = .804cm$, $h = .316cm$, $\varepsilon_{r_{DR}} = 10.5$, $w_{ap} = 0.12cm$, $L_{ap} = 0.56cm$, $L_s = 0.6cm$

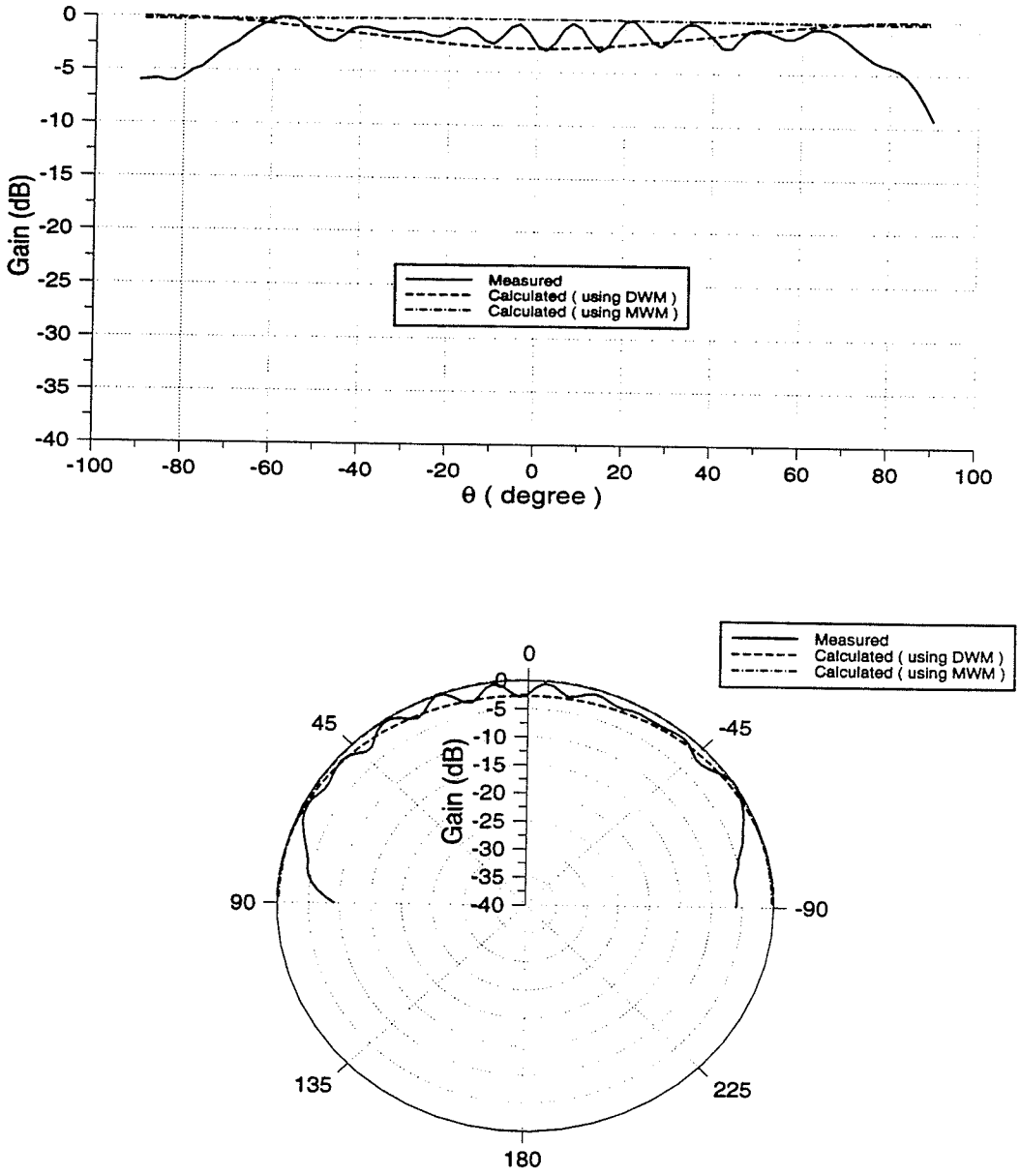

(a)

Figure 3.19 Theoretical and experimental radiation pattern for DRA (a) E–plane, (b) H–plane.

$d = .92cm$, $h = .316cm$, $\varepsilon_{r_{DR}} = 10.5$, $w_{ap} = 0.12cm$, $L_{ap} = 0.56cm$, $L_s = 0.6cm$

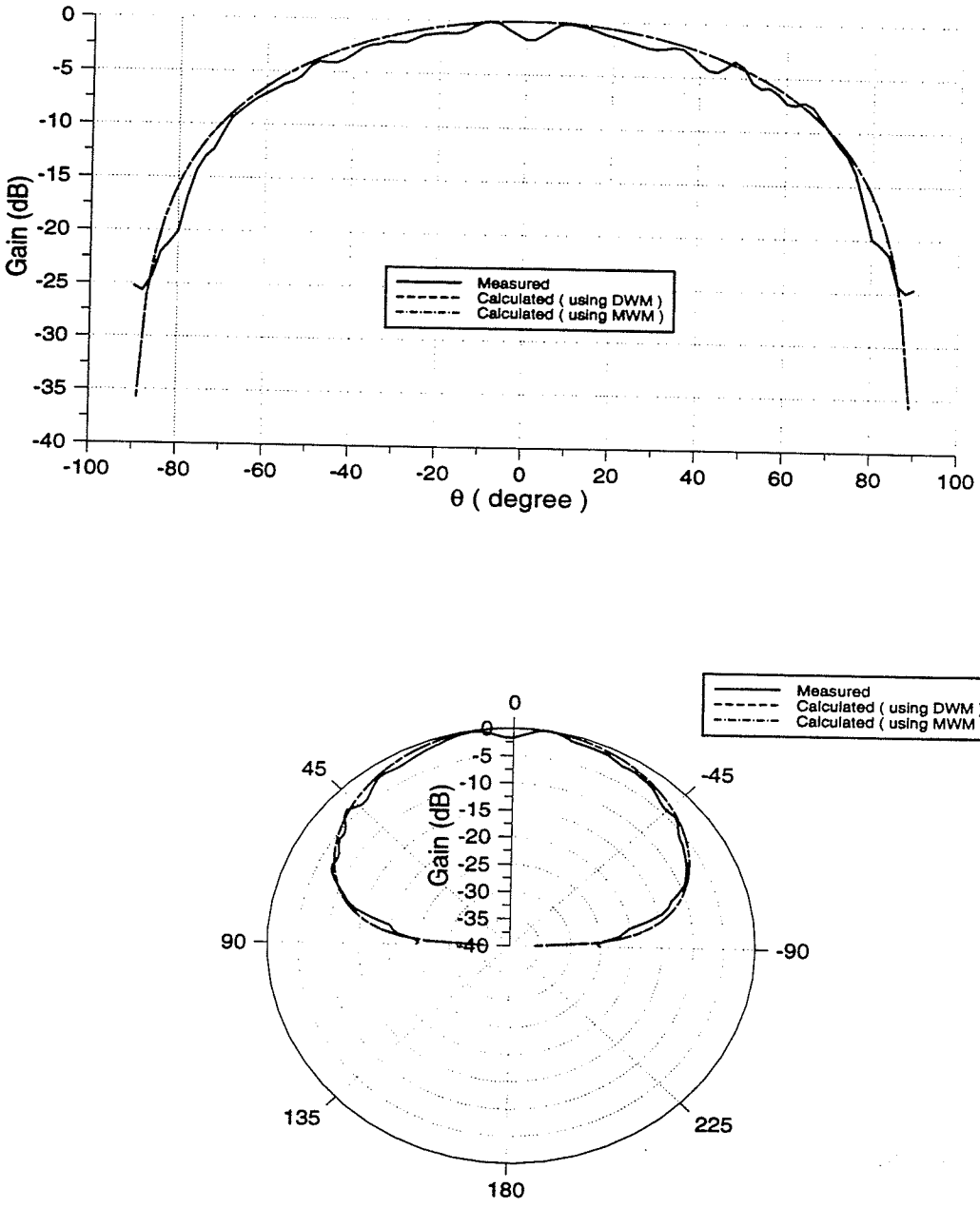

(b)

Figure 3.19 Theoretical and experimental radiation pattern for DRA (a) E–plane, (b) H–plane.

$d = .92cm$, $h = .316cm$, $\varepsilon_{r_{DR}} = 10.5$, $w_{ap} = 0.12cm$, $L_{ap} = 0.56cm$, $L_s = 0.6cm$

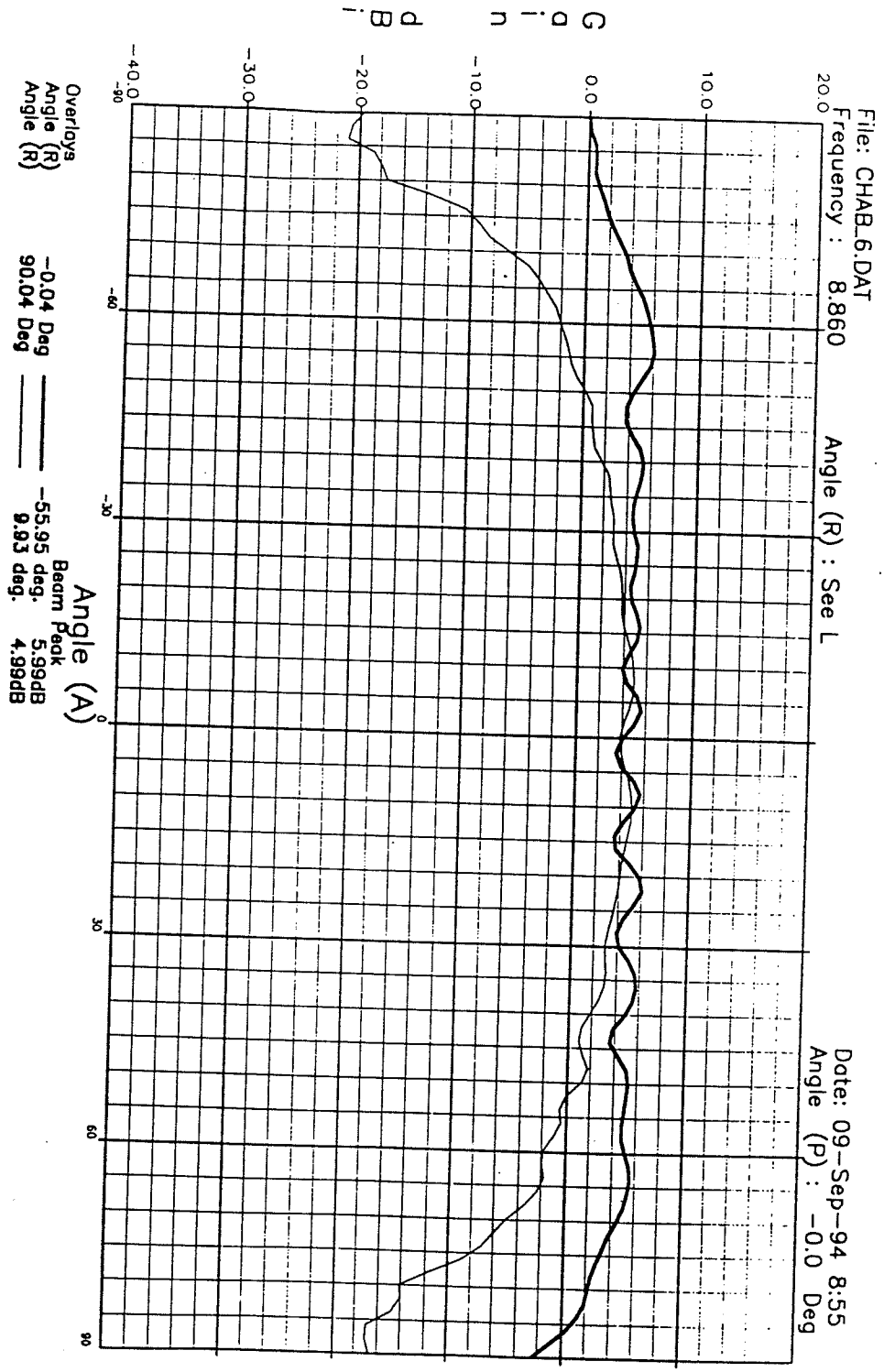

Figure 3.20 Measured radiation pattern for DRA at frequency 9.4 Ghz.

$d = .92cm$, $h = .316cm$, $\varepsilon_{r_{DR}} = 10.5$, $w_{ap} = 0.12cm$, $L_{ap} = 0.56cm$, $L_s = 0.6cm$

3.8 Gain Measurement of the DRA

The power gain of an antenna describes its performance. It takes into account the efficiency as well as the directional capabilities of the antenna. Also, it gives an indication of the operational pattern bandwidth of the antenna. The maximum power gain in the E–plane and the H–plane of a dielectric resonator antenna of $\varepsilon_{r_{DR}} = 10.5$, $h = 0.316\ cm$ and $d = 0.804\ cm$ is shown as function of frequency in Fig. 3.21. This plot was obtained by marking the maximum gain at each tested frequency of the measured radiation pattern of the antenna. It can be seen from this plot that pattern bandwidth is fairly broad. However, this graph can be misleading given the fact that it only takes into consideration the maximum location of the pattern of the tested antenna which was corrupted by the effects of the finite size of the ground plane.

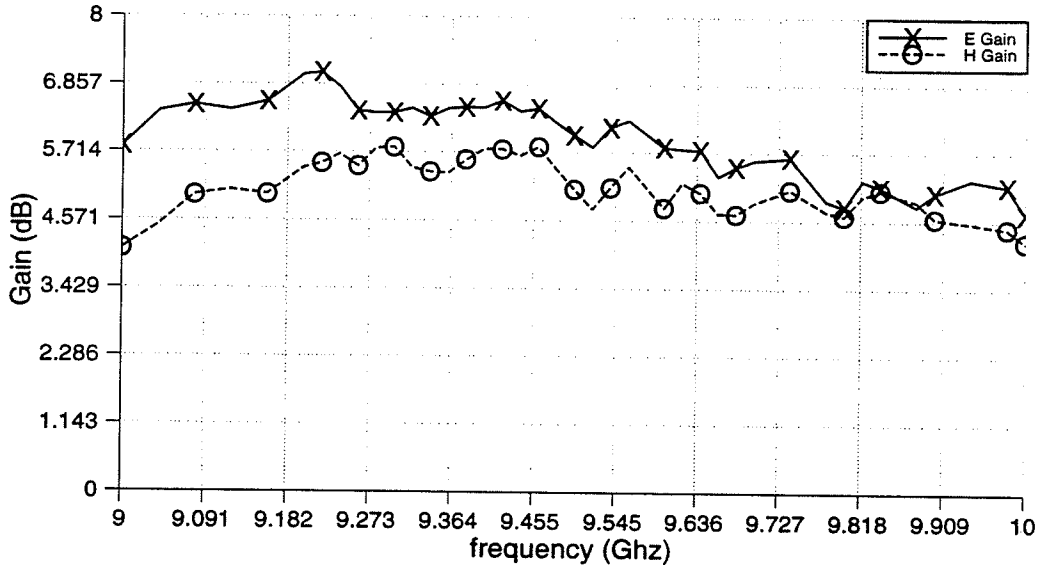

Figure 3.21 The measured maximum gain versus frequency for an aperture–coupled cylindrical DRA

$d = .92cm$, $h = .316cm$, $\varepsilon_{r_{DR}} = 10.5$, $w_{ap} = 0.12cm$, $L_{ap} = 0.56cm$, $L_s = 0.6cm$

CHAPTER 4

4.1 Conclusion

Dielectric resonators (DRs) seem to be very promising radiating elements which can be used in antennas that operate in the *mm* wave band and can be integrated with microwave integrated circuits (MIC). A theoretical and experimental investigation has been presented where an aperture–coupled cylindrical dielectric resonator antenna excited at the $HEM_{11\delta}$ dominant mode has been analyzed. The analysis method, which is based on modelling dielectric resonator as a dual dielectric waveguide, was introduced to calculate the dielectric resonator antenna properties. The investigated antenna properties in this thesis include the resonant frequency, far fields, near fields, and the radiated quality factor Q. The results obtained using the suggested dual dielectric waveguide model (DWM) for the DR are comparable to those of empirical and numerical methods found in the literature, and are far better than the results found by the use of a simple magnetic wall model for the DR.

To confirm the obtained theoretical results for the resonant frequency and the radiation pattern of the antenna experimental measurement have been conducted. Several dielectric resonator antennas were designed, fabricated, and tested in the frequency range of 8 to 10 GHz and in the range of 5 to 6 GHz. The measured results are in excellent agreement with the results obtained theoretically using the developed dual dielectric waveguide model for the DR.

4.2 Recommendation

The dielectric resonator antenna technology is still in its infancy and, therefore, there is a lot of room available for both theoretical and experimental investigation for this type of

antenna. Some possibilities for future research toward aperture coupled antennas are listed below.

One might use the developed DWM formulation for the resonant frequency and the Q– factor of the dielectric resonator antenna to find theoretically the input impedance of the presented circuit model for the antenna (as discussed in section 2.9) in terms of resonant frequency, stub length, and aperture dimensions. This would be of great importance in developing design curves for the input impedance of the antenna that would be useful for the antenna designer.

Using the developed DWM formulation for the near field, One can obtained the mutual coupling of two neighboring DRs. This is of great interest when designing an array of DR antennas.

Using the developed DWM formulation for the far fields in this thesis, and with the theory of diffraction developed in [36], one could include the effect of using a finite ground plane on the radiation pattern of the antenna.

REFERENCES

[1] R.D. Richtmyer, "Dielectric resonator" , J. Appl. Phys. vol. 10, pp. 391–398, June 1939.

[2] S.B. Cohn, "Microwave Bandpass Filters Containing High Q Dielectric Resonator" , IEEE Trans. Microwave Theory & Techniques, vol. MTT–16, pp. 218–227, April 1968.

[3] D.J. Masse et al, "A New Low–Loss High–k Temperature compensated Dielectric for Microwave Applications" , Proc. IEEE, vol. 59, pp. 1628–1629, November 1971.

[4] J.K. Ploured, D.F Linn, H.M. O'Brayn Jr., J. Thomson Jr., "$Ba_2Ti_9O_2O$ as a Microwave Dielectric Resonator", J. Amer. Ceram. Soc., vol. 58, pp. 418–420, October 1975.

[5] T. Nishikawa, Y. Ishikawa, H. Tamura, "Ceramic Material for Microwave applications", Electronic Ceramics, Spring Issue, Special Issue on Ceramic Materials for Microwave Applications, Japan 1979.

[6] A.P.S. Khanna, "Understanding DRO Design Methods and Operation," Microwaves & RF, vol. 31, pp. 120–124, April 1992.

[7] J.R. James & P.S. Hall (Editors), Handbook of Microstrip Antennas, Peter Peregrinus Ltd. 1989.

[8] Y.Kobayashi and S.Tanaka, "Resonant modes of a dielectric rod resonator short circuited at both ends by parallel conducting plates", IEEE Trans. Microwave Theory Tech., vol. MTT–28, pp. 1077–1085, October 1980.

[9] D.Kajfez & P.Guillon (Editors), Dielectric Resonators, Artech House Inc 1986.

[10] D. Kajfez, A. W. Glisson and J. James, " Computed Modal Field Distributions for Isolated Dielectric Resonator", IEEE Trans. on Microwave Theory &Techniques, vol. MTT–32, pp. 1609–1616, December 1984.

[11] S.A.Long, M.W.Mcallister, L.C.Shen, "The Resonant Cylindrical Dielectric Cavity Antenna" IEEE Trans. on Antenna and Propagation, vol. AP–31, pp. 406–412, May 1983.

[12] R.K.Mongia, "A Half–Split Dielectric Resonator Placed On Metallic Plane For Antenna Applications", Electronics Letters, vol. 25, pp. 462–464, August 1989.

[13] M.W. McAllister S.A.Long and G.L. Conwya, " Rectangular Dielectric resonator Antenna", Electronics Letters, vol. 19, pp. 218–219, March 1983.

[14] M.W. McAllister and S.A.Long, "Resonant Hemispherical Dielectric Antenna", Electronics Letters, vol. 20, pp 657–659, August 1984.

[15] R.A.Kranenburg and S.A.Long, "A Microstrip Transmission Line Excitation Of Dielectric Resonator Antennas ", Electronics Letters, vol. 24, pp. 1156–1157, September 1988.

[16] R.A.Kranenburg, S.A.Long and J.T.Williams, "A Coplanar Waveguide Excitation of Dielectric Resonator Antenna ", IEEE Trans. on Antenna And Propagation, vol. AP–39, pp. 119–122, January 1991.

[17] M.Haneishi and H.Takazawa , "Broadband Circularly Polarized Planar Array Composed Of A Pair Of Dielectric Resonator Antennas", Electronics Letters. vol. 21, pp. 437–438, May 1985.

[18] J.T.H.St.Martin Y.M.M Antar A.A Kisk A. Ittipiboon & M. Cuhaci, "Dielectric Resonator Antenna Using Aperture Coupling", Electronics Letters, vol. 26, pp. 2015–2016, November 1990.

[19] R.K.Mongia A.Ittipiboon Y.M.M Antar P.Bhartia & M.Cuhaci,"A Half–Split Cylindrical Dielectric Resonator Antenna using slot–coupling", IEEE Trans.on Microwave Theory & Techniques, vol.3, pp. 38–39, MTT–3, February 1993.

[20] A.A.Kishk A.Ittipiboon Y.M.M Antar & M.Cuhaci ," Dielectric Resonator Antenna fed by a Slot in the Ground Plane of a Microstripline", Proc. Eight Int. Conf. on Antennas and Propagation, ICAP'93, Part 1, pp. 540–543, April 1993.

[21] A.A.Kishk, A.W. Glisson, and D.Kajfez," Computed resonant frequency and far field of isolated disks, IEEE AP–S Int. Symp. Digest, pp. 408–411, Michigan, June28 – July2, 1993.

[22] A.Ittipiboon R.K.Mongia Y.M.M Antar & M.Cuhaci ," An Integrated Rectangular Dielectric Resonator Antenna", IEEE AP–S Int. Symp. Digest, pp. 604–607, Michigan, June 28– July 2, 1993.

[23] J.T.H.St–Martin, Aperture coupling of Circular cylindrical Dielectric Resonator Antenna, MEng Thesis, Royal Military College of Canada 1989.

[24] D.M.Pozar,"Microstrip Antenna Aperture–Coupled to a Microstripline", Electronics Letters, vol. 21, pp. 49–50, January 1985.

[25] D.M.Pozar,"A Reciprocity Method of Analysis for Printed Slot–Coupled Microstrip Antennas",IEEE Trans.on Antennas and Propagation , vol. AP–34, pp. 1439–1446, December 1986.

[26] R.K.Mongia and P. Bhartia "Dielectric Resonator Antennas– A Review and General Design Relations For Resonator Frequency and Bandwith", Int. journal of Microwave and millimeter wave Computer–Aided Engineering (to be published in 1994 issue)

[27] A.Ittipiboon R.Oostlander & Y.M.M Antar,"Modal Expansion Method of Analysis and Measurement on Aperture–Coupled Microstrip Antenna", IEEE Trans. on Antennas And Propagation, vol. AP–39, pp. 1567–1573, November 1991.

[28] R.F.Harrington,Time–Harmonic Electromagnetic Fields, MacGraw–Hill Book Company, 1960.

[29] E.A.J. Marcatili, "Dielectric rectangular waveguide and directional coupler for integrated optics," Bell Syst. Tech. J., vol.48, pp. 2071–2102, September 1969.

[30] Itoh,T. and Rudokas,"R.S.,New method for computing the resonant frequencies of dielectric resonator", IEEE Trans. Microwave Theory & Techniques, vol. MTT–25, pp. 52–54, 1977.

[31] R.K.Mongia & P.Bhartia,"Accurate Resonant frequencies of cylindrical dielectric resonators using a simple analytical technique," Electronics Letters, vol. 21 pp. 479–480, May 1985.

[32] R. K. Hoffman, Handbook of Microwave Integrated Circuits. Artech House, 1983.

[33] J.Van Bladel, "On the resonances frequency of a dielectric resonator of very high permittivity," IEEE Trans.on Microwave Theory and Tech., vol. MTT–23, pp 199–208, February 1975.

[34] K.C. Gupta, R. Garg and R. Chadha, Computer Aided Design Of Microwave Circuits. Handbook of Microwave Integrated Circuits. Artech House, 198?.

[35] R. K. Hoffman, Handbook of Microwave Integrated Circuits. Artech House, 1983.

[36] C.A.Balanis, Antenna Theory analysis and design , Harper & Row–Hill Publishers, 1982.

[37] R. F. Harrington, Field Computation by Moment Methods, Kreiger Publishing Company, 1983.

APPENDIX A

RADIATION PATTERN MEASUREMENT

This appendix contains the measured radiation patterns for the tested DRA DR_1 (A_1 to A_4) and DR_2(A_5 to A_8)

THE UNIVERSITY OF MANITOBA

Resonator 0.8cm, 10.5, 34cm gnd plane

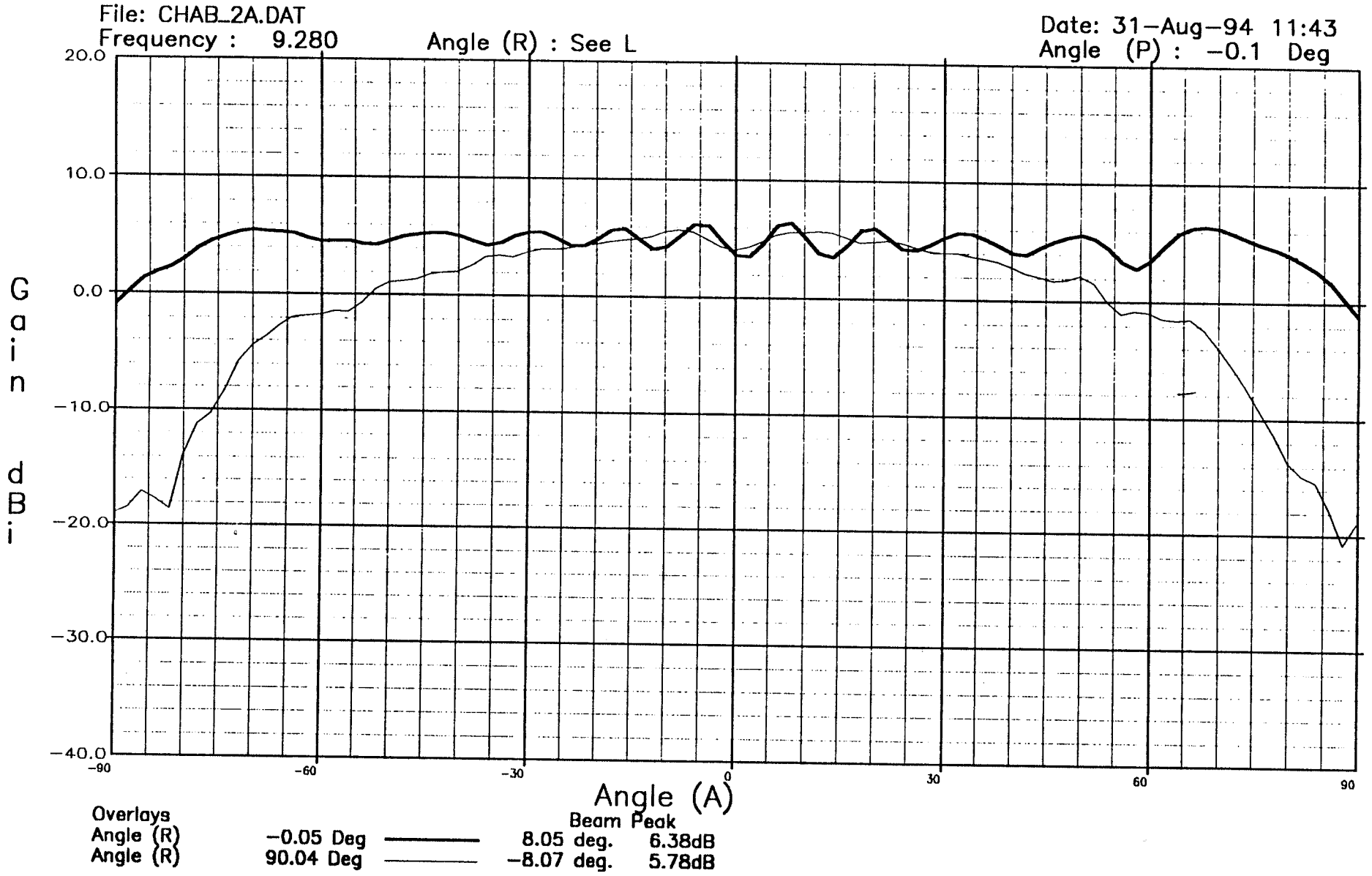

THE UNIVERSITY OF MANITOBA

Resonator 0.8cm, 10.5, 34cm gnd plane

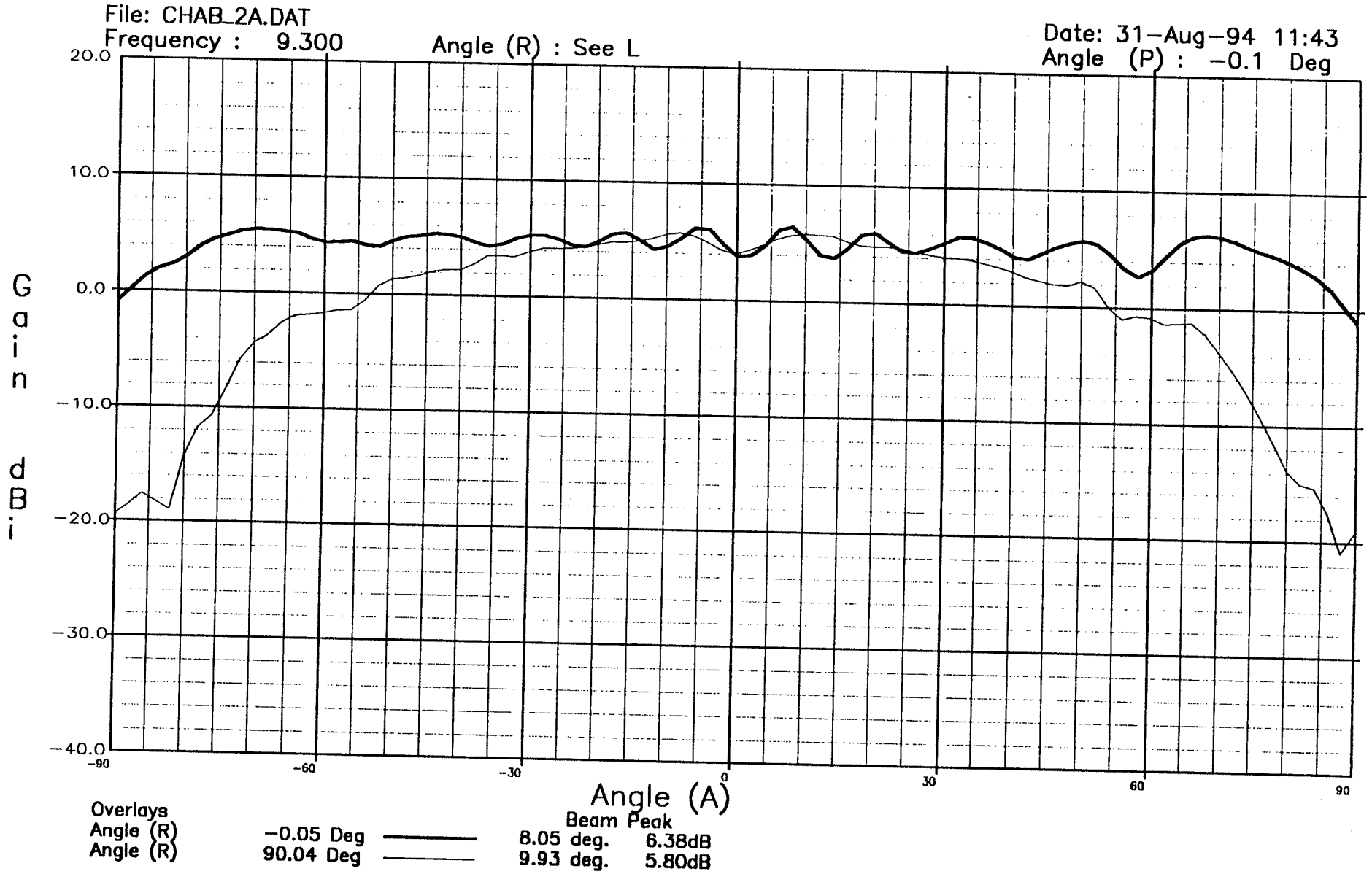

THE UNIVERSITY OF MANITOBA

Resonator 0.8cm, 10.5, 34cm gnd plane

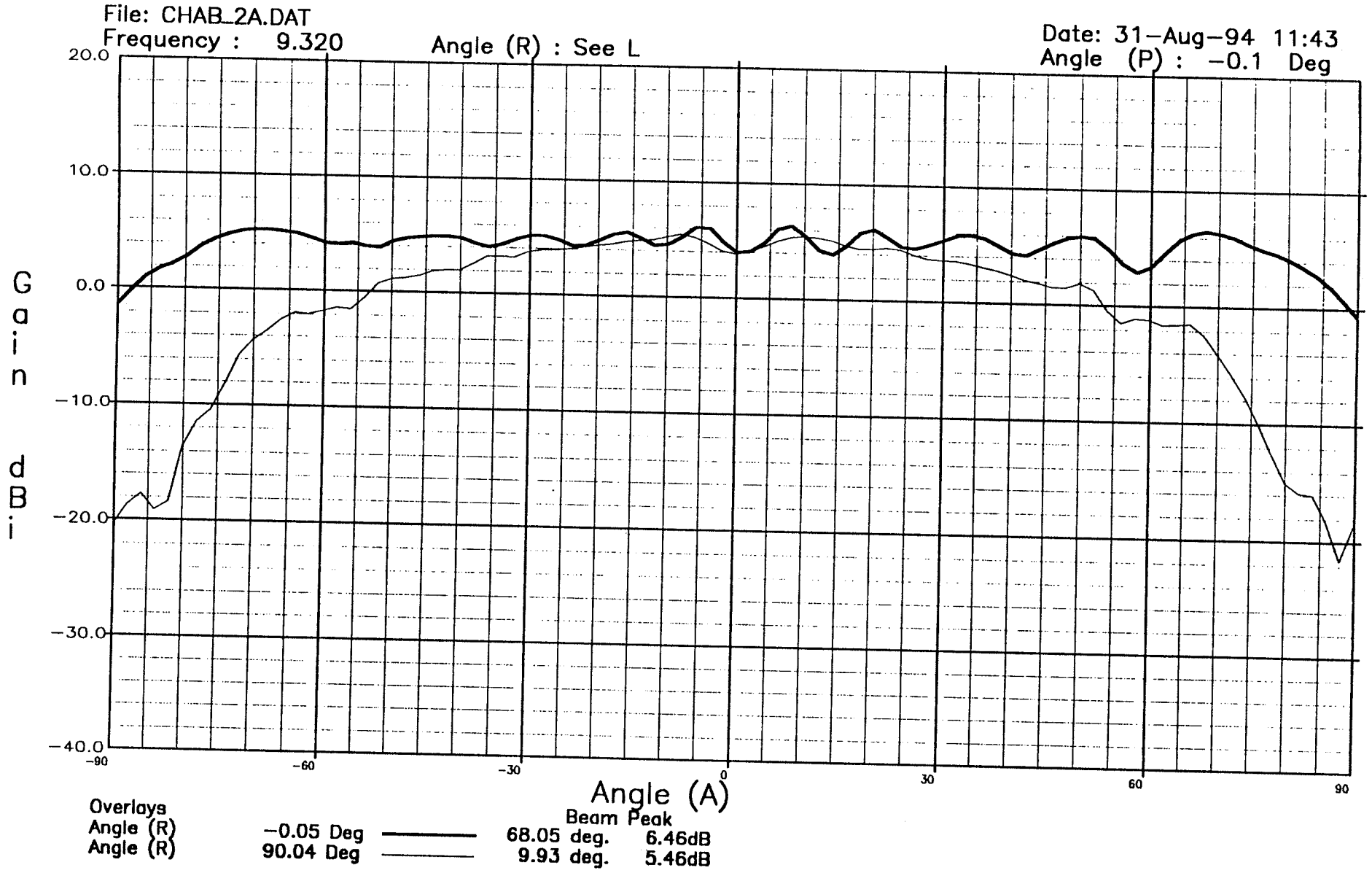

THE UNIVERSITY OF MANITOBA

Resonator 0.8cm, 10.5, 34cm gnd plane

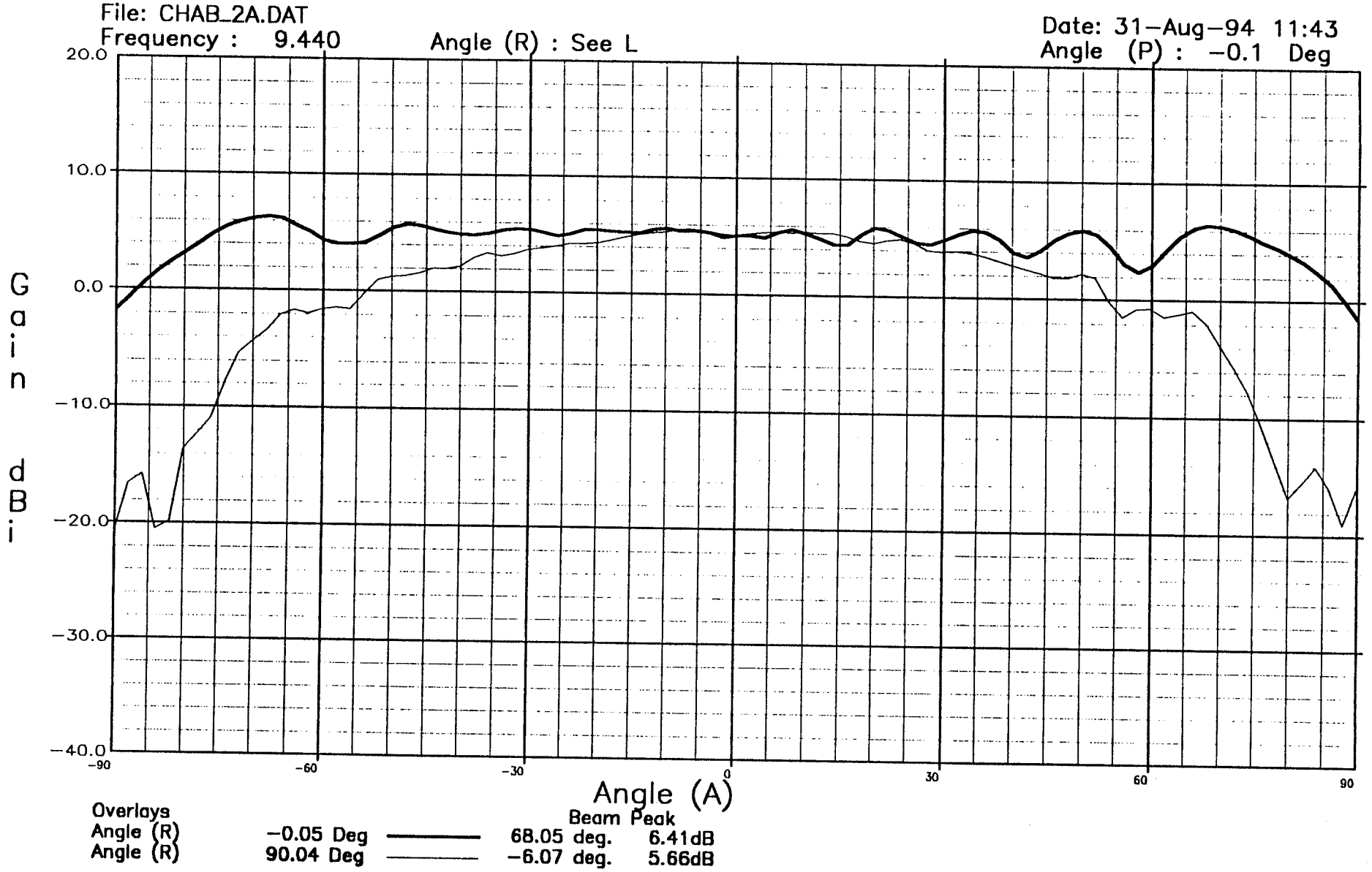

THE UNIVERSITY OF MANITOBA

Resonator 11cm, 10.2, 34 cm gnd plane,

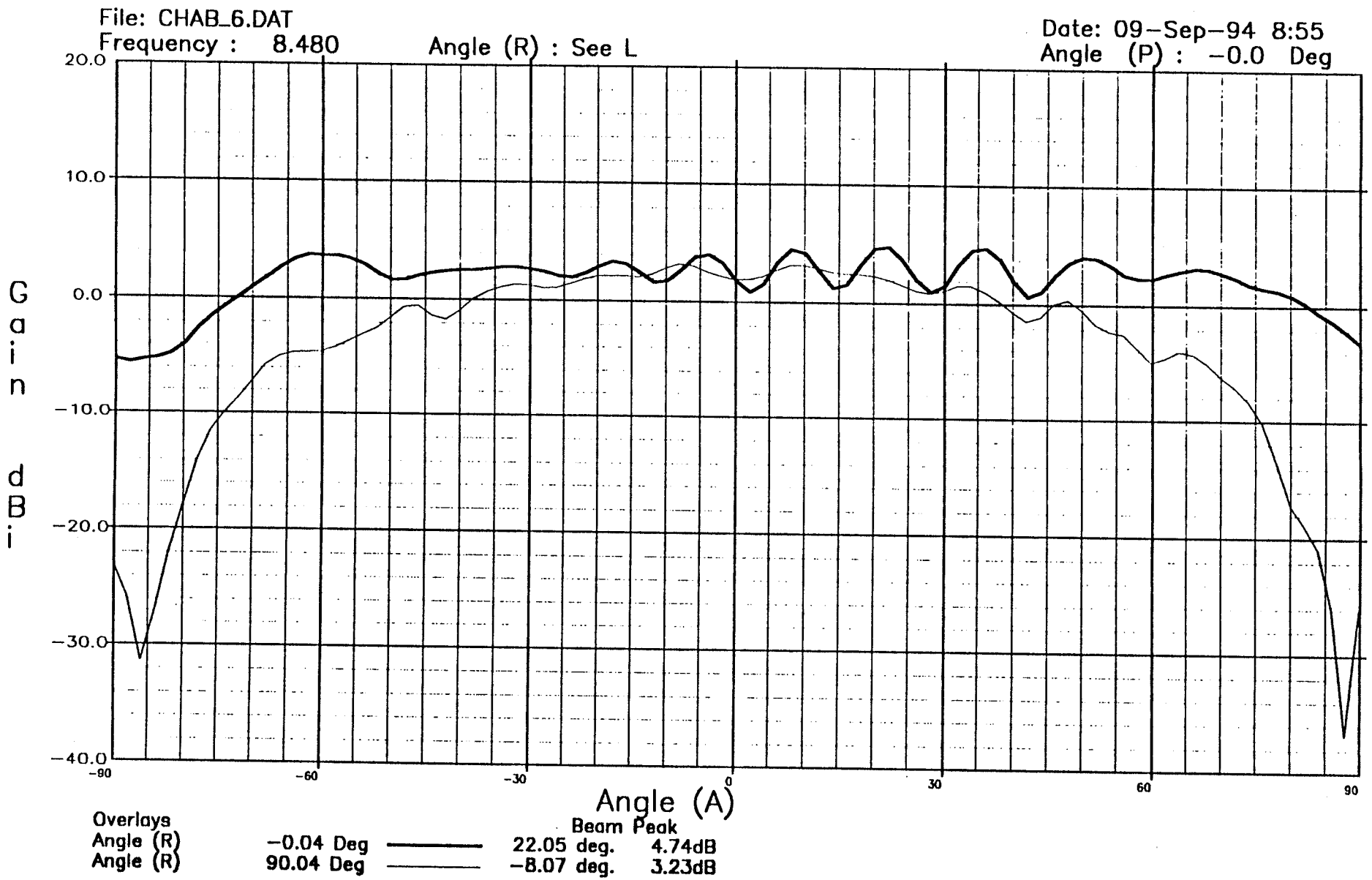

THE UNIVERSITY OF MANITOBA

Resonator 9cm, 10.2, 34 cm gnd plane,

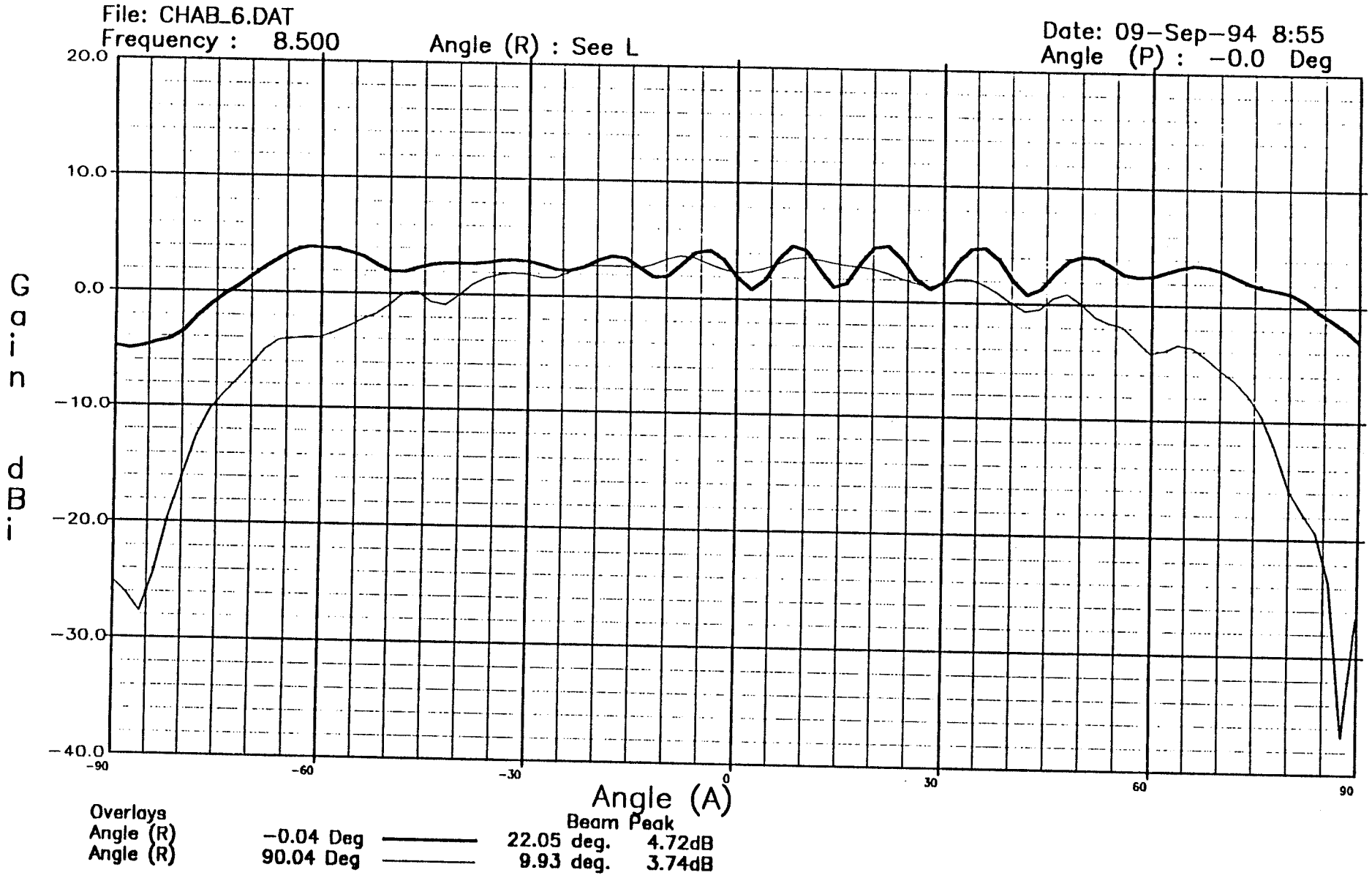

THE UNIVERSITY OF MANITOBA

Resonator 9.1 cm, 10.2, 34 cm gnd plane,

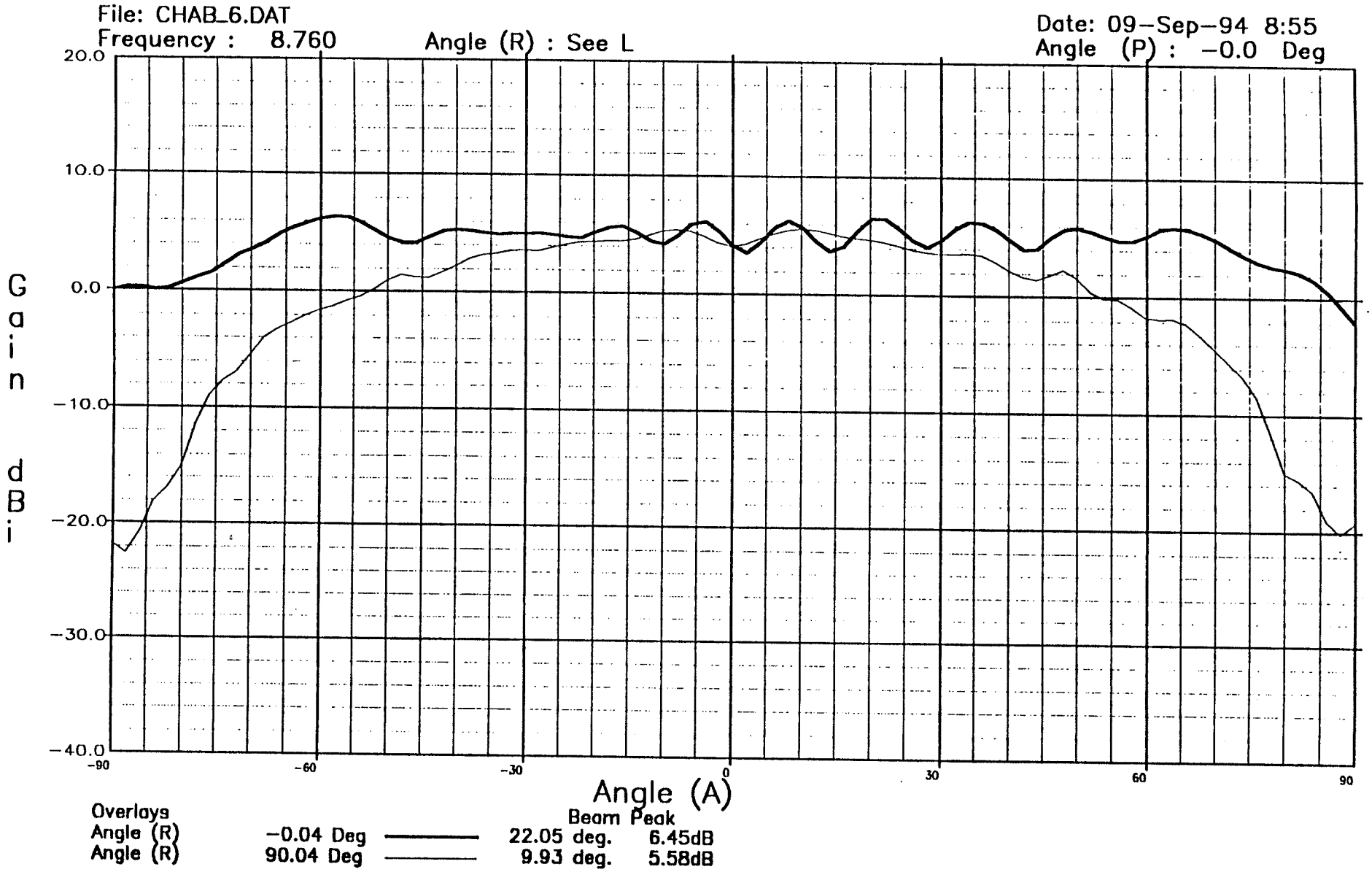

THE UNIVERSITY OF MANITOBA

Resonator 1cm, 10.2, 34 cm gnd plane,